Thermal metamorphism of CM chondrites: A dehydroxylation-based peak-temperature thermometer and implications for sample return from asteroids Ryugu and Bennu

Michael A. VELBEL [1,2]* and Michael E. ZOLENSKY [3]

[1]Department of Earth and Environmental Sciences, Michigan State University, 288 Farm Lane, Room 207, Natural Sciences Building, East Lansing, Michigan 48824–1115, USA
[2]Division of Meteorites, Department of Mineral Sciences, National Museum of Natural History, Smithsonian Institution, Washington, District of Columbia 20013–7012, USA
[3]X12 Astromaterials Research and Exploration Science, NASA Johnson Space Center, Houston, Texas 77058, USA
*Corresponding author. E-mail: velbel@msu.edu

Abstract–The target bodies of C-complex asteroid sample return missions are carbonaceous chondrite-like near-Earth asteroids (NEAs), chosen for the abundance and scientific importance of their organic compounds and "hydrous" (including hydroxylated) minerals, such as serpentine-group phyllosilicates. Science objectives include returning samples of pristine carbonaceous regolith from asteroids for study of the nature, history, and distribution of its constituent minerals, organic material, and other volatiles. Heating after the natural aqueous alteration that formed the abundant phyllosilicates in CM and similar carbonaceous chondrites dehydroxylated them and altered or decomposed other volumetrically minor constituents (e.g., carbonates, sulfides, organic molecules; Tonui et al. 2003, 2014). We propose a peak-temperature thermometer based on dehydroxylation as measured by analytical totals from electron probe microanalysis (EPMA) of matrices in a number of heated and aqueously altered (but not further heated) CM chondrites. Some CM lithologies in Maribo and Sutter's Mill do not exhibit the matrix dehydroxylation expected for surface temperatures expected from insolation of meteoroids with their known orbital perihelia. This suggests that insolated-heated meteoroid surfaces were lost by ablation during passage through Earth's atmosphere, and that insolation-heated material is more likely to be encountered among returned asteroid regolith samples than in meteorites. More generally, several published lines of evidence suggest that episodic heating of some CM material, most likely by impacts, continued intermittently and locally up to billions of years after assembly and early heating of ancestral CM chondrite bodies. Mission spectroscopic measures of hydration can be used to estimate the extent of dehydroxylation, and the new dehydroxylation thermometer can be used directly to select fragments of returned samples most likely to contain less thermally altered inventories of primitive organic molecules.

INTRODUCTION

Background and Statement of Problem

The target bodies of C-complex asteroid sample return missions Hayabusa2 and OSIRIS-REx (Origins, Spectral Interpretation, Resource Identification, and Security–Regolith Explorer) are, respectively, carbonaceous near-Earth asteroids (NEAs) Ryugu (provisional designation 1999 JU₃, Minor Planets Center [MPC] designation 162173) and Bennu (provisional designation 1999 RQ₃₆, MPC designation 101955). They were chosen for the abundance and scientific importance of the volatiles they contain (Lauretta et al. 2017; Wada et al. 2018). Volatile-rich constituents of interest include hydrated[1] crystalline silicates (phyllosilicates), amorphous

silicates, and associated organic compounds hosted by such volatile-rich phases. All spectroscopic matches (with varying degrees of success) between C-complex mission target asteroids and meteorites are with members of carbonaceous chondrite (CC) groups that contain H-hosting phyllosilicates and elevated abundances of reduced (organic) C compounds associated with the phyllosilicates (Grady 2000; Hutchison 2004; Kebukawa et al. 2009), suggesting surface materials related to CM2, CM1, and CI chondrites, or anomalous C chondrites (Lauretta et al. 2015, 2017; Wada et al. 2018). Specific associations of organic compounds with host phases in carbonaceous chondrites are influenced by the nature and initial abundance of each, and subsequent redistribution of volatiles, both spatially and among reactant and product phases, during aqueous and thermal alteration (Glavin and Dworkin 2009; Kebukawa et al. 2009; Herd et al. 2011; Glavin et al. 2018).

CM (Mighei-like) chondrites are sufficiently numerous and abundant among carbonaceous chondrite falls and finds that available samples encompass well-studied ranges of both

1. Multiple subtle compositional variations that indicate different degrees/extents of aqueous alteration and are classified using any of a number of aqueous alteration scales[2] and
2. Varying degrees of natural thermal dehydroxylation after aqueous alteration (e.g., Tonui et al. 2014).

A number of heat sources have been hypothesized to account for both the mild heating required for aqueous alteration and the additional post-hydration heating observed in carbonaceous chondrite meteorites and inferred spectroscopically from surfaces of C-complex asteroids. These include:

1. Heating in grandparent body interiors (larger planetesimal ancestral bodies subsequently disrupted into fragments, from which assembled the rubble-pile asteroid that was the immediate parent body of a meteoroid; cf. Sugita et al. 2019, their fig. 8; Keane 2019) by decay of early solar system short-lived radionuclides (mainly ^{26}Al) driving internal thermal metamorphism (Akai 1988),
2. Sub-body scale conversion of kinetic energy to heat in CM chondrite target rock during impact, driving widespread subsurface metamorphism of target material (Akai 1988; Choe et al. 2010; Davison et al. 2012; Garenne et al. 2014; King et al. 2015a; Trigo-Rodríguez 2015),
3. Conversion of kinetic energy to heat in submillimeter- to centimeter-scale heating of small projectiles and immediately adjacent target regolith

during high-velocity impact (Gounelle et al. 2003; Rubin 2004, 2012; Trigo-Rodríguez et al. 2019),
4. Insolation heating of asteroid surfaces during passage near the Sun during past low-perihelion orbital epochs (Akai 1988; Nakamura 2005; Licandro et al. 2007; Nakato et al. 2008; Michel and Delbo 2010; Delbo and Michel 2011; King et al. 2015b; de León et al. 2018; Quirico et al. 2018),
5. Space weathering (Lantz et al. 2018), and
6. Some small (submillimeter- to centimeter-scale) volatile-rich projectiles may arrive at asteroid surfaces as small meteorites at sufficiently high velocities that impact heating partially devolatilizes but does not vaporize them. Otherwise identical small meteorite projectiles, and spall fragments from larger CM projectiles, arrive at lower velocities and consequently retain their volatiles. Both subpopulations become incorporated into target-body regoliths (and their subsequently lithified regolith breccia counterparts) as clast-like fossil meteorites and fossil micrometeorites in regolith breccias (Gounelle et al. 2003; Rubin and Bottke 2009; Reddy et al. 2012; Patzek et al. 2018).

Aqueous alteration in CM chondrites was driven by mild heating that caused melting of water ice physically intermixed with silicate matter. The former presence of water ice has long been inferred by many studies of CM chondrites and was recently convincingly demonstrated by Matsumoto et al. (2019). Such CMs are commonly referred to as aqueously altered. An ever-growing number of CM chondrites is recognized as having been heated—well beyond the melting temperature of $H_2O_{(s)}$ ice—after aqueous alteration (e.g., Tonui et al. 2002, 2014). Such CMs are referred to as "heated" (e.g., Akai 1990; Tonui et al. 2002), "naturally heated" (to be distinguished from experimentally heated; Hiroi et al. 1996), or "thermally metamorphosed" (e.g., Akai 1990; Hiroi et al. 1993; Tonui et al. 2003, 2014; Nakamura 2005). Nomenclatural confusion abounds.

Aqueous alteration of CMs was recognized first (e.g., DuFresne and Anders 1962; Bunch and Chang 1980), and only later were observations made that required hypothesizing additional heat beyond that required for aqueous alteration. Relative to the emergingly recognized "thermally metamorphosed" CM chondrites, CM chondrites that were merely "aqueously altered" (the required heat being implicit in the term) became contrasted with their (naturally) "heated" counterparts by being labeled "unheated" (relative to those metamorphosed beyond the temperature range of aqueous alteration; Hiroi et al. 1996; Tonui et al. 2003, 2014; Nakamura 2005) or "common" (relative to their at-the-time still uncommon heated counterparts; Hiroi et al. 1996). Nakamura (2005) referred to "post-

hydration thermal metamorphism" and Cloutis et al. (2012, p. 587) introduced the term ATCCs ("aqueously altered and thermally metamorphosed CCs"; Cloutis et al. 2018, p. 284) for "CCs that show evidence of aqueous alteration followed by thermal metamorphism." These papers applied their suggested terms to CCs affected by *both* aqueous alteration *and* thermal metamorphism, to distinguish them from CCs affected *only* by aqueous alteration. Rather than introduce yet another term, this article will use the existing term ATCC, with the implicit understanding that aqueous alteration ("hydration") of CCs—mainly large subsets of CMs and CIs that are *not* ATCCs, but aqueously altered without *further* heating— also required heating, but only to temperatures not as high as the temperatures of thermal metamorphism.

The meteorites with the best spectroscopic matches to the recent C-complex sample-return mission target asteroids include thermally anomalous C chondrites and experimentally heated CM2s (e.g., Hiroi et al. 1993, 1996; Nakamura 2005; Choe et al. 2010; Clark et al. 2011; Moskovitz et al. 2013; Sugita et al. 2013; Tonui et al. 2014; Perna et al. 2017). Meteorite spectra vary with particle size, viewing geometry, illumination conditions, and terrestrial weathering (McAdam et al. 2015; Campins et al. 2018; Cloutis et al. 2018; Takir et al. 2018). Spectroscopic measurements of asteroids provide information only about the optically active outermost surface that (1) may not be representative of the composition of bulk materials collected below the surface by sample return missions and (2) may have been affected by phenomena that modify their spectra relative to (a) conditions of acquisition of laboratory spectra from meteorites (e.g., temperature, vacuum versus laboratory ambient atmosphere) and (b) material that was never exposed to processes at the parent body's surface such as space weathering (Takir et al. 2018; Kaplan et al. 2020). Hypotheses for the interpretation of asteroid surface composition from some spacecraft-measured spectral properties will ultimately be tested and understood only by terrestrial laboratory analyses of the returned sample (Kaplan et al. 2020).

Surface phenomena including space weathering (Lantz et al. 2018) and the thermal effects of an asteroid being much closer to the Sun than the inner Main Belt collisional famil(y/ies) to which it is related (de Léon et al. 2018) have both been suggested as processes affecting some NEA spectra. Spectroscopically similar anomalous CM chondrites have mineral inventories and attributes that indicate they were dehydroxylated during heating to peak temperatures of 400–750 °C (~670–1020 K), higher than peak temperatures experienced by aqueously altered (but not further heated) CCs (e.g., Akai 1988, 1990, 1992; Ikeda 1992; Tonui et al. 2002, 2003, 2014) (Table 1). Spectral reflectance data in the ultraviolet (UV), visible

(Vis), and near-infrared (NIR) for thermally metamorphosed carbonaceous chondrites (e.g., Tonui et al. 2014) suggest that carbonaceous chondrite-like material that has been metamorphosed over the aforementioned range of temperatures occurs at the surfaces of a number of C-, G-, B-, and F- asteroids (Hiroi et al. 1993, 1994, 1996).

Early Hayabusa2 and OSIRIS-REx data from Ryugu and Bennu support prelaunch expectations that material depleted in H (measured as OH, depleted by loss as H_2O) and other volatile elements and compounds relative to aqueously altered (but not further heated) CM chondrite material (1) would be encountered at these B- and C-type asteroids (e.g., Bennu and Ryugu, respectively) and (2) will be present among the samples returned by these missions. It is essential to both (1) continued interpretation of data acquired during sample site selection and characterization, and (2) examination of the returned samples, to establish the specific surface material with which the spectral signature of the desired volatile-rich target material is associated.

This project builds on existing knowledge (from meteorites) of thermal metamorphism and its effects, to develop a regimen of specific simple measurements for peak-temperature lithothermometry of mission-returned samples. The purposes of this article are to (1) propose a quantitative measure of thermally induced loss of phyllosilicate-hosted hydroxyl from carbonaceous (CM) chondrite lithologies, from a compilation and synthesis of published data from CM meteorites and clasts of CM lithologies in meteoritic breccias; (2) propose a corresponding preliminary peak-temperature lithothermometer for heating effects on CM lithologies; and (3) discuss some implications of the results from peak-temperature lithothermometry for previously hypothesized heat sources of CM carbonaceous chondrites, and for spacecraft spectroscopic characterization of sample sites and preliminary examination of mission-returned samples.

Sample Return Mission Target Asteroids and Corresponding Meteorite Groups

The target asteroids of the Hayabusa2 and OSIRIS-REx sample return missions, Ryugu and Bennu, respectively, were selected in part on the basis of the expected presence of volatiles, including hydrated silicates and associated reduced carbon compounds (Lauretta et al. 2015, 2017; Wada et al. 2018). Spectroscopic near-matches include both (1) "common" CM chondrites (sensu Hiroi et al. [1996]; aqueously altered but not further heated, and rich in OH-bearing phyllosilicates, and thus among the most aqueously altered meteorites available for study in terrestrial laboratories) and (2)

Table 1. Compositional properties and estimated peak metamorphic temperature of thermally altered C chondrites.

Meteorite	Classification[a]	$T_{\text{peak metamorphism}}$ (°C)[b]	Matrix EPMA total (wt%)[a]	$T_{\text{peak metamorphism}}$ (°C) from matrix EPMAΣ (1 significant figure)	$T_{\text{peak metamorphism}}$ (°C) from matrix EPMAΣ (2 significant figures)
Y-86789	CM2TIV	≥750 =↓	98.7[c]	800	760
Y-86720	CM2TIV	=↑	96.54[d]	700	660
Y-82162	CI1TII/III		96.6	700	660
Y-86029	CI1TIII	=↓	95.0	600	590
B-7904	CM2TIV	=↑ ≈600	91.5[e]	*400*	*440*
PCA 91008	CM2TIII		97.3	700	690
A-881655	CM2TIII	=↓ ≈500	98.17[f]	600	730
WIS 91600	CM2TII	=↑	94.4	*600*	*570*
Y-793321	CM2TII	≥400	91.8	400	450
Y-791198	CM2		88.3[d]	300	300
Compiled	Non-ATCC CM	<400	84–88	<300	<300

As arranged by Tonui et al. (2014); modified and corrected from Zolensky et al. (2018), their table 2.5. Arrows point to adjacent listed samples identified as having equal peak temperatures of metamorphism. Italicized T_{peak} values fall outside the range of the Nakamura (2005) Stage to which the meteorite was assigned by Tonui et al. (2014).
[a]From Tonui et al. (2014) unless otherwise credited.
[b]From Tonui et al. (2014), estimated from similarity of labile-element depletion to Murchison experimentally heated to the indicated temperature.
[c]From Matsuoka et al. (1996).
[d]TEM EDX analysis of matrix serpentine, with several minor elements not determined; from Lipschutz et al. (1999) their table 2.
[e]From Zolensky et al. (1993).
[f]Desiccated high Al, Mg serpentine from matrix (Lipschutz et al. 1999).

naturally heated, both aqueously and thermally altered (dehydroxylated) (ATCC sensu Cloutis et al. 2012, 2018) meteorites.

The disk-averaged thermal inertia of Ryugu is high, suggesting that the asteroid's surface materials are dominated by boulders and bare rock, generally lacking thick regolith (Hasegawa et al. 2008; regolith is defined elsewhere as unconsolidated particulate matter smaller than the thermal skin depth, Rozitis et al. 2020). Diverse spectroscopic observations of Ryugu by ground-based telescopes vary and are attributed to spatial heterogeneity of the surface material (Binzel et al. 2004; Vilas 2008; Sugita et al. 2013; Moskovitz et al. 2013). A small number of ground-based astronomical observations yielded spectra with a 0.7 μm absorption feature, suggesting that a small part of the asteroid's surface (a surface that rotation only occasionally exposes to ground-based telescopes) consists of aqueously altered (but not further heated) CM2-like phyllosilicate-rich carbonaceous chondrite material (e.g., ALHA81002 [CM2]; Vilas 2008; Sugita et al. 2013). At the group level, the best spectroscopic matches to the most frequently observed surfaces of Ryugu are (Moskovitz et al. 2013; Sugita et al. 2013; Perna et al. 2017) partially devolatilized (1) CM-like carbonaceous chondrite material (the <63 μm particle size fraction of Murchison [CM2] experimentally heated to 900 °C and 1000 °C), and (2) CI material (the <125 μm fraction of naturally thermally altered [ATCC] Yamato [Y]-86029 [CI1TIII in

the classification of Nakamura [2005]—more on this classification below; 500 °C < inferred T_{peak} < 700 °C; also classified as CY by King et al. 2019a[3]]). Based on early Hayabusa2 mission data (Kitazato et al. 2019), Ryugu is still most similar to MET 01072 (shocked CM2) and heated CCs (Ivuna [CI] experimentally heated to 500 °C), although not an exact match to any one as-recovered meteorite or experimentally heated meteorite.

At the *group* level, CI and/or CM chondrites are the best spectroscopic matches to Bennu. Clark et al. (2011) suggested "CM1"-like material. The best spectroscopic matches between Bennu and library spectra of *individual* meteorites are a sample of Ivuna (CI) experimentally heated to 700 °C, the anomalous CM carbonaceous chondrite Dhofar 225 (possibly part of a CM-like Belgica [B]-7904 grouplet[4]; Choe et al. 2010), and a matrix-rich fraction of Mighei, all examined as powders of 100–200 μm grains (Clark et al. 2011). Space weathering (Lantz et al. 2018) and the thermal effects of Bennu being much closer to the Sun than the inner Main Belt collisional families to which it is related (de León et al. 2018) have both been suggested as processes affecting the spectra of Bennu. Based on early OSIRIS-REx mission data (Hamilton et al. 2019), Bennu is still most similar to CM2s, now more specifically Cold Bokkeveld (CM2.2 in the classification of Rubin et al. 2007), other CM2.2 and CM2.1 chondrites, and CM1/2 chondrites, although not an exact match to any one as-recovered meteorite.

As new meteorite spectra are acquired and added to spectral libraries (Takir et al. 2013; McAdam et al. 2015; Garenne et al. 2016; Kaplan and Milliken 2016; Beck et al. 2018; Lantz et al. 2018; Bates et al. 2020; Kaplan et al. 2020), additional good matches may be recognized, enabling refined interpretation.

Phyllosilicates and Associated Minerals in CM Chondrite Matrices: Their Aqueous Alteration and Heating

Phyllosilicates in CM chondrites are mainly serpentine group minerals, $(Mg,Fe)_3Si_2O_5(OH)_4$, some with more complex substitutions of trivalent cations in either or both octahedral and tetrahedral sites (Zolensky et al. 2018, their table 2.4). They occur mainly in matrix (Buseck and Hua [1993]; see review by Velbel and Palmer [2011], and the pioneering primary references cited therein). Many CM chondrites also contain smaller abundances of phyllosilicates in fine-grained rims around chondrules (e.g., Metzler et al. 1992; Lauretta et al. 2000; Chizmadia and Brearley 2008), although in some CM chondrites (e.g., ALH 88045; Zolensky et al. 1997), the fine-grained material occurs almost entirely as rims on chondrules rather than matrix. Phyllosilicates in CM chondrites also occur locally but significantly as pseudomorphs after anhydrous silicates (pyroxene, olivine; Bunch and Chang 1980; Kojima et al. 1984; Barber 1985; Browning et al. 2000; Hanowski and Brearley 2001; Velbel et al. 2012, 2015; Lee et al. 2014; Velbel 2014; Leroux et al. 2015; Lee and Lindgren 2016; Pignatelli et al. 2016, 2017; King et al. 2019b), where their microscopic textures demonstrate unequivocally that the hydrous (phyllosilicate) phase formed by a hydration reaction of water with primary anhydrous silicates.

Different groups of carbonaceous chondrites differ in their modal abundances of matrix (Krot et al. 2005; Hutchison 2004; Weisberg et al. 2006; Howard et al. 2009, 2011, 2015; King et al. 2015b) and in the ranges of EPMA (anhydrous) analytical totals (EPMAΣ) of their matrices (McSween and Richardson 1977; Zolensky et al. 1993, 1997), among other important factors. As noted above, CM- and CI-like lithologies are the best spectroscopic matches to date between recent C-complex mission target asteroids and meteorites. CM chondrites are dominated by serpentine-group minerals (e.g., 56–91 modal%, Howard et al. 2015; King et al. 2017; Bates et al. 2020), most of which are in matrix that constitutes 40–91 (but mainly 50–91) modal% of CMs (McSween 1979; Zolensky et al. 1997; Garenne et al. 2014; Hewins et al. 2014; King et al. 2017). A few CM chondrites, including Bells (Zolensky et al. 1993; Brearley 1995) and Belgica-7904 (Kojima et al. 1984; Akai 1988, 1992; Tomeoka 1990; Ikeda 1992; Kimura and Ikeda 1992;

Tonui et al. 2014), contain appreciable smectite-like phyllosilicate—commonly identified as saponite—in various states of dehydroxylation ("dehydration"), or other non-serpentine-group minerals (talc, clinochlore) among their phyllosilicates.

Temperature Range for Serpentine-Forming Aqueous Alteration

CM chondrites experienced a range of aqueous alteration (e.g., Zolensky and McSween 1988; Brearley 2003, 2006, 2014; Velbel et al. 2015, their table 1; Zolensky et al. 2018, their table 2.2). The precise conditions under which the parent body aqueous alteration that formed these phyllosilicates took place are loosely constrained. Primary research papers and review papers generally indicate that aqueous alteration products (including serpentine group phyllosilicates) in CM chondrites formed at temperatures broadly between −20 °C and 300 °C (~250–575 K, a range of >300 °C; see brief review with numerous older references in Velbel et al. 2012, p. 128; and more recent papers including Alexander et al. 2015; Verdier-Paoletti et al. 2017; Glavin et al. 2018, their table 3.2; Vacher et al. 2018, 2019; Telus et al. 2019).

Mineralogic Consequences from Heating of CM Chondrite Lithologies

Several observable changes are known to result from thermal metamorphism of CM lithologies. One result of thermal metamorphism of CM lithologies is dehydroxylation ("dehydration") of the phyllosilicate minerals that dominate the abundant matrix.

Phyllosilicate Dehydroxylation Textures in Transmission Electron Microscopy (TEM) and Synchrotron X-ray Diffraction (SXRD)

Ikeda (1992) reviewed the results of a consortium study of three Yamato and Belgica C-chondrites that were among the first recognized (Akai 1988) as being distinct from other C-chondrites in exhibiting evidence for dehydration of matrix phyllosilicates (including high EPMA analytical totals; Tomeoka 1990; Kimura and Ikeda 1992; Ikeda et al. 1992; see below). These three meteorites (Tomeoka et al. 1989a, 1989b) were the first members of the CY group (Ikeda 1992; King et al. 2019a). To support interpretation of these meteorites, Akai (1992) heated powdered Murchison matrix and terrestrial saponite in vacuo to temperatures between 250 and 1100 °C for 1–350 h. Akai (1992) then compared TEM, selected area electron diffraction (SAED), and analytical (transmission) electron microscope (AEM) images and data from the experimentally heated materials with similarly acquired results from a number of

Antarctic meteorites (including Ikeda's [1992] CY chondrites) that had previously shown indications of partial progressive dehydroxylation of phyllosilicates and formation of olivine (Akai 1988; Tomeoka 1990; Ikeda et al. 1992; Kimura and Ikeda 1992). Long (>50 h) heating at a given temperature yielded the same TEM and SAED characteristics as shorter duration (<24 h) of heating at slightly higher temperature. For earlier stage, lower T phenomena, short durations at ~325 °C produce the same observable effects as longer durations at ~300 °C. For later stage, higher T features, phenomena that form rapidly at ~850 °C take >50 h to form at ~700 °C (Akai 1990). The highest temperatures determined from SAED patterns and textures in TEM images differed by up to ~150 °C depending on whether short- or long-duration experimental counterparts were the comparison set, but between-sample relative temperature differences were similar whether short- or long-duration scales were used.

Nakamura (2005) reviewed previous literature and examined by SXRD most of the heated C chondrites recognized at the time. On the combined basis of previous work and new SXRD measurements, Nakamura (2005) proposed a four-stage scale of silicate-mineral/temperature relationships. Samples showing heating effects by reflectance spectroscopy and TEM but no heat-induced mineralogical changes in XRD patterns were assigned to Stage I (corresponding to short-duration exposure to $T < 250$–300 °C; cf. Akai 1992; CM2TI). Samples with XRD patterns lacking diffraction peaks for either serpentine or secondary olivine (formed by dehydroxylation of serpentine) were assigned to Stage II (CM2TII, corresponding to short-duration exposure to T 300–500 °C). Samples showing XRD peaks indicative of low-crystallinity secondary olivine (Tonui et al. 2003) were assigned to Stage III (CM2TIII, corresponding to short-duration exposure to T 500–700 °C). Samples showing XRD peaks of only anhydrous minerals (indicating essentially complete dehydroxylation of phyllosilicates) were assigned to Stage IV (CM2TIV, corresponding to short-duration exposure to $T > 750$ °C). The temperatures at which a given ensemble of mineral relations occurs were typically ~100 °C lower for longer heating periods (cf. Akai 1992). The short-duration (<24 h) relationships between mineral relations, time, and peak temperature may be applicable if a small local high-velocity impact was the source of heat, whereas long-duration (>50 h) time-peak temperature relationships may be applicable if early solar system short-lived radionuclides or solar insolation provided the heat. For simplicity, note that intermediate values between Akai's (1992) short- and long-duration experimental "calibrations" of temperature–time–texture relationships are consistent with subsequent serpentine-based CM matrix peak-temperature estimates for the same meteorites by other means (e.g., Tonui et al. 2002, 2003, 2014), and are used here.

Temperature Ranges for Heating of Serpentine Group and Associated CM Matrix Minerals

Serpentine

Thermal analysis (thermogravimetric analysis, TGA; differential thermal gravimetry, DTG; and differential thermal analysis, DTA) of natural terrestrial serpentine group minerals reveals that mass loss with gradual heating is nonlinear over the temperature range of interest (400 °C < T_{peak} < 750 °C; upper Stage II through Stage IV of Nakamura 2005).[5] For most serpentines, thermogravimetric (TG) curves of mass change with increasing T are typically sigmoidal (Martinez 1961; Faust and Fahey 1962; Hršak et al. 2005, 2008; Viti 2010; Alizadehhesari et al. 2012), with different samples exhibiting a variety of steep and shallow mass-loss curves (Fig. 1). In monomineralic samples, most mass loss occurs over a narrow T range (clinochrysotile in sample F-41a in Fig. 1), whereas in polymineralic samples, most mass loss occurs over a broad T range (chrysotile and lizardite in sample F-69 in Fig. 1). Variations in particle size of prepared powders can shift the temperature range of the sigmoid (e.g., ~10 °C for chlorite; Bish and Duffy 1990), and the particle-/crystallite-size distribution and packing may be expected to introduce some variation in weight loss properties of natural materials examined in an intact (unpowdered) state.

Following Bish and Duffy (1990) and Guggenheim and Koster van Groos (2001), a sigmoidal TG curve (e.g., Fig. 1) is here treated as three line segments—the low-temperature asymptote, the reaction interval (steep sigmoid), and the high-temperature asymptote—and the intersections of the reaction interval with the low- and high-temperature asymptotes are, respectively, T_o and T_c, the onset and completion temperatures of the reaction.

Tochilinite

The "poorly characterized phase" (PCP) described by Fuchs et al. (1973) from Murchison (CM2.5 in the Rubin et al. [2007] classification) was initially estimated to have an upper thermal stability limit of ~245 °C. Subsequently, PCP was (much better) characterized and subdivided into Type I (discrete tochilinite, $Fe_{0.9}S \cdot 5(Fe, Mg)(OH)_2$) and Type II (tochilinite–cronstedtite intergrowths, TCI) PCP (see Velbel et al. [2015], pp. 414–415 for a brief review with numerous pioneering references). TCIs are widespread in most aqueously altered (but not further heated) CM chondrites (Rubin et al. [2007] based their classification of CM2 petrologic subtypes on the compositions of "PCP" [TCI]), but some (e.g., LEW 85311; Lee et al. 2019)
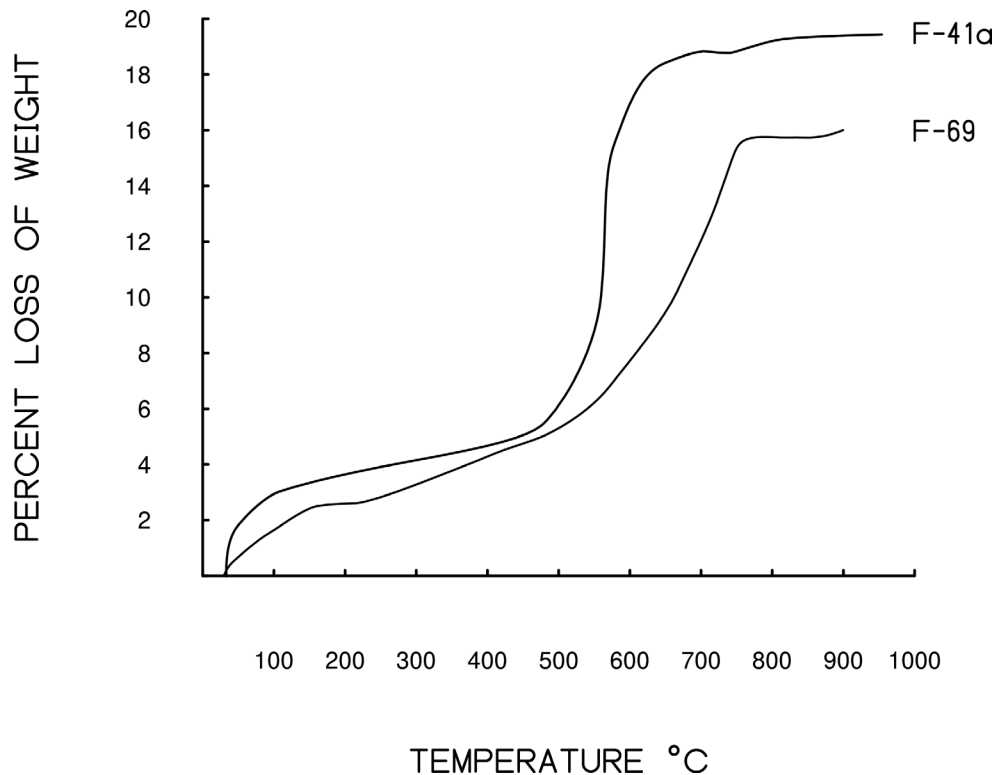
Fig. 1. Thermogravimetric analysis (TGA) curves of representative serpentine-group minerals redrawn from figures in Faust and Fahey (1962); temperature in degrees Centigrade. Bish and Duffy (1990) and Guggenheim and Koster van Groos (2001) distinguish three intervals on a TGA curve each of which can be approximated by a straight line. In these examples, the gently sloping portion of each curve below ~400 °C corresponds to that curve's low-temperature asymptote; the nearly horizontal portion of each curve above ~700 °C corresponds to that curve's high-temperature asymptote; and the steep sigmoidal interval in between corresponds to the reaction interval. Sample F-41a is Globe-type clinochrysotile, from Currant Creek, Nevada, USA (Faust and Fahey, 1962, fig. 26). Sample F-69 is chrysotile and some lizardite(?), from Webster, North Carolina, USA (Faust and Fahey, 1962, fig. 25).

contain very little. Many CM1s contain no tochilinite at all (as summarized by Zolensky et al. 1997).

Discrete Fe-rich tochilinite has a calculated upper stability limit of approximately 120 °C under reducing conditions (Zolensky et al. [1997] and references therein) and has broken down completely in Murchison experimentally heated to ~300 °C (Tonui et al. 2014). CMs clasts in the complex breccia Kaidun all lack tochilinite, which led Zolensky and Ivanov (2003) to suggest that an upper thermal stability limit for tochilinite of ~350 °C was exceeded. Persistence of tochilinite in a CM chondrite is interpreted to indicate that that chondrite was not heated above the upper thermal stability limit of tochilinite. Above this (not especially well-constrained) temperature, tochilinite would have been converted to troilite or pyrrhotite (Zolensky et al. 1997; Zolensky and Ivanov 2003; Tonui et al. 2014).

Carbonates, Sulfides, and Sulfates

Minor amounts of carbonates, sulfides, and sulfates occur in CM chondrites (Howard et al. 2015). Carbonates

and sulfides (mostly pyrrhotite and pentlandite; Howard et al. 2009) constitute, respectively, <4.5 (mean 2.3) and <5.5 (mean 2.1) modal % of most CM chondrites (Howard et al. 2015), on average less than 8% combined of the modal abundance of serpentine group minerals.

Thermal decomposition (decarbonation) of calcite occurs very near and above 700 °C (Bish and Duffy 1990; Beck et al. 2014; Garenne et al. 2014; King et al. 2015a, 2019a, 2019b). This is near the high end of the temperature range considered in the study. Given that the modal abundance of carbonate minerals in CM chondrites is no greater than 8% and usually <4% that of serpentine (Howard et al. 2015), the contribution of carbonate mineral thermal decarbonation is only a small fraction of the mass lost by thermal devolatilization of CM matrix and even then only at or beyond the highest temperatures of interest here.

Similarly, thermal dehydration (sensu stricto) of hydrous Ca- and Mg-sulfates occurs over a temperature range of 0–350 °C (Bish and Duffy 1990; Vaniman et al. 2004; Vaniman and Chipera 2006), below the

temperature range of interest to this study. Some CM chondrites contain a few modal % sulfate (Howard et al. 2015), but these sulfates are products of terrestrial oxidation of meteoritic sulfides (Gounelle and Zolensky 2001; Losiak and Velbel 2011; Velbel and Palmer 2011).

Synthetic pyrrhotite and pentlandite of 45–75 μm particle size lose mass upon heating through the 500–800 °C range in an oxygenated (terrestrial air) furnace atmosphere (Dunn and Mackey 1991). In nitrogen (inert) furnace atmosphere, synthetic pyrrhotites ranging in composition from $Fe_{0.83}S$ to $Fe_{1.00}S$ and grain sizes between 45 and 125 μm have decomposition temperatures of 500–700 °C and lose only 1–3% of their mass by 800 °C (Dunn and Chamberlin 1991; Garenne et al. [2014] indicate a slightly lower temperature range of 400–650 °C). If all 5.5 modal% CM sulfide (the maximum reported by Howard et al. 2015) were decomposed by natural heating in an inert (not oxidizing) medium in the same manner as synthetic pyrrhotite in an inert atmosphere, mass loss from CM sulfides would be a fraction of a weight percent of the bulk CM or its matrix. Pentlandite decomposes to other phases at 610 °C in an inert (nitrogen) atmosphere without mass loss and loses only ~1 wt% from 800 to 1000 °C (Dunn 1997), entirely above the temperature range of concern to this study.

In summary, and in agreement with Garenne et al. (2014) and King et al. (2015a, 2019b), most weight loss from heating CM matrix other than weight loss from thermal dehydroxylation of serpentine group phyllosilicates—including loss of sorbed molecular H_2O ($H_2O(-)$) and dehydration ($H_2O(+)$) of non-silicate minerals—occurs outside the ~400 to ~750 °C temperature range of serpentine dehydroxylation. Weight losses with increasing temperature due to dehydroxylation of hydroxides (possibly including the hydroxide layers in tochilinite and TCI) and oxyhydroxides, hydrous sulfate mineral thermal decomposition, thermal decomposition of CM-relevant sulfides, and carbonate mineral thermal decarbonation occur mainly outside of, or are only a small fraction of, the weight lost by thermal devolatilization of serpentine-dominated CM matrix over the ~400 to ~750 °C temperature range of interest here (corresponding to upper Stage II to Stage IV of Nakamura 2005). Consequently, the minor contributions from non-phyllosilicate minerals to cumulative thermal weight loss from CM matrix are not considered further in this study.

Matrix Analytical Totals by Electron Probe Microanalysis (Matrix EPMAΣ) Vary with Temperature

A quantitative measurable compositional change known to result from thermal metamorphism of CM lithologies is the shortfall of analytical matrix EPMA totals that results mainly from matrix EPMA not analyzing the H and assigning associated O in any phyllosilicate's OH group (Reed 1996). Other contributors to low EPMA analytical totals for CC matrix include the presence in the analyzed volume of other volatile matrix species not measurable by EPMA (e.g., C-bearing) and matrix microporosity of any origin (e.g., Matsuoka et al. 1996; Reed 1996; Patzek et al. 2018).

Matrices in most CM falls, and many finds, consist mainly of serpentine group minerals (Howard et al. 2009, 2011, 2015), especially serpentine–greenalite and serpentine–cronstedtite solid solutions (Velbel 2014). "Anhydrous" wet-chemical analyses (analysis minus wt% H_2O; $H_2O = H_2O[+] + H_2O[-]$) of serpentine-group minerals fall within the ~83–89 wt% range (Deer et al. 1962). If CM matrix were all (non-porous) serpentine, and no volatiles other than H were present, then the anhydrous totals from wet-chemical analyses (in wt%) would equal 100 minus (wt% $H_2O[+]$ + wt% $H_2O[-]$). All wet-chemical analyses of (non-ATCC) CM2 falls and finds shown in Table 2 fall within the ~83–89 wt% range for high-quality analyses of terrestrial serpentine (Deer et al. 1962).

EPMA does not detect H and does not assign any O to the undetected H when cations are reported as oxides; this is why the O associated with H as OH or $H_2O(+)$ is excluded from the oxygen number used in calculating mineral stoichiometric and structural formulae of "hydrous" minerals (Reed 1996). The resulting EPMAΣs for CM matrices yield values conceptually identical with the anhydrous portion of wet-chemical analyses (i.o.w., the sums of all oxides of analyzed major elements except sorbed water $H_2O[-]$ and bound or "structural" water $H_2O[+]$; Table 2). EPMAΣ analytical totals of ~83–89 wt% for CM matrices (e.g., Zolensky et al. 1993) indicate that those CM chondrites experienced little or no thermal metamorphism above ~300–400 °C (e.g., Tonui et al. 2014) (Table 1).

CM chondrites that were aqueously altered but not further heated and therefore have CM volatile abundances that include OH have matrix EPMAΣ between 77.4 and ~90 wt% (Zolensky et al. 1993), encompassing the ~83–89 wt% range of serpentine-group minerals (Deer et al. 1962; Faust and Fahey 1962). EPMAΣs < 83% are reported (e.g., McSween and Richardson 1977; Zolensky et al. 1993) and are likely due to microporosity (e.g., Matsuoka et al. 1996); EPMA matrix analyses with totals <83% are therefore excluded from this study.

Recent CM matrix EPMAΣ means accompanied by measures of variance mostly fall within the same range (Table 3). NWA 11024, the first possible CM3 (Ebert et al. 2019), experienced less aqueous alteration than previously characterized CM2s, and partial thermal dehydration; this meteorite, the only ATCC shown in

Table 2. Comparison of analyzed wt% H_2O = $H_2O(+)$ + $H_2O(-)$ with EPMA analytical totals for matrix from several CM2 chondrites.

Meteorite	$H_2O(+)$	$H_2O(-)$	H_2O_{tot}	$100 - H_2O_{tot}$	Matrix EPMAΣ
Murchison matrix 1	10.08	2.37	12.45	87.55	86.04[a]
Murchison matrix 2	11.61	2.61	14.22	85.78	85.43[b]
Cold Bokkeveld			15.17[c]	84.83	84.98[b]
Murray	9.98[c]	2.44[c]	12.42[c]	87.58	85.89[a]
Mighei			12.86[c]	87.14	83.19[a]
Nogoya	10.85[c]	3.43[c]	14.28[c]	85.72	83.39[a]
Y-791198	12.81[d]	2.85[d]	15.66[d]	84.34	88.30[a]
ALH 83100	12.05	1.33	13.38	86.62	87.91[a]
ALH 83102	11.01	1.93	12.94	87.06	n.a.
Y-791824	10.28	2.22	12.50	87.50	n.a.

Wet-chemical analysis data compiled by Jarosewich (1990) except as noted.

n.a. = no EPMA matrix analysis available; wet-chemical analysis shown to illustrate that entries higher in this table are representative of wet chemical analyses from CM2 chondrites.

[a]Zolensky et al. (1993); this analysis is not of the same sample as the wet-chemical analysis.

[b]McSween and Richardson (1977); this analysis is not of the same sample as the wet-chemical analysis.

[c]Wiik (1956); this analysis is not of the same sample as the EPMA analysis.

[d]Haramura et al. (1983).

Table 3, is included here for the documented variance of its matrix EPMAΣ. The two least-aqueously altered non-ATCC CM chondrites presently known, Paris and EET 96029, contain lithologies classified as CM 2.7–2.9 using the Rubin et al. (2007) classification; all their mean matrix EPMA totals fall within or near the low end of the range for ideal serpentine (Table 3). Mean matrix EPMA totals for Paris from three different research groups are all within ~2 wt% of one another (Table 3). Matrix EPMA totals for EET 96029 fall within the range of means reported for Paris. It is assumed here that all "normal" (not C2, C2-anomalous, C2-unique, C2-ungrouped, or subsequently thermally metamorphosed ATCC) CM chondrite matrices ended their aqueous alteration episode, and began any post-aqueous alteration (additional) heating, with the OH inventory and corresponding "anhydrous" analytical totals of serpentine (Deer et al. 1962), the dominant mineral group in CM matrix (Howard et al. 2009, 2011, 2015). Values below ~83 wt% likely (as noted above) represent analyses in which factors other than serpentine's OH (specimen microporosity and/or other volatile matrix species such as those containing C) contributed to low EPMA totals. EPMA totals above ~89 wt% in serpentine-bearing CM matrix indicate either dehydroxylation of serpentine (to, e.g., olivine, directly or by way of a disordered intermediate; Akai 1988, 1990, 1992) or the presence within the analyzed volume of primary anhydrous (OH and H_2O-free) minerals (metal, sulfide, silicate). Discrete metal and sulfide minerals with their very high atomic number (Z-)contrast in backscattered scanning electron microscope images are easily avoided during selection of spots for EPMA analyses of matrix.

EPMA totals of ~83–89 wt% for CM chondrite matrices (e.g., Zolensky et al. 1993) indicate that they experienced little or no thermal metamorphism above ~300–400 °C (e.g., Tonui et al. 2014). On this basis, a CM matrix EPMAΣ total of ~87 wt% is chosen as the threshold value between (possibly microporous) CM matrices that were altered only by aqueous solutions to varying degrees and CMs that were subsequently thermally altered (ATCCs) under open-system conditions in which dehydroxylated H and O were lost from the analyzed volume as $H_2O(+)$.

Natural terrestrial serpentine-group minerals dehydroxylate and lose weight during TGA, with most of the weight loss occurring between 400 and 700 °C (e.g., Faust and Fahey 1962; Fig. 1 herein). Dehydroxylation weight losses of a few percent (indicated by CM matrix EPMAΣ of ~91–93 wt%) occur gradually over a range of temperatures from ~200 °C up to $T \approx$ ~550–680 °C (~470 to ~820–950 K; e.g., Faust and Fahey 1962) and correspond to the low-temperature TGA asymptote and the steep part of the asymptote that is transitional to the reaction interval as defined by Bish and Duffy (1990). Thermally metamorphosed CM2s that contain evidence of heating to maximum temperatures of 400–750 °C (~670–1020 K) have partially dehydroxylated matrices, yielding matrix EPMAΣ above ~91 wt% (Zolensky et al. 1993; Tonui et al. 2014) (Table 1); recent TGA studies of CM chondrites ascribe weight loss between 400 and 770 °C to dehydroxylation of phyllosilicates (Garenne et al. 2014; King et al. 2019b). More extensive dehydroxylation weight losses (indicated by matrix EPMAΣ ~94 to >99 wt%) commonly occur over (and DTA curves exhibit a deep minimum just above) a much narrower range of $T \approx$ ~550–730 °C (~820–1000 K); this interval is referred to as the reaction interval (Bish and Duffy 1990). The TGA "plateau" at temperatures above the reaction interval is the high-temperature ($T >$ ~730 °C) asymptote (Bish and Duffy 1990).

Bracketing T_Peak Between the Upper Thermal Limit of Tochilinite Persistence and the Onset Temperature of Serpentine Dehydroxylation

Y-791198 (Metzler et al. 1992; CM2.4 in the Rubin et al. [2007] classification) and ALH 81002 (CM2) have matrix EPMA analytical totals of 88.30 wt% and 77.4 wt%,

Table 3. Mean and variation of EPMA analytical totals in matrices from recently reported CM chondrites including the least aqueously altered CMs presently known.

Meteorite	Petrologic CM subtype[a]	Matrix EPMA total (wt%) mean	s.d.	n	Reference
NWA 11024	3[b]	92.9	4.1	72	Ebert et al. (2019)
Paris	2.9	84.95	2.43	20	Hewins et al. (2014)
Paris	2.7	83.48	2.36	8	Calculated from Marrocchi et al. (2014)
Paris	2.7 – 2.9	82.91	n.r.	10	Rubin (2015) oxides as cited and correctly summed by Lee et al. (2016)
EET 96029	2.7, 1.6[c]	83.55	3.32	28	Lee et al. (2016) and Alexander et al. (2013), respectively
Jbilet Winselwan	2.7 - <2.3	82.3	4.0	58	King et al. (2019b) JW-1-A
Jbilet Winselwan	2.7 - <2.3	83.5	3.1	73	King et al. (2019b) JW-1-E
Sutter's Mill SM51-1	2.1 – 2.0	87.1	0.9	4	Jenniskens et al. (2012)
LAP 02277	1.4[c]	86.3	3.1	187	Alexander et al. (2013); King et al. (2019b)

From the top downward, meteorites are listed in order of increasing aqueous alteration (decreasing Rubin et al. [2007] petrologic subtype).
[a]Petrologic subtype of Rubin et al. (2007) as assigned by the paper listed in the Reference column, except as otherwise noted.
[b]Petrologic type of Van Schmus and Wood (1967) as assigned by the paper(s) listed in the Reference column.
[c]Petrologic subtype of Alexander et al. (2013) as assigned by Alexander et al. (2013) their table 2.

respectively (Zolensky et al. 1993), and abundant tochilinite is preserved in their fine-grained rims (Lauretta et al. 2000; Chizmadia and Brearley 2008, respectively). Carbonaceous clasts in Kapoeta (howardite; $EPMA\Sigma$ = 88.66 wt%) contain tochilinite; a similar clast in Jodzie (howardite; $EPMA\Sigma$ = 86.25 wt%) contains minor tochilinite and TCI (Zolensky et al. 1996a). These relationships are consistent with lack of dehydroxylation in Nakamura's (2005) CM2TI stage and a T_{peak} < 250–350 (~300 ± 50) °C.

Sutter's Mill is a unique regolith breccia with some lithologies separated from others as individual stones during breakup in Earth's atmosphere (Zolensky et al. 2014) consisting mainly of diverse CM carbonaceous chondrite lithologies spanning a range of matrix dehydroxylation (Table 4). Reported matrix EPMA totals are 87.1 wt% in lithologies classified as CM2.1 and CM2.0 on the scale of Rubin et al. (2007; sample SM51-1 from stone 51; Jenniskens et al. 2012) and 97.17 wt% in a thermally metamorphosed clast (from stone SM2; Zolensky et al. 2014). Sutter's Mill CM2.1 and CM2.0 clasts (e.g., SM51-1; EPMA totals of 87.1 wt%) contain tochilinite and TCI. The persistence of tochilinite (Tonui et al. 2014) and TCI indicates that these clasts were not heated above ~300 ± 50 °C (~570 ± 50 K). This inferred peak temperature limit is consistent with the temperatures that various aqueously altered (but not further heated) Sutter's Mill lithologies reached as estimated using other methods (Jenniskens et al. 2012), including thermoluminescence (300 ± 20 °C), and Raman spectroscopy of macromolecular carbon in two samples (153 ± 27 °C and 268 ± 42 °C). These Sutter's Mill measurements also overlap the <250–350 (~300 ± 50) °C "consensus" upper thermal limit for TCI

inferred from the meteorites discussed in the previous paragraph.

The persistence of discrete or interstratified tochilinite in Y-791198, ALH 81002, carbonaceous clasts in Kapoeta and Jodzie, and especially Sutter's Mill sample SM2 (for which independent T_{peak} determinations exist) indicates that they were not heated above tochilinite's upper stability limit (~300 °C; Tonui et al. 2014). On this basis, the highest of their $EPMA\Sigma$'s (~89 wt%) anchors T_{peak} as <~300 ± 50 °C.

Matrix in CM2 clast N in EET 87513 (howardite; matrix $EPMA\Sigma$ = 92.2 wt%) exhibits corrugated matrix-serpentine lattice fringes in TEM and contains tochilinite and TCI (Buchanan et al. 1993). A carbonaceous chondrite clast in the G-Day (Mundrabilla 020) howardite (matrix $EPMA\Sigma$ = 90.67 wt%) contains sparse discrete tochilinite and TCI (Zolensky et al. 1996a). This suggests that matrix dehydroxylation to an $EPMA\Sigma$ of ~91–92 wt% can occur without exceeding tochilinite's upper thermal stability threshold. Alternatively, it may reflect kinetic constraints on the thermal decomposition of tochilinite or mixing of heated and aqueously altered (but not further heated) fine-grained matrix materials after peak heating.

The thermally metamorphosed CM lithology in Sutter's Mill sample SM2 ($EPMA\Sigma$ = 97.17 wt%) lacks tochilinite and has other attributes assigning it to Nakamura's (2005) Stage III, indicating it was heated above the upper thermal stability limit for tochilinite (possibly as high as 500–700 °C; Zolensky et al. 2014).

The upper bound of aqueous alteration that forms hydroxyl-bearing (serpentine-group) minerals in CM chondrites is ~35–120 °C (~300–390 K). The lower end of the temperature range over which thermal

Table 4. Compositional properties and estimated peak metamorphic temperature of thermally altered CM chondrites (including CM clasts in HEDs and lunar breccia, and the CM-like Belgica subgroup).

Meteorite	Classification[a]	Matrix EPMAΣ (wt%)[a]	$T_{\text{peak metamorphism}}$ (± <80 °C) from matrix EPMAΣ	$T_{\text{peak metamorphism}}$ (±100 °C) from matrix EPMAΣ (1 sign. figure ± 200 °C)
ATCCs				
Plainview	CM clast	99.8[d]	800	800
Y-86789	CY[b]/CM2TIV	98.7[e]	**760**	**800**
Y-86720	CY[b]/CM-like Bg[b]TIV	98.66[f]	**750**	**800**
A-881655	CM2TIII	98.17[g]	**730**	**700**
PCA 91008	CM2TIII	97.3	**690**	**700**
Sutter's Mill SM2	CM heated	97.17[h]	690	700
Y-82162	CY[b]/CI1TII/III	96.6	**660**	**700**
Y-86720	CY[b]/CM-like Bg[b]TIV	96.54[i]	*660*	*700*
LEW 87295	CM2(unusual) clast	96.45[j]	660	700
Y-86029	CY[b] / CI1TIII	95.5[k]	**610**	**600**
Y-86029	CY[b]/CI1TIII	95.0	**590**	**600**
WIS 91600	CM-like Bg[b]TII	94.4	*560*	*600*
Bench Crater	CM1 clast	94.29[j]	560	600
Y-82162	CY[b]/CI1TII/III	94.21[l]	**560**	**600**
Y-86720	CY[b]/CM-like Bg[b]TIV	93.43[l]	*520*	*500*
B-7904	CY[b]/CM-like Bg[b]TIV	93.07[m]	*510*	*500*
NWA 11024	CM3?	92.9[n]	500	500
EET 87513	CM2 clast	92.2[o]	470	500
Y-793497	C unclassified microclast	91.95[p]	460	500
Y-86029	CY[b]/CI1TIII	91.9[k]	*450*	*500*
Y-793321	CM2TII	91.8	**450**	**400**
B-7904	CY[b]/CM-like Bg[b]TIV	91.48[k]	*440*	*400*
G'Day	CM2 clast	90.67[j]	400	400
B-7904	CY[b]/CM-like Bg[b]TIV	89.7[q]	*360*	*400*
Y-793321	CM2TII	89.03[j]	**330**	**300**
Aqueous alteration without subsequent additional heat				
Y-791198	CM2	88.3[j]	300	300
Sutter's Mill SM51-1	CM unheated	87.1[r]	240	200
LAP 02277	CM1	86.3[s]	210	200
	CM[c]	84–88	<300	<300

Arranged downward from most to least dehydroxylated. Meteorites for which multiple published matrix analyses exist are listed as many times as there are published analyses. **Boldface** T_{peak} values fall **within** the range of the Nakamura (2005) stage to which the meteorite was assigned by Tonui et al. (2014). *Italicized* T_{peak} values fall *outside* the range of the Nakamura (2005) stage to which the meteorite was assigned by Tonui et al. (2014). *All that fall outside are in the CM-like Belgica subgroup.*

[a]From Tonui et al. (2014) unless otherwise credited.

[b]CY from Ikeda (1992) and King et al. (2019a), CM-like Bg = Belgica grouplet (Choe et al. 2010).

[c]From Zolensky et al. (1993) and including aqueously altered (but not further heated) CM clasts in Kaidun, Kapoeta, and Jodzie, from Zolensky et al. (1996a, 1996b) and Buchanan et al. (1993).

[d]From Rubin and Bottke (2009) their table 3.

[e]From Matsuoka et al. (1996).

[f]From Ikeda et al. (1992) their table 2 highest matrix EPMAΣ is analysis 523; Y-86720 is a breccia with multiple types of clasts of matrix-like lithologies.

[g]Desiccated high Al, Mg serpentine from matrix (Lipschutz et al. 1999).

[h]From Zolensky et al. (2014).

[i]TEM EDX analysis of matrix serpentine, with several minor elements not determined; from Lipschutz et al. (1999) their table 2.

[j]From Zolensky et al. (1996b).

[k]From Tonui et al. (2003).

[l]From Zolensky et al. (1993).

[m]From Kimura and Ikeda (1992) their table 3b highest matrix EPMAΣ; B-7904 is a breccia with multiple types of clasts of matrix-like lithologies.

[n]From Ebert et al. (2019).

[o]From Buchanan et al. (1993).

[p]From Gounelle et al. (2003) their table 2.

[q]From Tomeoka (1990) their table 4 analysis 3.

[r]From Jenniskens et al. (2012).

[s]From King et al. (2019a).

dehydroxylation of CM matrix has been demonstrated (lower limit of Stage II of Nakamura 2005) is ~250–400 °C (~520–670 K). Between aqueous alteration and dehydroxylation of hydroxyl-bearing products of aqueous alteration is Nakamura's (2005) Stage I (~120 °C < T_{peak} < ~250–300 °C); the range of Stage I temperatures is not amenable to measurement by the EPMAΣ measure of dehydroxylation. Phenomena below ~250 °C are deemed to be mostly outside the scope of this article.[6]

Thermal Stability of Organics and the Effects of Heating

Insoluble Organic Matter (IOM)

Temperatures of chondrite parent body thermal metamorphism have been estimated from Raman and carbon-XANES measurements of the meteoritic insoluble organic matter (IOM) of a variety of chondrites, including CM, CI, and C2-ungr. Temperatures estimated from various spectroscopies of IOM in CM chondrites that experienced only aqueous alteration vary among laboratories by more than 300 °C. For example, for Murchison, Raman spectroscopy yielded estimates of <220 °C (Busemann et al. 2007), 309.2 ± 6.3 °C for matrix IOM (Chan et al. 2017), 60 °C using an equation for long-duration geological maturation of OM and 222 °C using an equation for rapid carbonization of OM (Schmidt and Hinrichs 2020), four values using an equation for long-duration geological maturation of OM ranging from 396 ± 47 to 443 ± 51 °C (Kiryu et al. 2020), and carbon-XANES measurements yielded 96 ± 65 °C (Cody et al. 2008). Similarly, for Nogoya, Raman spectroscopy yielded estimates of 291.7 ± 15.2 °C for matrix IOM (Chan et al. 2017), 77 °C using an equation for long-duration geological maturation of OM, and 260 °C using an equation for rapid carbonization of OM (Schmidt and Hinrichs 2020).

Many workers observe that T estimated from Raman spectroscopy of IOM in chondrites in general (e.g., Cody et al. 2008; Schmidt and Hinrichs 2020) and ATCC chondrites in particular (e.g., Quirico et al. 2014; Schmidt and Hinrichs 2020) are significantly (up to ~600 °C) lower than those estimated from mineralogical and textural parameters. For example, for Y-86720 (metamorphism stage IV of Nakamura [2005], >750 °C), Raman spectroscopy yielded estimates of <230 °C (Busemann et al. 2007), 70 °C using an equation for long-duration geological maturation of OM and 245 °C using an equation for rapid carbonization of OM (Schmidt and Hinrichs 2020), 496 ± 55 °C using an equation for long-duration geological maturation of OM (Kiryu et al. 2020), and carbon-XANES measurements yielded 265 ± 42 °C (Cody et al. 2008). Similarly, for WIS 91600 (metamorphism stage II of Nakamura [2005], 300–500 °C),

Raman spectroscopy yielded estimates of 362.2 ± 49.8 °C for matrix IOM (Chan et al. 2017), 67 °C using an equation for long-duration geological maturation of OM, and 277 °C using an equation for rapid carbonization of OM (Schmidt and Hinrichs 2020). Such differences are attributed to differences between the kinetics of IOM and mineral responses to the temperatures and durations of heating events, with mineral-textural indicators responding much more rapidly to short, rapid heating events such as impacts (e.g., Cody et al. [2008]; Quirico et al. [2014] and references therein; Schmidt and Hinrichs 2020).

Some spectroscopic measurements and their corresponding cosmothermometer equations provide peak temperature estimates for organics that are below the ~250–300 °C threshold for serpentine dehydroxylation and the EPMA dehydroxylation peak temperature thermometer proposed below; other measurement-equation couples yield values in the serpentine dehydroxylation range (>300 °C).

Solute Extractable OM: Amino Acids

Amino acid abundances in Sutter's Mill stone SM2—the most highly metamorphosed sample of the heterogenous Sutter's Mill shower fall for which such data have been reported to date—are at least a factor of 20-fold lower than amino acid abundances in the Murchison meteorite (Burton et al. 2014). This is consistent with a higher temperature of metamorphism on the SM2 ancestral body prior to SM2's incorporation into the heterogenous Sutter's Mill meteoroid (Burton et al. 2014). A recent experimental study by Weiss et al. (2018) found significant thermal decomposition of amino acids in the 200–300 °C range which is consistent with the previous temperature estimates of all but the least metamorphosed fragments (from stone 51) of Sutter's Mill.

MATERIALS AND METHODS

This study (Table 4) compiles published data from more than 20 ATCC CM chondrites and CM clasts in breccias. These include more than a dozen previously studied whole meteorites containing evidence of post-aqueous alteration heating (e.g., Akai 1988, 1990, 1992; Tonui et al. 2002, 2003, 2014; Nakamura 2005), most of which are finds, and which have been previously interpreted to have been heated above ~400 °C (Table 1). Also considered (Table 4) is the subset of CM carbonaceous chondrite lithologies that show similar thermal effects and occur as clasts in polymict breccias, including howardites (Buchanan et al. 1993; Zolensky et al. 1996a), polymict eucrites (Zolensky et al. 1992, 1996a), more complex polymict breccias (e.g., Kaidun; Zolensky et al. 1996b), and lunar regolith (Bench Crater; Zolensky et al. 1996a). Data from CM clasts that do not

exhibit heating after aqueous alteration were also compiled (above) but are not shown in Table 4. In order to investigate specifically the hypothesis of insolation heating, data from two CM chondrite falls (Maribo and Sutter's Mill) with known present-epoch orbital elements are also examined (below).

Except for a few instances where only defocused beam EPMA data or TEM EDS data were available, most matrix analyses selected for this study are individual spot analyses or averages of multiple spot analyses, all acquired in the same manner. For CM chondrites from which matrix in the same meteorite has been analyzed by both averages of spot analyses and defocused beam EPMA, the analytical totals from defocused beam analyses are in all instances lower (in several instances as low as ~71–72 wt%, i.e., ~12–13 wt% lower) than the averaged spot analyses. Likely reasons are that, in addition to materials containing H (in OH) with too low an atomic number to generate characteristic X-ray signals, defocused beams will interact with (1) materials containing other minor elements too low in atomic number to generate characteristic X-ray signals (e.g., C), and (2) microporosity in the matrix, which will also not produce an X-ray signal (Matsuoka et al. 1996; Reed 1996; Patzek et al. 2018).

Many (generally older) papers about aqueously altered CM chondrites that did not experience post-aqueous alteration heating to higher temperatures report the number of spots analyzed and averaged (typically 10–40, averaging 25), and some plot bar charts showing the distribution of selected elements in individual analyses, but do not provide individual analyses, ranges, or measures of variance (e.g., standard deviations). Some more recent papers about aqueously altered CM chondrites that did not experience post-aqueous alteration heating to higher temperatures report means and standard deviations; studies reporting averaged EPMA totals within the range of interest of this study (~82–88 wt%; Jenniskens et al. 2012; Hewins et al. 2014; Lee et al. 2016; King et al. 2019b) yielded standard deviations of ~1–4 wt% (Table 3). One recent paper about an ATCC (NWA 11024; Ebert et al. 2019) reported EPMA data from which mean matrix composition and a standard deviation of 4.1 wt% could be calculated. Garenne et al. (2014) performed replicate TGA analyses of LAP 02336 (CM2) as a test of specimen homogeneity, yielding an average total weight loss of 15.1 ± 1.1 wt% ($n = 6$); assuming that analytical totals for the entire specimen summed to 100 wt%, the TGA results would correspond to EPMAΣ = 84.9 ± 1.1 wt%. This mean and standard deviation fall within the range of EPMAΣ determinations compiled in Table 3.

Interlaboratory variation is similar; where matrix in the same meteorite has been analyzed by two or more research groups by the averaging of spot analyses approach (and, in a few cases, by the defocused-beam approach) average matrix totals differ by no more than ~1–2 wt% (Table 3). This also suggests that (1) CM matrix compositions are generally homogenous within a few wt% among different matrix specimens of individual CMs, and (2) differences of means greater than ~3–4 wt% are significant.

Reported standard deviations of CM chondrite matrix EPMA totals are proportional to the number of spots analyzed (n in Table 3) for $n \leq$ ~30; for $n >$ 30, all standard deviations are ~3–4 wt% (Table 3). For this study, the largest standard deviations of analyses (±4.0–4.1 wt%) are the basis for the estimation uncertainty range of the resulting inferred temperatures discussed below and reported in Table 4. For these reasons, the averaged spot measurements are all regarded here as being intercomparable *for the purposes of this study*. For future application of the peak temperature thermometer proposed below, a preconsidered regimen of factors including EPMA operating conditions, sample area examined, and number of spots analyzed will need to be uniformly applied to future analyses of meteorites and mission-returned samples to ensure intercomparability among analyses and inferences (including estimated peak metamorphic temperatures) drawn from the measurements.

A Dehydroxylation Peak-Temperature Thermometer

Based on the preceding sections, with some additional explanation below, the assumptions underlying this approach are (re-)stated here:

- *CM chondrite matrices ended their aqueous alteration episode, and began any post-aqueous alteration (additional) heating, with the OH inventory and corresponding "anhydrous" analytical totals of serpentine (~83–89 wt%), the dominant mineral group in CM matrix.* In most non-ATCC CMs, matrix is dominated by phyllosilicates. All "normal" (not C2, C2-anomalous, C2-unique, C2-ungrouped, or subsequently thermally metamorphosed ATCC) CM chondrites in which the matrix is not dominated by phyllosilicates are ATCCs, all of which contain textural evidence that the matrix anhydrous silicates formed by dehydroxylation of matrix phyllosilicates (references above to early recognized CY group and Belgica subgroup ATCCs; and NWA 11024 per Ebert et al. 2019). Until a phyllosilicate-free O-isotopically CM chondrite with no ATCC textures (e.g., pseudomorphism of anhydrous after hydroxylated minerals) is recognized and characterized, the very existence, let alone the nature and significance of,

such a not-yet-observed CM chondrite is only speculative, and in that way is beyond the scope of this paper. This paper begins in parts of parameter space where extant samples are—numerous CM chondrites with phyllosilicate-dominated matrices, and a growing number of recognized ATCC CMs with textural evidence that anhydrous silicates formed pseudomorphically after familiar textures and habits of hydroxylated CM matrix minerals.

- *Contributions to EPMAΣ from non-phyllosilicate (e.g., anhydrous) minerals to cumulative thermal weight loss, and non-contributions from microporosity and host phases of other light elements, in CM matrix are too small over the T range of interest (~400–750 °C)* relative to both (1) the weight loss attributable to dehydroxylation of matrix serpentine and (2) the measurement variance, *to require further specific consideration in this study.*
- *Matrices efficiently lose all their water upon heating.* This assumption is consistent with the small particle sizes of CM matrix (e.g., Scott et al. 1988), and the short timescales for experimental dehydroxylation (e.g., Akai 1992).
- As noted above, TGA (devolatilization weight loss) curves are generally sigmoidal but are commonly quantified as line segments; the slope of the reaction interval is used here to infer T from EPMAΣ. *The representativeness of a straight-line approximation* to diverse observed sigmoids from published TGA plots for serpentine and the associated range of estimation error are discussed shortly after the introduction of Equation 1 immediately below.

Proposed Dehydroxylation Peak-Temperature Thermometer

A preliminary equation for inferring T from EPMAΣ over the previously estimated range 400 °C $< T_{peak} <$ 750 °C (mainly from the breadth and slope of the reaction interval) is

$$T_{peak}(^{\circ}C) \approx 240 + (44 \times (\text{matrix EPMA}\Sigma(\text{wt\%}) - 87\,\text{wt\%}))$$
$$T_{peak}(K) \approx 510 + (44 \times (\text{matrix EPMA}\Sigma(\text{wt\%}) - 87\,\text{wt\%})).$$
$$(1)$$

Coefficients are selected so that the equation recovers (1) the mean of the three T_{peak} measurements from Sutter's Mill sample SM51-1 (~240 °C; Jenniskens et al. 2012); and (2) a $T >$ 750 °C for Y-86789 (CM2TIV), as estimated by Tonui et al. (2014). Estimated T_{peaks} (using Equation 1) for Y-791198 (Table 4) and Kaidun CM1 (88.56 wt%; Zolensky et al. 1992), with EPMAs near 89 wt% and the presence of tochilinite, are just under the ~300 (±75) °C upper thermal stability limit for

tochilinite persistence. This suggests that the equation and coefficients used yield values consistent with observations even somewhat below the temperature range of intended application.

Estimation errors for Equation 1 are on the order of ±75 °C (±75 K). The more broad the sigmoid of the TG curve (e.g., sample F-69 in Fig. 1), the more closely the linear approximation will conform to the TG curve. The steeper the sigmoid (the narrower the T range over which most dehydroxylation occurs; e.g., sample F-41a in Fig. 1), the greater the deviation of the linear approximation from the actual curve. In the latter cases, the linear equation will overestimate T_{peak} by up to ~75 °C at Ts between the sigmoid's midpoint and the high-T asymptote, and will underestimate T_{peak} by up to ~75 °C at Ts between the sigmoid's midpoint and the low-T asymptote. The linear equation yields estimates much closer to the actual TG curve near the transitions to the asymptotes (because the coefficients were chosen to anchor the line representing the reaction interval to previously observed EPMAΣ-temperature pair values at the transition points), and near the midpoint of the sigmoid. Similarly, the projection of the linear trend to below 400 °C (and below the low-temperature asymptote) yields estimates closer to the TG curve (smaller estimation error) near the transition between the low-T asymptote and the reaction interval, and progressively farther (larger estimation error) at progressively lower T. The total range of the deviation between any actual sigmoidal TG curve and Ts estimated by Equation 1 within the reaction interval (variance range = 150 °C) is the same as (1) the range in absolute temperatures determined from SAED patterns and textures in TEM images of the products of experimental heating of Murchison (CM2) (~150 °C; Akai 1990, 1992; see above) and (2) the range of temperatures inferred for various aqueously altered (but not further heated) Sutter's Mill lithologies estimated using thermoluminescence and Raman spectroscopy (~150 °C; Jenniskens et al. 2012; see above), and less than the estimation error (2σ) for thermometry using Raman spectroscopic parameters Γ_G and Γ_D, ±118–120 °C (~240 °C, Cody et al. 2008). This linear relationship (Equation 1) between ~400 and 750 °C is used to estimate T_{peak} in Tables 1 and 4.

Given that (1) the linear approximation of the TGA reaction interval (Equation 1 herein), (2) variations in time–temperature relations for experimental heating of reference samples (Akai 1990, 1992), and (3) multiple measurements of similar materials by several methods in Sutter's Mill (Jenniskens et al. 2012) all have a similar ~150 °C range of inferred Ts, a variance of ±75 °C is assumed for T_{peak} values estimated from a specific value of EPMAΣ using Equation 1. This is conservative; TGA

curves for powdered CM and CI chondrites are commonly nearly linear over the temperature range of serpentine dehydroxylation (e.g., Garenne et al. 2014; King et al. 2015a).

Tonui et al. (2014) examined data for 10 ATCCs (mostly CMs and a few CIs) and ranked them from least to most thermally metamorphosed, based on several observational attributes including matrix EPMAΣ. Table 1 lists the nine for which EPMA data were available (thus excluding only EET 90043). Also shown in Table 1 is a specific CM that experienced only aqueous alteration without subsequent thermal metamorphism for which EPMAΣ is available (Y-791198) and the range of EPMAΣ for other CMs that experienced only aqueous alteration without subsequent thermal metamorphism (Zolensky et al. 1993). All that were considered by Tonui et al. (2014) are listed in the same order as they were ranked. Each meteorite's classification by group, petrologic type, and Nakamura (2005) stage is shown in Table 1 as they were understood at the time of the Tonui et al. (2014) study.

RESULTS

For comparison with previous T_{peak} estimates (Tonui et al. 2014), T_{peak} estimates from Equation 1 using EPMAΣ are shown in Table 1 reported to only one significant figure (nearest hundred degrees Centigrade) and to two significant figures to illustrate the basis for the rounding to one significant figure. Table 4 applies Equation 1 to the same meteorites and a number of other CM meteorites and CM clasts for which sufficient data are available (including updated group/subgroup classifications); meteorites are listed in Table 4 in order of decreasing EPMAΣ. Meteorites for which multiple published matrix analyses exist are listed as many times as there are published analyses, so there are more lines in Table 4 than the number of meteorites represented there.

Elevated EPMA totals (above the range for serpentine, EPMAΣ > ˜87–89 wt%) among the CM chondrites considered here correspond to T_{peak} up to 750 °C (Tables 1 and 4). Table 1 shows that, with only two exceptions (Belgica-7904, because it dehydroxylated from a saponite-dominated CI-like precursor, and WIS 91600, another member of the CM-like Belgica subgroup proposed by Choe et al. 2010), Equation 1 quantitatively estimates temperatures of peak metamorphism that (when rounded to one significant figure) for the most part conform to (1) the limiting T_{peak} values and ranges inferred semiquantitatively using the Nakamura (2005) stage classification and (2) the relative heating relationships (e.g., ranking by inferred T_{peak}) for the same meteorites previously

estimated semiquantitatively (to one significant figure) by other means (Akai 1988, 1990, 1992; Tonui et al. 2002, 2003, 2014; Nakamura 2005).

Carbonaceous chondrite lithologies, including specifically CM, have been documented to occur as clasts in polymict breccias, including howardites (Bunch et al. 1979; Buchanan et al. 1993; Zolensky et al. 1996a), polymict eucrites (Zolensky et al. 1992, 1996a), H chondrites (Rubin and Bottke 2009), more complex polymict breccias (e.g., Kaidun; Zolensky et al. 1996b), and lunar regolith (Bench Crater; Zolensky et al. 1996a). Matrix EPMA totals of CM2 clasts in the howardites Kapoeta (86.66 wt%; Zolensky et al. 1996a) and Jodzie (83.48 wt%, Bunch et al. 1979; and 86.25 wt%, Zolensky et al. 1996a), and CM1 in Kaidun (ungrouped polymict chondrite breccia, 88.56 wt%; Zolensky et al. 1996b), all fall in the normal range for CM not heated beyond ~400 °C (Tables 2 and 4). However, CM clasts in other howardites (Mundrabilla 020, also informally known as G'Day, 90.67 wt%, Zolensky et al. 1996a; EET 87513, 92.2 wt%, Zolensky et al. 1996a), H-chondrite regolith breccias (including Plainview clast PV3, 99.5 wt%, Rubin and Bottke 2009), and lunar breccia (Bench Crater, 94.29 wt%, Zolensky et al. 1996a) are elevated and in the range corresponding to heating to peak temperatures above 400 °C (Table 4). Similar objects interpreted as fossil micrometeorites rather than clasts have been documented from howardites and polymict eucrites (Gounelle et al. 2003; Patzek et al. 2018).

DISCUSSION

Variability and Heterogeneity—Brecciation, Heterogenous Heating

Variability among different analyses of the same meteorite in Table 4 may indicate either the replication error range of analyzed compositions if a meteorite's matrix is homogenous among all analyzed specimens of that meteorite (cf. Table 3), or heterogeneity of matrix (including variation among C-chondrite clasts consisting mainly or entirely of matrix in polymict breccias) among all analyzed specimens of that meteorite (Lentfort et al. 2021).

QUE 93005 as an Example of Heterogeneity

CM between-sample and within-sample heterogeneity (variations among different allocated splits from the same meteorite, and within single allocations) most likely results from the (micro)brecciated character of CM chondrites. CM breccias consist of different proportions of clasts of different petrologic subtypes (sensu Rubin et al. 2007) or chondrule alteration stages (sensu Endreß

and Bischoff 1993; Metzler 1995; Hanowski and Brearley 2001; Morlok et al. 2006; Velbel et al. 2012, 2015; Lentfort et al. 2021). For example, Queen Alexandra Range 93005 (hereinafter, QUE 93005) is a CM2 Antarctic find. It is a single 13.4 g stone approximately 2.5 cm in longest dimension. QUE 93005 has been previously studied for several aqueous alteration phenomena and is one of the more highly altered CM2 chondrites known (Trigo-Rodríguez et al. 2006; Rubin et al. 2007; de Leuw et al. 2009, 2010; Howard et al. 2011; Lee et al. 2012; Velbel et al. 2015). Although this meteorite is not discernibly brecciated at hand specimen scale, considerable heterogeneity of some petrographic attributes among multiple allocations have been reported. QUE 93005 contains multiple occurrences of olivine partially replaced by serpentine in allocation QUE 93005,9 examined by Rubin et al. (2007), and in one but not both fragments in the thin section allocations (QUE 93005,14–16) examined by Velbel et al. (2015; see fig. 1 therein, showing that all occurrences of olivine partially replaced by serpentine are in the larger of the two fragments). However, other workers received allocations almost completely devoid of intact olivine or olivine partially replaced by serpentine (e.g., Grossman et al. [2005], unspecified allocation(s); Lee et al. [2012, 2014]; Lindgren et al. [2015], allocation QUE 93005,10). The observed pronounced heterogeneity between different fragments in thin sections suggests that QUE 93005 is a breccia at larger-than-fragment scale that disaggregated (fragmented) mainly along clast boundaries during curatorial subdivision and preparation for thin sectioning (Velbel et al. 2015). Because of this within-stone heterogeneity, different polished thin section allocations would be assigned to different petrologic subtypes (as was done for Sutter's Mill by Jenniskens et al. 2012, their fig. 2B).

Heating of QUE 93005 was suggested by (1) Alexander et al. (2012, 2013) on the basis of bulk H, C, and N abundances and isotopic compositions and (2) Quirico et al. (2014, 2018) on the basis of Raman spectroscopic characterization of insoluble organic matter (IOM). The coexistence in QUE 93005 of volumes some of which experienced and others of which escaped such heating indicates that clast heating above ~120 °C predates the assembly of the clasts into the immediate parent object of QUE 93005 (Velbel et al. 2015). Complex natural histories of sufficient heating for aqueous alteration of silicate minerals followed by additional heating (indicated by the spectroscopy and composition of IOM), followed by another episode of hydration by "retrograde" aqueous alteration reactions (Quiricio et al. 2018) are certainly possible. However, heterogeneity of thermal and aqueous alteration and dehydroxylation phenomena in diverse individual clasts

subsequently mixed and juxtaposed (as suggested for the general case by Trigo-Rodríguez 2015; Trigo-Rodríguez et al. 2019) into in the small but subtly complex QUE 93005 breccia perhaps ought to be considered the null hypothesis that needs to be refuted before invoking more complex scenarios. The persistence of TCI in allocation QUE 93005,16 (Fig. 2) indicates no alteration at $T > 300$ °C before or after assembly of the QUE 93005 breccia (Velbel et al. 2015).

Similar heterogeneity of CM lithologies, petrologic subtypes (Lentfort et al. 2021)—and thermal metamorphism stages (e.g., Y-86029 and Sutter's Mill; Table 4)—may be expected within single fragments of returned asteroid regolith. Heterogeneity among clast lithologies in such breccias may best be described by indicating the range of petrologic subtypes as suggested by Lentfort et al. (2021). Similar heterogeneity of thermal metamorphism after aqueous alteration (TMA[3]) in ATCCs can be indicated by the range of Nakamura (2005) thermal stages.

Expectations and Exceptions: CM Versus CY/CM-like Belgica

In Table 4, **boldface** and *italicized* T_{peak} values fall, respectively, **within** and *outside* the temperature range of the Nakamura (2005) stage to which the meteorite was assigned by Tonui et al. (2014). Of the nine (represented by 12 analyses in Table 4), the six (represented by eight analyses) that fall within the Nakamura (2005) range to which Tonui et al. (2014) assigned them are all CM2 or CI1. The dehydroxylation peak temperature thermometer proposed here (Equation 1) quantitatively places these meteorites properly in the same Nakamura (2005) stage as the semiquantitative multi-proxy approach of Tonui et al. (2014). All four meteorites (represented by seven analyses) that fall *outside* the previously proposed Nakamura (2005) stage all are in either or both the long-proposed CY group (Ikeda 1992; King et al. 2019a) and/or the more recently proposed CM-like Belgica subgroup (Choe et al. 2010). It remains to be established whether this is because lithologies of the CY and CM-like Belgica subgroup result from initial mineral proportions, compositions, and textures that (1) differ from CM lithologies and respond differently to thermal metamorphism than CM and CI lithologies or (2) were subjected to different heating or evolutionary processes than CMs and CIs (Choe et al. 2010; King et al. 2019a).

Heterogeneity of Heating Effects at Thin Section Scale

The matrix EPMA data compiled in Table 3 satisfy the selection criterion that they fall within a predefined range based on anhydrous totals from wet-chemical analyses of serpentine (except for NWA 11024, the only ATCC shown in Table 3, included for the reasons

discussed above). These selected mean matrix EPMAΣ analytical totals typically vary among the different analyzed subsamples of the same meteorite. Multiple matrix EPMAΣs for different subsamples of individual non-ATCC falls vary by approximately 2 wt% (Murchison in Table 2 [$n = 2$]; Paris [$n = 3$] and Jbilet Winselwan [$n = 2$] in Table 3). Multiple EPMAΣ means for different subsamples of individual ATCC finds (Table 4) vary by typically approximately 3 wt% (ranges of EPMAΣ means for Y-82162 [~2.4 wt%, $n = 2$], Y-96029 [~3.6 wt%, $n = 3$], and B-7904 [~3.4 wt%, $n = 3$] in Table 4) but by as much as ~5 wt% in Y-86720 ($n = 3$, in Table 4). The within-sample variance among individual EPMA spots contributing to a mean value (standard deviation if reported) ranges up to 3–4 wt% for analyzed spot $n > ~25$ spots (Table 3); all CM chondrites so thoroughly and rigorously analyzed are recently analyzed non-ATCC finds. As discussed above, variations in EPMAΣ among spots within an individual subsample and among means from multiple subsamples may be due to heterogeneity in the distribution of anhydrous minerals and porosity among analyzed matrix spots. However, the population of EPMA spots may also measure actual within-subsample variation in EPMAΣ among spots with heterogeneous responses to short-lived heating events (Bland et al. 2014).

Bland et al. (2014) demonstrated by modeling supported by novel mineralogical observations on an example meteorite that impact velocities as low as 1.5 km s^{-1} were capable of heating localized and heterogeneously distributed volumes of porous chondrite matrix to >1000 K, with pressure–temperature varying by >10 GPa and >1000 K over length scales of ~100 μm. In pre-compacted chondrites, porous matrix consisting of sub-μm mineral grains can, immediately after shock compaction, locally reach higher temperatures than the adjacent non-porous μm-sized spherical chondrules. After the shock wave passes, heated matrix cools as adjacent chondrules act as heat sinks. Fourier's Law temperature gradients from hot porous matrix to adjacent cold nonporous chondrule immediately after shock heating could be on the order of 10^3 K/10 μm, so the high-temperature excursions that affect some of the matrix are brief (less than tens of seconds; Bland et al. 2014). Latent heat of melting or vaporization, phase changes (e.g., dehydroxylation of pre-impact matrix phyllosilicates to anhydrous phases), and the postimpact cooling rate of the impact-heated volume are commonly not addressed in exploratory implementations of thermomechanical models of the shock event and its immediate aftermath (Bland et al. 2014; Michel et al. 2020), but estimates of postimpact cooling rates have been modeled (Davison et al. 2012). However, modeled peak impact shock-induced temperatures of serpentine matrix are lower than
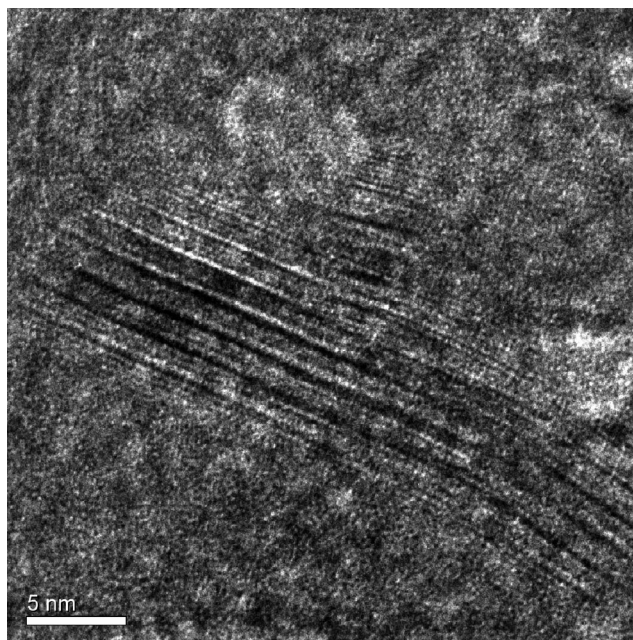

Fig. 2. TEM image of 1:1 regularly interstratified serpentine–tochilinite (a.k.a. tochilinite–cronstedtite intergrowth, TCI) with d(001) = 1.8 nm in QUE 93005,16 matrix. The persistence of TCI in this allocation indicates no alteration at $T > 300$ °C before or after assembly of the QUE 93005 breccia (see also Velbel et al. 2015, and fig. 3 therein).

those of forsterite matrix, so at least in this regard model behavior is consistent with expectations of realistic model outcomes for phyllosilicate-rich matrix (Bland et al. 2014).

Large impacts into a uniformly porous asteroid will compact the porous material and heat a large volume around the crater, which then cools and thermally equilibrates over timescales up to 10^6–10^7 yr (Davison et al. 2012). The volumes (several cm in size) modeled by Bland et al. (2014) would experience short-term (tens of seconds; Bland et al. 2014) local thermal re-equilibration as hot porous matrix regions lost heat to cold non-porous chondrules. Volumes of the same size would also experience longer term re-equilibration with their surroundings. Centimeter-size fragments ejected from the impact target area would cool rapidly (minutes to hours) to the ambient temperature around the target body, whereas volumes of identical size and shock-heating response would equilibrate with their surrounding rock volumes that experienced similar shock heating on much longer timescales. Bulk temperatures would fall on even longer timescales after low-velocity impact and up to 10^5–10^7 yr in around larger impacts (Bland et al. 2014). Observations of minerals that are known thermal indicators in one CR thin section identified that (1) 46 area % showed no evidence of heating and (2) at least 5 area % contained evidence consistent with heating to each of the

following maximum temperature ranges—493 K $\leq T \leq$ 873 K (~12%), 873 K $\leq T \leq$ 1023 K (~28%), 1023 $\leq T \leq$ 1178 K (~9%), and $\geq$1178 K (~5%). Thermopetrographic observations of sub-mm heterogeneity of heating effects in that thin section are consistent with the hypothesis formulated in the smallest spatial-scale modeling of Bland et al. (2014). The ranges of T_{peak} estimated from the observed within-sample ranges of EPMAΣ in this study are similarly consistent with the hypothesis of Bland et al. (2014).

Multiple studies of some mineral-water reactions and organic maturation phenomena in a variety of chondrite classes have quantitatively estimated "short" durations of some heating–cooling episodes and specific associated chemical reactions. Insoluble macromolecular organic matter in some chondrites regarded as more strongly metamorphosed than the usual meteorites of the same group (including CM-like, CR) exhibits spectroscopic signatures consistent with those produced by experimental heating episodes of seconds or minutes to weeks durations (Yabuta et al. 2010; Briani et al. 2013; Schmidt and Hinrichs 2020). Several studies of secondary mineral production by aqueous alteration in both ordinary and carbonaceous chondrites have quantitatively estimated reaction durations to be in the range of approximately 10^0–10^1 yr (Dyl et al. 2012; Velbel et al. 2012). Such a duration is too long for insolation heating during a single perihelion passage of a chondritic small body but short enough to be consistent with a single heating and cooling episode caused locally on a chondritic asteroid by a small impact with a velocity as low as 1.5 km s^{-1} (Bland et al. 2014).

Distinguishing highly localized effects of transient localized heating from mixing of discrete millimeter-to-centimeter-size fragments with different thermal histories in CM breccias will require (1) linking each analysis with the specific allocation of a meteorite (cf. discussion of QUE 93005 above) and (2) acquiring and interpreting analyses (e.g., EPMA spots) in their textural context relative to clasts, clast-host boundaries, and lithologic boundaries (e.g., Metzler 1995, fig. 1; Morlok et al. 2006, fig. 3; Jenniskens et al. 2012, fig. 2B; Zolensky et al. 2014, fig. 2; Lentfort et al. 2021, fig. 1) and/or (3) highly spatially resolved measurements of heat-sensitive phases and their compositions (e.g., Bland et al. 2014).

Thermally Driven Devolatilization—Interior or Surface?

Several possible sources for the heat required to dehydroxylate OH-bearing CM chondrites have been considered by previous workers (see list in the Introduction). The location of the thermal alteration is long and widely accepted as having been in the interior of CM parent small bodies. Hiroi et al. (1993, 1996) suggested that spectroscopic signatures of thermally altered CM materials observed in asteroid spectra indicate the exhumation of thermally altered materials from the small body's interior. The occurrence of thermally dehydroxylated CM clasts in some howardite, CM-chondrite, and complex breccias, and thermally unmodified CM clasts in others, and the coexistence of heated (ATCC) and aqueously altered (but not further heated) CM clasts in some meteorite breccias, suggests that CM lithologies now occurring as clasts reached a wide range of peak temperatures *before* assembly of the various clasts into the diverse now-lithified breccias hosting the CM clasts. Possible settings for such pre-assembly heating include grandparent body heating at depth by short-lived radionuclides (e.g., ^{26}Al), in the shallow subsurface following impact while the impact-heated target region cooled (Davison et al. 2012; followed by another impact to disrupt the impact-heated material and incorporate fragments of it into the eventual breccia), or being heated by an impact and immediately incorporated into the pre-lithification breccia. However, heated clasts in meteorite breccias do not support testing of the surface insolation-heating hypothesis.

Testing the ^{26}Al Hypothesis for Heating ATCCS

Table 5 compiles K-Ar gas retention ages of aqueously altered but not subsequently metamorphosed CM chondrites compiled and determined by Mazor et al. (1970) and new Rb-Sr model ages of ATCCs determined by Amsellem et al. (2020). From the top downward, meteorites are listed in Table 5 in order of increasing aqueous alteration (decreasing Rubin et al. [2007] petrologic subtype and increasing chondrule alteration stages of Hanowski and Brearley [2001] and Velbel et al. [2012, 2015]) followed by ATCCs in order of increasing Nakamura (2005) thermal metamorphic stage.

Mazor et al. (1970, p. 801) interpreted K-Ar ages as "not true ages recording a discrete event, but apparent ages, reflecting incomplete retention of radiogenic Ar^{40}." Noting that "meteorites with low K-Ar ages tend to have low He$_c^3$/Ne$_c^{21}$ ratios," they suggested that Ar$_r^{40}$ and He$_c^3$ "were lost concurrently, during the cosmic-ray exposure era, when the meteorite had a perihelion less than 1.02 AU, and hence was subject to appreciable solar heating (Eugster et al. 1998) Mazor et al. wrote everything in quotes. Eugster et al. did not write any of the quotes, but they concurred with what Mazor et al. had written.

Amsellem et al. (2020) determined Rb-Sr model ages of five Antarctic CM finds identified by previous work to have been metamorphosed beyond the temperatures of aqueous alteration (ATCCs), up to stages III/IV of the Nakamura (2005) CM thermal

metamorphism scale. All have lower Rb concentrations, and most have lower Sr concentrations, than "typical" CMs (Amsellem et al. 2020, their fig. 3). Amsellem et al. (2020) considered and rejected Rb depletion by terrestrial (specifically Antarctic) weathering. However, Velbel (1988) added the "e" (evaporite-efflorescence-bearing) designation to the Antarctic Search for Meteorites (ANSMET) curatorial classification of meteorite weathering, and re-examined three published data sets for Antarctic H-chondrites for a relationship between the distributions of Rb concentrations and terrestrial evaporite efflorescence formation. In all three data sets, evaporite-bearing samples are clustered at the low end of the distribution of Rb concentrations (Velbel 1988, fig. 1 therein). Ratios of alkalis and alkaline earths (including specifically Rb) to Mg in the evaporites on one such meteorite indicate minimal elemental fractionation relative to the corresponding ratios in the meteorite (Velbel et al. 1991, their fig. 3), suggesting that the evaporite efflorescences on weathered Antarctic chondrites contain alkalis and alkaline earths (including Rb) leached from the interiors of those meteorites on which the evaporite efflorescences formed. One (1) of the two (2) youngest Rb-Sr model ages reported by Amsellem et al. (2020) is from an evaporite-bearing sample (MIL 07675, weathering category Be). However, although both PCA 02010 and PCA 02012 are depleted in Rb (by 40% and 90%, respectively; Amsellem et al. 2020), neither is evaporite-bearing (Antarctic Meteorite Classification Database), although the lack of evaporites on the sample when received and curated does not preclude the possibility that evaporites were formed by leaching in Antarctic but naturally removed (e.g., abraded by wind) before sample collection and curation. Rubidium abundances may have been influenced by Antarctic weathering, but not in any obvious way related to the Rb-Sr models ages, so it remains reasonable to consider alternatives to Antarctic weathering to explain the Rb abundances in the samples analyzed by Amsellem et al. (2020).

All Rb-Sr model ages for the ATCC finds analyzed by Amsellem et al. (2020) are <2 Ga (with large standard errors up ~1 Ga). Amsellem et al. (2020) interpret this to mean that such young Rb-Sr model ages indicate that the thermal metamorphism of these ATCCs occurred relatively recently in solar system history, and specifically long after the decay of primordial ^{26}Al during the solar system's first few tens of millions of years. This refutes the hypothesis of ^{26}Al as the heat source for CM ATCC metamorphism. Of the K-Ar gas retention ages compiled by Eugster et al. (1998) for 10 non-ATCC CM2s (nine falls, one Antarctic find; Table 5), half are <2 Ga, in the same range as the five ATCCs examined by Amsellem et al. (2020). CMs that experienced only aqueous alteration (but were not heated to the point of phyllosilicate dehydroxylation) and have K-Ar gas retention ages <2 Ga include meteorites with low degrees of aqueous alteration (petrologic subtype 2.5, chondrule alteration stage 1) and CMs with extensive aqueous alteration (petrologic type 2.2). In other words, some "common" CMs have CM K-Ar gas retention ages as "young" as the Rb-Sr model ages of the ATCCs reported by Amsellem et al. (2020)—young radioisotope ages are not unique to ATCCs. CMs with petrologic subtypes between 2.5 and 2.2 and chondrule alteration stages between 1 and 5 (inclusive) have K-Ar gas retention ages >2 Ga—older (gas retention) ages have to date only been measured from CMs that experienced aqueous alteration but not subsequent thermal dehydroxylation. It remains possible that ^{26}Al was an important heat source for early aqueous alteration, but metamorphism of ATCCs beyond the temperature range of aqueous alteration by ^{26}Al-sourced heating is precluded by the Rb-Sr and K-Ar ages.

The range of Rb-Sr model ages for the five ATCCs analyzed by Amsellem et al. (2020)—and the range of K-Ar gas retention ages for approximately half on non-ATCC CMs (Mazor et al. 1970) (Table 5)—corresponds to the range of collision ages of C-type asteroid families, favoring a large impact origin (cf. Davison et al. 2012) for the heat that metamorphosed these ATCCs. Older K-Ar gas retention ages for other CMs (Mazor et al. 1970) (Table 5) pre-date any dynamic collision ages considered by Amsellem et al. (2020), instead falling mainly in the ~1.3–3.5 Ga gap in impact-reset ^{39}Ar-^{40}Ar ages of ordinary chondrites (Bogard 1995, 2011).

Returned samples will provide an opportunity to better understand the chronology and nature of thermal metamorphism in C-complex asteroids.

Testing the Insolation Hypothesis for Heating ATCCS

Asteroid regolith sample return missions will enable observations relevant to the hypothesis of insolation heating during small-perihelion passages of the asteroid past the Sun. A governing question that frames potential tests of this hypothesis is: Are dehydroxylated materials at the surfaces of mission target carbonaceous asteroids because they have been exhumed from asteroid interiors that were heated to such high temperatures, or might such thermally metamorphosed material have *formed* by dehydroxylation *at* these asteroids' surfaces (Zolensky et al. 2018)? Heating at or near (<1 m depth) the CM parent body's surface, by insolation heating at an NEA's surface during an epoch of low-perihelion orbit, has long been considered (e.g., Akai 1988; Nakamura 2005; Nakato et al. 2008; Marchi et al. 2009; Michel and Delbo 2010; Delbo and Michel 2011; King et al. [2015b] and references therein; de León et al. 2018; Quirico et al. 2018). The next sections explore various aspects of this question.

Table 5. K-Ar gas retention ages (Mazor et al. 1970; Eugster et al. 1998) and Rb-Sr model ages (Amsellem et al. 2020) for CM chondrites.

Meteorite	Petrologic subtype	Chondrule alteration stage[d]	Thermal metamorphism stage[e]	^{40}K-^{40}Ar gas retention age (Ma)[f]	^{87}Rb/^{86}Sr model age (Ma)[g]
Aqueous alteration without subsequent additional heating (non-ATCCs)					
Murchison	2.5[a]1.6[b]1.5[c]	1		1030	
Pollen				2010 ± 700	
Erakot				3100 ± 1100	
Boriskino				3770 ± 900	
Murray	2.4/5[a]1.5[b]1.5[c]	1		2700 ± 900	
Mighei	1.6[b]1.4[c]	2		3080 ± 900	
LEW 90500	1.6[b]1.4[c]	3		2670	
Haripura				1780 ± 600	
Nogoya	2.2[a] 1.1–1.2[b] 1.2–1.4[c]	5		2460 ± 1100	
Cold Bokkeveld	2.2[a]1.3[b]1.4[c]			1160 ± 300	
QUE 93005	2.1[a]1.5[b]1.3[c]	6	I/II		1274 ± 708
MIL 07675					699 ± 531
ATCCs					
PCA 91008			III		1544 ± 475
PCA 02012 #1	CM2TIII/IV[e]		III/IV		1161 ± 1059
PCA 02012 #2					1417 ± 1163
PCA 02010					607 ± 614

From the top downward, meteorites are listed in Table 5 in order of increasing aqueous alteration (decreasing Rubin et al. [2007] petrologic subtype and increasing chondrule alteration stages of Hanowski and Brearley 2001; Velbel et al. 2012, 2015) followed by ATCCs in order of increasing Nakamura (2005) thermal metamorphic stage.
[a]Classified by Rubin et al. (2007) using their aqueous alteration scale.
[b]Classified by Alexander et al. (2013) using their aqueous alteration scale.
[c]Classified by Howard et al. (2011, 2015) using their aqueous alteration scale.
[d]Hanowski and Brearley (2001), extended by Velbel et al. (2012, 2015).
[e]Classified by Amsellem et al. (2020) using Nakamura's (2005) thermal metamorphism scale (see also Quirico et al. 2018, their table 4).
[f]Eugster et al. (1998). Error ranges on K-Ar gas retentions ages are estimated from Mazor et al. (1970), their table 3, the source of some of the data compiled by Eugster et al. (1998), their table 5.
[g]Amsellem et al. (2020), their table 2.

Earth-Crossing Asteroid and Meteoroid Orbits and Insolation Heating of Surface Materials

It is tautological that meteorites recovered on Earth were delivered by meteoroids with Earth-crossing orbits in the present epoch. The pre-atmospheric orbits of witnessed and recovered meteorite falls mostly have perihelion distances ~0.7–1.0 AU (mean of perihelion distances calculated from orbital elements compiled by Jenniskens et al. 2012; Meier 2017). Similarly, the orbits of sample return mission target asteroids Itokawa, Ryugu, and Bennu all have perihelion distances q of $0.90 < q < 0.96$ AU (Fujiwara et al. 2006; Michel and Delbo 2010; Delbo and Michel 2011; Lauretta et al. 2015, 2017; Wada et al. 2018). At these heliocentric distances in the present epoch, neither category of objects experiences insolation heating above that experienced *in vacuo* by the Moon at 1 AU.

Marchi et al. (2009) noted that, over the orbital lifetimes of asteroids (including recent and current C-complex mission target asteroids and other NEAs) and meteoroids, there exists a finite probability that some of them experienced epochs during which their orbital perihelia were closer to the Sun than both their Main Belt progenitors and most NEAs. During such possible orbital passes near the Sun (<<1 AU), surfaces of such NEAs may have been exposed to insolation heating to temperatures (Marchi et al. 2009; Michel and Delbo 2010; Delbo and Michel 2011; de Léon et al. 2018) well above either the ambient temperature of their source bodies (Main Belt asteroids) or the majority of meteorite-delivering NEAs. Marchi et al. (2009) calculated that surfaces of NEAs with perihelia of < 0.5 AU or < 0.1 AU may have been heated to temperatures as high as 400–600 K or 1200–2000 K, respectively. These potentially accessible surface temperatures include the range of peak metamorphic temperatures inferred from matrix dehydroxylation from thermally metamorphosed CM and CI chondrites (e.g., Akai 1988, 1990, 1992; Tonui et al. 2002, 2003, 2014; Nakamura 2005; Tables 1 and 4 herein).

Attenuated effects of surface heating penetrate from the surface to the (spin-rate controlled) diurnal heat

penetration (thermal skin) depth (Marchi et al. 2009). For an object with a rotation period on the order of hours (e.g., Ryugu's rotation period is ~7.6 h; Wada et al. 2018; and Bennu's rotation period is ~4 h; Lauretta et al. 2015, 2017), the thermal skin depth is on the order of 2–3 cm (e.g., Delbo and Michel 2011; DellaGiustina et al. 2019). The thermal skin depth for annual (orbital) heating is ~1.5 m (Mazanek et al. 2016). If surface material is porous rather than non-porous, thermal effects penetrate more deeply (Molaro et al. 2020).

Michel and Delbo (2010) investigated orbital and thermal evolutions (the latter due to solar radiative heating during low-perihelion orbital epochs) of four prospective sample return mission target NEAs, including Ryugu. Michel and Delbo (2010) consider it improbable (<50%) that Ryugu's peak temperatures exceeded 500 K (~230 °C) and 450 K (~180 °C) at the surface and 3 cm depth, respectively.

Delbo and Michel (2011) investigated orbital and thermal evolution (the latter due to solar radiative heating during low-perihelion orbital epochs) of Bennu. Delbo and Michel (2011) consider it improbable (<50%) that Bennu's peak temperatures exceeded 500 K (~230 °C) and 400 K (~130 °C) at the surface and 5 cm depth, respectively.

Application of Thermal Dehydroxylation Measures to CM Falls: Maribo and Sutter's Mill

The recent CM2 falls Maribo and Sutter's Mill had orbital perihelia between 0.45 and 0.5 AU (between the orbits of Venus and Mercury; perihelion distances from Jenniskens et al. 2012) in their immediately pre-fall epochs. Thus, the meteoroids that delivered those meteorites to Earth ought to have experienced perihelion surface temperatures of 420–650 K (~180–380 °C, the upper portion of the range of Nakamura's [2005] Stage I and approximately the lower half of the temperature range of Stage II) in the present orbital epoch (Marchi et al. 2009).

Maribo

On the basis of its pre-entry orbit and the modeling of Marchi et al. (2009), Maribo matrix might have been heated to T_{peak} as high as the maximum T consistent with its observed orbital perihelion (~380 °C). In the absence of data on the matrix EPMA total for Maribo, heating to ~380 °C cannot be excluded. However, Maribo contains the largest tochilinite aggregates of any CM (Haack et al. 2012). The persistence of tochilinite, with its upper thermal stability limit of <350 °C (see discussion of PCP, tochilinite, and TCI above), militates against even this modest amount of heating after aqueous alteration for the recovered mass (<30 g) of Maribo. The outermost material of the pre-atmospheric Maribo meteoroid

(estimated radius 10–20 cm, and mass 9–74 kg; Haack et al. 2012) may have achieved surface temperatures as high as those modeled for its pre-atmospheric perihelion, but such surface material would have been the first material lost to ablation during bright flight.

Sutter's Mill

Sutter's Mill (CM) contains diverse CM carbonaceous chondrite lithologies spanning a range of matrix dehydroxylation (Table 4), with reported matrix EPMA totals of 87.1 wt% in lithologies classified as CM2.1 and CM2.0 on the scale of Rubin et al. (2007) SM51-1; Jenniskens et al. 2012) and 97.17 wt% in a thermally metamorphosed clast (SM2; Zolensky et al. 2014). Several different Sutter's Mill stones were not heated to temperatures ≥400 °C (~670 K), as indicated by three T_{peak} measurements by Jenniskens et al. (2012) using thermoluminescence (300 ± 20 °C), and Raman spectroscopy of macromolecular carbon in two samples (153 ± 27 °C and 268 ± 42 °C). As noted above, Equation 1 was calibrated to the mean of those three measurements ($T_{peak} \approx$ 240 °C). Minimal heating of most Sutter's Mill stones is further indicated by the widespread persistence of both discrete tochilinite and TCI in many Sutter's Mill samples (Zolensky et al. 2014).

Application of Equation 1 to the EMPA data from the thermally metamorphosed lithology (SM2) reported from Sutter's Mill by Zolensky et al. (2014) gives $T_{peak} \approx$ 690 °C (≈960 K). As with CM clasts in achondritic and complex breccias, intimate juxtaposition of such diverse lithologies within a single CM meteoroid suggests that peak temperatures of all individual clasts were reached before assembly of the various clasts into the meteoroid that broke up into the lithified stones that fell and were recovered. Zolensky et al. (2014) suggest that carbonaceous asteroid regolith may consist of a similar (Sutter's Mill-like) variety of C-chondrite lithologies.

Synthesis

In the pre-fall epoch, the Maribo and Sutter's Mill parent meteoroids passed close enough to the Sun for their surfaces to have been heated by insolation to up to ~380 °C, beyond the T required for the onset of metamorphism as observed in other CMs. However, the recovered masses of Maribo and Sutter's Mill contain CM lithologies that do not exhibit matrix dehydroxylation (matrix EPMA totals >91 wt%) that is evident in CM2 chondrites that were thermally altered above ~400 °C. Also, neither Maribo nor Sutter's Mill show evidence of heating of bulk matrix beyond the upper temperature limit of tochilinite stability during possible closer approaches to the Sun in either the present (immediately pre-fall) orbital epoch or possible past low-perihelion orbital epochs.

If the recovered masses of Maribo and Sutter's Mill were within the thermal skin depth of their meteoroid's surfaces, they might have been heated during perihelion passage to the onset temperatures of the thermal effects reported by Tonui et al. (2002, 2003, 2014). However, the recovered meteoroid volumes sampled by Maribo and Sutter's Mill are highly unlikely to have been exposed at the surfaces of their parent meteoroids. Material within tens of cm of a meteoroid's surface would not survive atmospheric entry (e.g., Michel and Delbo 2010; Delbo and Michel 2011), during which typically >90% of an incoming stony meteoroid is ablated. Consequently, material with measurable manifestations of surface exposure to insolation heating (such as the dehydroxylation considered in this paper) may be underrepresented among meteorites relative to asteroid regoliths because the insolation-heated material does not survive ablation during falls of boulder size or larger meteoroids (Zolensky et al. 2018).

It is much more likely that those thermally metamorphosed CM and CI chondrites that do exhibit measurable effects of heating (Akai 1990, 1992; Tonui et al. 2002, 2003, 2014; Nakamura 2005) were heated either in interiors of their parent bodies early in solar system history or by impact at any time, than that they were heated during a recent orbital epoch with small perihelia. This being the case, heated meteorites are uninformative regarding insolation heating of their parent bodies during low-perihelion passage near the Sun in a former orbital epoch. However, we should expect to find CM and related lithologies with indications of heating at the surfaces of NEAs if those NEAs approached the Sun more closely during a previous orbital epoch, because such surfaces will have not been lost to atmospheric ablation of meteoroids, the natural filtering mechanism that prevents boulder size meteoroidal parent body regolith surface-exposed materials from reaching Earth's surface.

Testing the Insolation Hypothesis for Dehydroxylation of Regolith on C-Complex Mission Target Asteroids

Ryugu

Orbital Evolution and Insolation

Michel and Delbo (2010) calculated that the probability of Ryugu having spent time in an orbit with perihelion at $<n$ AU during its (chaotic) orbital evolution from the Main Belt to its current orbit is ~0.30, ~0.16, ~0.07, and ~0.03 for perihelia (n) of 0.4 (approximately the average distance of Mercury from the Sun), 0.3, 0.2, and 0.1 AU, respectively. The maximum amount of time spent at such low perihelion distance was ~10^6 yr for minimum perihelion of 0.4 AU,

decreasing to near zero at 0.1 AU (Michel and Delbo 2010). Michel and Delbo (2010) also calculated that the probabilities that 50% of the surface of Ryugu and 50% of shallow subsurface material at 3 and 5 cm depth were heated above a given temperature during Ryugu's past dynamical lifetime. Assuming that labile and refractory organic molecules start to thermally decompose at temperatures of 520 K (~250 °C) and 620 K (~350 °C), respectively, corresponding to an NEA's surface temperature at heliocentric distances between 0.7 and 0.5 AU and about 0.5 and 0.35 AU, respectively, from the Sun, Michel and Delbo (2010) estimated probabilities of ~40% and ~10% that Ryugu had 50% of its surface heated above the temperatures of thermal decomposition of labile and refractory organic matter. The shallow subsurface (<5 cm) did not reach their assumed thermal decomposition temperature of these carbon compounds unless the asteroid was closer than 0.25 AU from the Sun; the estimated probability of this is ≤0.16 (Michel and Delbo 2010).

Surface Materials as Inferred from Early Mission Data

The Hayabusa2 spacecraft carries several instruments capable of making measurements relevant to characterization of minerals on asteroid Ryugu. The Hayabusa2 Optical Navigation Camera Telescope (ONC-T) has seven color channels (0.40 μm [ul], 0.48 μm [b], 0.55 μm [v], 0.59 μm [Na], 0.70 μm [w], 0.86 μm [x], and 0.95 μm [p]) for photometry in visible and shortwave infrared light (Kameda et al. 2017; Sugita et al. 2019). The Hayabusa2 near-infrared spectrometer 3 μm (NIRS3) has a spectral range of 1.8–3.2 μm (Iwata et al. 2017; Kitazato et al. 2019). The Hayabusa2 thermal infrared imager (TIR) is a single-band imager sensitive to wavelengths between 8 and 12 μm (Okada et al. 2017). The Hayabusa2 Mobile Asteroid surface SCOuT (MASCOT) lander (Ho et al. 2017) carries the MicrOmega hyperspectral microscope and the MASCOT Camera (MASCam; Jaumann et al. 2017). MicrOmega is a miniaturized descendent of the Mars Express Observatoire pour la Minéralogie, l'Eau, les Glaces et l'Activité (OMEGA) Infrared Mineralogical Mapping Spectrometer. MicrOmega has a spectral range of 0.99–3.65 μm (Bibring et al. 2017). MASCam acquired grayscale images (depth of field 150 mm to infinity; nominal ground resolution of 150 μm/pixel at 150 mm distance) in natural (clear filter) light when viewing the asteroid's daylight side, and was equipped with LEDs in blue, green, red, and shortwave infrared wavelengths (bandcenters at 0.465, 0.523, 0.633, and 0.812 μm, respectively; Jaumann et al. 2017, 2019) to illuminate MASCOT's immediate surroundings for simulating color imaging on the asteroid's nighttime surface (Jaumann et al. 2017). MASCam had a spatial resolution for

imaging and spatially resolved spectrophotometry of 200 µm/pixel (Jaumann et al. 2017).

Hayabusa2 MASCam acquired images during descent and while resting on the surface, and spatially resolved four-channel photometry in both daylight and artificially illuminated nightside image fields. Rocks of decimeter- to tens of meters size dominate the imaged surface, without visible fine-grained material atop or between the boulders. Two types of rock surfaces were identified and characterized, including (1) bright rocks with smooth faces and sharp edges, and (2) dark rocks with cauliflower-like, crumbly surfaces. Bright and spectrally diverse inclusions occur in the dark lithology. These inclusions are sub-mm to several mm in size and visually (Jaumann et al. 2019) and dimensionally (Jaumann et al. (2019), their supplementary materials) similar to coarse-grained inclusions (chondrules, chondrule fragments, Ca-Al-rich and other refractory inclusions) in CI2, CM, and CO carbonaceous chondrites. That such features could be readily discerned in MASCam images indicates the absence of covering fines (Jaumann et al. 2019).

Based on their colors in the LED-illuminated nighttime MASCam images, two dominant types of inclusions—blue and red—dominate the diverse inclusion population. The bright inclusions were interpreted to be anhydrous materials that would have been vulnerable to aqueous alteration (e.g., olivine) but had been only moderately and not extensively aqueously altered (hydroxylated; Jaumann et al. 2019). Chondrule-hosted olivine of similar dimensions persists abundantly in minimally altered CM2 chondrites (stage 1 of Hanowski and Brearley 2001; petrologic subtypes 2.9-2.4 of Rubin et al. 2007). Partially altered olivine remnants slightly reduced in volume due to partial centripetal/peripheral replacement by phyllosilicates persist up through alteration stages 2–4 of Hanowski and Brearley (2001) and down to subtype ~2.3 of Rubin et al. (2007; cf. Velbel et al. 2015, their table 1; Zolensky et al. 2018, their table 2.2).

Hayabusa2 ONC-T spectra vary among several different regolith and boulder types (Sugita et al. 2019), but ONC-T and NIRS3 spectra of prospective landing sites at low-(equatorial) and midlatitudes vary little, suggesting a homogeneous global surface layer consisting of a mixture of different lithologies (Kitazato et al. 2019; Sugita et al. 2019; Watanabe et al. 2019). The type 1 dark rugged boulders and type 2 bright smooth boulders described from remote ONC-T data by Sugita et al. (2019) correspond, respectively, to the dark rocks with cauliflower-like, rough and crumbly surfaces at small scale and the bright rocks with planar smooth slabby faces and sharp edges discerned in MASCOT MASCam imagery and photometry (Jaumann et al. 2019). Okada et al. (2020) determined from global one-rotation thermographic TIR images that most boulders

on Ryugu have a lower-than-expected thermal inertia suggesting microporosities of 30–50% whereas some ("cold spot") boulders have significantly higher thermal inertia. The inferred high microporosities for the dominant Ryugu boulder type are much higher than porosities of most interplanetary dust particles (IDPs) and all CM2 and CI1 chondrites but correspond to the porosities of the most porous chondritic IDPs (Corrigan et al. 1997).

Hayabusa2 results to date from both ONC-T color observations and the NIRS3 spectra are consistent with moderately dehydroxylated carbonaceous chondrites (Kitazato et al. 2019; Sugita et al. 2019). Ryugu's globally averaged near-infrared spectrum lacks both the 0.7 µm charge transfer band observed in ground-based spectra of Ryugu (Vilas 2008; Sugita et al. 2013) and any strong OH absorption band signature around 2.8 µm, both of which are common spectroscopic signals of hydrous phyllosilicates (e.g., Beck et al. 2018; Cloutis et al. 2018); however, a weak absorption band at 2.72 µm is ubiquitous on Ryugu's lithologically well-mixed surface (Kitazato et al. 2019; Sugita et al. 2019). The 2.72 µm absorption band is widely understood to be a vibration band of Mg-OH in octahedral sites of Mg-phyllosilicates (Kitazato et al. 2019; Bates et al. 2020). The absolute 2.72 µm band depth in processed reflectance data is positively correlated with estimated surface temperatures at the time of spectrum acquisition, indicating that uncertainties in the radiometric calibration and/or correction for the thermal emission component could account for the entire range of observed variations in the 2.72 µm band depth (Kitazato et al. 2019). The 2.72 µm band depth is not obviously correlated with topographic or morphologic features when normalized by the observed temperature trend (Kitazato et al. 2019). Spatial invariance of the 2.72 µm band depth at the ~18 m spatial resolution of the global standoff spectra indicates compositional homogeneity of the phyllosilicates at ~18 m and larger spatial scales (Kitazato et al. 2019).

Principle components analysis of ONC-T data indicates that Ryugu regolith spectra are consistent with moderately dehydroxylated carbonaceous chondrites and plot near the dehydroxylation trajectories for CM and CI chondrites (Sugita et al. 2019). ONC-T color spectra are bluer on Ryugu's equatorial ridge, one of several types of topographic highs "which may be subject to gradual erosion, leading to the exposure of fresh surface material" (Sugita et al. 2019, p. 4). Prospective landing sites along the equatorial ridge (especially L08, the site eventually selected for Hayabusa2's first sample acquisition) have brighter bluish spectra relative to sites at higher latitudes with their darker reddish spectra (Sugita et al. 2019; Watanabe et al.

2019). Mixing of different lithologies by impact gardening of regolith and boulders was favored by Sugita et al. (2019) as the cause for the observed large-scale homogeneity of color observations and Vis-NIR spectroscopic observations of Ryugu. Taken together, ONC-T, NIRS3, and MASCam data permit the interpretation of partial dehydroxylation of previously moderately hydrated CM- or CI-chondrite-like material (e.g., CM $\geq$ 2.3 of Rubin et al. 2007; CI2, Grott et al. 2019), most likely in the grandparent body in the early solar system (Kitazato et al. 2019; Sugita et al. 2019).

Sugita et al. (2019) considered a solar insolation-driven dehydroxylation hypothesis (Marchi et al. 2009) for the weak hydration signal (0.7 μm absorption feature) in visible and near-infrared spectra of some NEAs, including Hayabusa2 spectra from Ryugu. Sugita et al. (2019) noted that the timescale for resurfacing Ryugu (from the retention age of 10 m craters, $<2 \times 10^6$ yr) and excavating material by impacts from below the orbital-period skin depth (tens of cm; Michel and Delbo 2010) for insolation heating during episodes of past higher eccentricity orbits is shorter than the timescale for excursions of NEAs with Ryugu-like orbits to or from different orbits (for Ryugu, $\sim 4 \times 10^7$ yr; Michel and Delbo 2010). From this, Sugita et al. (2019) inferred that it is unlikely that weakness of Ryugu's hydration signal (2.72 μm absorption band; Kitazato et al. 2019) is due to solar heating during a recent orbital excursion to low perihelion, although they recognized that the permissive but less than compelling evidence for this interpretation means that this hypothesis cannot be readily dismissed. Furthermore, modeling of thermal fatigue on Bennu by Molaro et al. (2020) suggests that more rapid resurfacing of an asteroid (by several orders of magnitude) after migration from a Main Belt orbit to an NEA orbit could change that asteroid's surface over a short period of time relative to its previous long residence in the Main Belt. Molaro et al. (2020) suggest that this solar proximity driven accelerated thermal fatigue and resurfacing may contribute to the lack of small craters observed on surfaces of some NEAs, specifically including Ryugu.

Morota et al. (2020) inferred the impact, insolation, and episodic regolith history of Ryugu by combining observations of two-channel VisSWIR photometry—spectral (b–x) slope from blue (b-band; 0.48 μm) to red (x-band 0.86 μm; near-infrared) to distinguish "blue" from "red" surfaces—with multiscale geomorphic observations of natural and experimental impact cratering phenomena including detailed before-and-after observations of Hayabusa2's first sampling site, relative age dating principles of cross-cutting and superposition relationships among craters and surrounding surfaces, and crater chronometry.

At the largest spatial scale, the globally nearly uniform (Sugita et al. 2019) layer of mixed redder and bluer materials is estimated to be a few meters thick, based on previously determined depth/diameter ratios of 0.14–0.2 for Ryugu's craters (Sugita et al. 2019) and the minimum crater size (~10 m in diameter) that penetrates to and exposes the underlying bluer materials (Morota et al. 2020). Ryugu's polar regions are bluer than its equatorial ridge (Morota et al. 2020, their fig. S3), suggesting that the reddening process may be related to solar illumination.

Craters on Ryugu can be divided into two groups: red craters with interiors showing a b-x slope similar to that of their surroundings and blue craters with bluer interiors (Morota et al. 2020, their fig. 3). Some craters >20 m in diameter that cross-cut (and are thus younger than) other craters expose materials that are spectrally bluer than their surroundings (Morota et al. 2020, their fig. 1C). Craters with redder interiors pre-date surface reddening; bluer craters formed after surface reddening, by impacts that exposed the underlying bluer materials. Differences between the b-x slopes of crater interiors and the b-x slopes of their surroundings are bimodal (Morota et al. 2020, fig. 3). This "suggests that the surface reddening has not been active throughout the whole of Ryugu's history and occurred mainly after the formation of redder craters and before the formation of bluer craters" (Morota et al. 2020, p. 658).

Observations of Ryugu's boulders are compatible with the interpretation that they are originally bluer, with redder materials produced by one or more of several previously hypothesized surface processes including space weathering, insolation (solar) heating, and regolith gardening by small impacts (Morota et al. 2020). Impact disruption or thermal fatigue are favored hypotheses for the production of red fine-grained materials by shedding from boulder surface (Morota et al. 2020). Persistence of bluer spectroscopic character on boulder interiors exposed on split surfaces or by selective comminution at boulder edges implies that the timescale for surface reddening is longer (reddening is slower) than that of boulder resurfacing (Morota et al. 2020).

The surfaces artificially disturbed during the touchdown operation that acquired the first sample from Ryugu were imaged with resolutions as fine as ~1 mm per pixel. The color of the sampling site (location L08-E1) was slightly bluer and brighter than that of the surrounding region prior to touchdown, but became redder after the deposition of the dark, redder fine grains lofted by the sampling projectile's impact and the firing of the spacecraft's thruster gas jets (Morota et al. 2020). Observations with the near-infrared spectrometer (NIRS3) before and after the touchdown and surface disruption showed slightly bluer

and brighter spectra after the touchdown than before but little change in the hydroxide (OH) band depth (Morota et al. 2020). Morota et al. (2020) found this consistent with the previously reported global lack of correlation between the spatial distribution of the OH band depth in NIRS3 spectra and the red-blue color variations in the corresponding ONC observations (Kitazato et al. 2019; Sugita et al. 2019).

Morota et al. (2020) inferred that Ryugu arrived at its present state through multiple generations of parent body disruptions and/or global resurfacing processes. Ryugu's current spinning top shape must be at least 8.5 Ma old (Morota et al. 2020). Both crater size–frequency model ages, including that from an NEA collision model, are younger than the typical dynamical lifetime of NEAs and the median orbital lifetime of Ryugu (Morota et al. 2020). Morota et al. (2020) suggested that the reddening of Ryugu's surface occurred after its orbit shifted from the Main Belt to its current near-Earth orbit (Sugita et al. 2019).

If surface reddening occurred mainly after the formation of redder craters and before the exhumation of bluer material by the formation of younger (post-reddening) craters as inferred on the basis of crater and surface cross-cutting and superposition relationships (Morota et al. 2020, p. 658), then the lack of correlation between the spatially uniformly shallow OH band depth in Hayabusa2 NIRS3 spectra (Kitazato et al. 2019) and latitudinal and local (crater–crater and crater–surface cross-cutting-controlled) variations in ONC-T red-blue color (Sugita et al. 2019; Morota et al. 2020, respectively) suggest that the processes of thermally driven partial dehydroxylation and surface reddening are independent of one another (Morota et al. 2020). Morota et al. (2020) favor solar heating during a brief orbital excursion near the Sun over space weathering as the cause of Ryugu's surface reddening. However, solar heating on Ryugu during an orbital excursion that reddened surface materials cannot also account for the low abundance of hydrous minerals revealed by global NIRS3 observations (Kitazato et al. 2019); the reddened material has the same low abundance of hydrous minerals as the bluish or brighter areas on Ryugu, which did not experience the intense solar heating hypothesized to have caused the reddening (Kitazato et al. 2019; Morota et al. 2020).

Morota et al. (2020) predict that the Hayabusa2 returned sample from sampling site L08-E1 will contain a mix of bluer (previously thermally dehydroxylated but not insolation-heated) and redder (previously thermally dehydroxylated and more recently reddened) materials, with only the latter recording a solar heating event. On the evidence to date from the Hayabusa2 mission, a brief (low probability) low-perihelion orbital epoch of Ryugu would not be sufficient to account for the uniformly partially dehydroxylated state indicated by NIRS3 spectra (Kitazato et al. 2019) for materials exhumed and exposed from depths below the diurnal and annual thermal skin depths (Delbo and Michel 2011; Mazanek et al. 2016; Morota et al. 2020).

Bennu:

Orbital Evolution and Insolation

The median lifetime for Bennu's orbit is $\sim 3.4 \times 10^7$ yr (Delbo and Michel 2011). Delbo and Michel (2011) calculated that the probability of Bennu having spent time in an orbit with perihelion at $<n$ AU during its (chaotic) orbital evolution from the Main Belt to its current orbit is ~0.14, ~0.10, ~0.08, and ~0.02 for perihelia (n) of 0.4, 0.3, 0.2, and 0.1 AU, respectively. The maximum amount of time spent at such low perihelion distance was $\sim 3–5 \times 10^5$ yr for minimum perihelion of 0.4 AU, decreasing to near zero at 0.1 AU (Delbo and Michel 2011). The thermal skin depth of Bennu is ~1–5 cm (Rozitis et al. 2020). Delbo and Michel (2011) also calculated that the probabilities that 50% of the surface of Bennu and 50% of shallow subsurface material at 3 and 5 cm depth were heated above a given temperature during Bennu's past dynamical lifetime. Making the same assumptions about the thermal decomposition temperatures of labile and refractory organic molecules as Michel and Delbo (2010) made for Ryugu, Delbo and Michel (2011) estimate there is a 50% probability that the surface of Bennu was heated at temperatures ≥ 500 K (~230 °C), with regolith at 3–5 cm depth ~100 K lower than the surface temperature. Delbo and Michel (2011) estimate a probability of $\leq 20\%$ and ~10% that Bennu had, respectively, peak surface and 3–5 cm depth temperatures above 600 K (~330 °C), still below the onset temperature of thermal dehydroxylation of phyllosilicates. The shallow subsurface (<5 cm) does not reach the thermal decomposition temperature of these carbon compounds unless the asteroid is closer than 0.25 AU from the Sun; the estimated probability of this is ≤ 0.10 (Delbo and Michel 2011).

Surface Materials as Inferred from Early Mission Data

OSIRIS-REx carries the OSIRIS-REx Camera Suite (OCAMS), which includes the MapCam, a four-color imager for intermediate spatial resolution spectrophotometry; the PolyCam, to observe the sample site at sub-cm resolution; and the SamCam for documenting the sample site before, during, and after disturbance of the site by the TAGSAM sampling mechanism (Rizk et al. 2018). OSIRIS-REx also carries VIR spectrometers with spectral ranges of 0.4–4.3 μm (OSIRIS-REx Visible and near-Infrared Spectrometer, OVIRS; Reuter et al. 2018) and 5.71–100 μm (OSIRIS-REx Thermal Emission Spectrometer, OTES; Christensen et al. 2018).

Boulders on Bennu fall into two categories, similar to those of Ryugu—hummocky boulders with rough surface textures and apparent brecciation, and bright, smooth boulders with angular shapes (DellaGiustina et al. 2019; Molaro et al. 2020; Rozitis et al. 2020).

Early OSIRIS-REx OVIRS and OTES whole-disk-integrated spectra are spatially uniform across Bennu's surface at the spatial resolutions of tens to hundreds of meters reported to date; acquisition, reduction, and interpretation of spatially resolved data are ongoing (Hamilton et al. 2019; Kaplan et al. 2020). A strong absorption feature at ~2.7 μm in OVIRS spectra is ubiquitous on Bennu's surface (Hamilton et al. 2019; Kaplan et al. 2020). The rounded shape of the feature resembles those of intermediately altered CMs (e.g., Cold Bokkeveld, CM2.2 in the classification of Rubin et al. 2007, and MET 00639; Hamilton et al. 2019) but also resembles Murchison (CM2.5; Bates et al. 2020). The position of the observed feature, 2.74 μm (±0.01) corresponds to highly aqueously altered CM2.1 to CM2.2 chondrites (Hamilton et al. 2019; classification of Rubin et al. 2007) and CM1/2 and CM1 (PSF 1.2 and 1.1; classification of Howard et al. [2015] applied by King et al. 2017) chondrites including NWA 8534, NWA 4765, and LAP 02277 (Bates et al. 2020), all of which contain abundant and Mg-rich phyllosilicates. The early Bennu surface spectrum in the 2.3–3.4 μm range (Hamilton et al. 2019, their fig. 2) resembles two highly hydrated CM chondrites assigned to subtype 1.1 in the classification of Alexander et al. (2013):

- DOM 08003 (Beck et al. 2018, their fig. 1) with (1) the highest H content measured by Alexander et al. (2013) and (2) a TGA mass loss of 11.6 wt% between 400 and 770 °C, fourth highest among 26 CM chondrites examined by Garenne et al. (2014); and
- ALH 83100 (Garenne et al. 2016, their fig. 1) with (1) the second highest H content measured by Alexander et al. (2013) and (2) a TGA mass loss of 12.9 wt% between 400 and 770 °C, the highest among 26 CM chondrites examined by Garenne et al. (2014).

Hamilton et al. (2019) show subtle features between 10 and 13 μm in OTES spectra. McAdam et al. (2015) examined a suite of 16 CM, CI, and C2-ungrouped chondrites (seven falls, nine finds), that included varying degrees of aqueous alteration, with some examples of subsequent thermal modification. Samples examined spectroscopically were from the same powdered samples that had been examined by X-ray diffraction by Howard et al. (2009, 2011). Tetrahedral layer vibrations of phyllosilicates and fundamental stretching vibrations of olivine both contribute to the 10–13 μm spectral feature (McAdam et al. [2015], and references therein).

Less altered CM/CI chondrites with relict primary olivine, or thermally altered CM chondrites with secondary olivine formed by phyllosilicate dehydroxylation, produce an ~12.3 μm peak. CM/CI chondrites with abundant Mg-rich phyllosilicates not subsequently dehydroxylated (which occur mainly in the more extensively altered carbonaceous chondrites) have a 11.4 μm peak. Intermediately altered CM/CI chondrites (with more extensive partial alteration of olivine to phyllosilicates, or partial thermal dehydroxylation of phyllosilicate to olivine) exhibit subequal contributions of both peaks (McAdam et al. 2015). The overall peak position (average of two where both are present) is strongly correlated with modal vol% Fe- and Mg-phyllosilicates, such that peak positions of ~12.2–12.5 μm indicate ~71 ± 6 vol% phyllosilicates, whereas peak positions between ~11.4 and 11.5 μm indicate >77 vol% phyllosilicates (McAdam et al. 2015). Peak positions in the range between the two aforementioned ranges (between ~11.6 and 12.1 μm) indicate ~75 ± 5 vol% phyllosilicates. The one (moderately) thermally altered CM chondrite examined by McAdam et al. (2015) exhibited a reflection peak position of ~12.0–12.1 μm. OTES spectra in the 11.6–12.4 μm range (Hamilton et al. 2019) may indicate variations in the proportions of hydrous phyllosilicate and corresponding variations in degree of hydration across the surface of Bennu.

No specific CM, CI, or similar ungrouped or anomalous C-chondrite (including naturally heated CM) matches all attributes of any OVIRS or OTIS spectra (Hamilton et al. 2019). The smooth rise of Bennu's spectrum, from 2.85 to ~3.3 μm and blue spectral slope, resembles spectra of Pallas-like asteroids, which are inferred to have a phyllosilicate-dominated composition (Hamilton et al. 2019).

Spatial invariance of the OVIRS or OTIS spectra at the ~80 m spatial resolution of the early global stand-off spectra indicates that the distribution of mixed mostly coarse (>125 μm) particles and boulders with a small fraction of fine (<125 μm) particles does not vary at the observed spatial scale (Hamilton et al. 2019). However, visual (e.g., albedo, size, shape, surface texture) variability in visual grayscale images (with image resolutions as small as 0.33 m/pixel at the time the reported images were acquired) of boulders indicates a variety of boulder types that may indicate that large-scale spectroscopic uniformity is caused by either redistribution processes or compositional uniformity (DellaGiustina et al. 2019). Lateral compositional homogeneity at spatial scales of meter to tens of meters may be facilitated in part by episodic particle ejection from Bennu's surface (Lauretta et al. 2019; Hergenrother et al. 2020). These particle ejection events on Bennu are estimated to redistribute ~10^4 g surface

material per orbit (437 days), most of which (70–85%) falls back onto Bennu's surface (DellaGiustina et al. 2020; Hergenrother et al. 2020). Diversity of boulder albedos is greater on Bennu than Ryugu, and "(s)maller and brighter boulders may represent younger, more recently fragmented material" (DellaGiustina et al. 2019). Large (>20 m) boulders occur mainly at Bennu's mid- to high latitudes, exhumed as smaller particles migrate away from the higher latitude regions (DellaGiustina et al. 2019).

OTES and OVIRS data and high spatial resolution images (~0.4 cm/pixel) obtained during the Recon C phase from an altitude of ~250 m suggest that the material exposed at the bottom of Nightingale crater, the primary OSIRIS-REx sampling site, has a lower thermal inertia than its surroundings and an abundance of centimeter-scale regolith (smaller than the ~1–5 cm thermal skin depth) atypical of Bennu surface (Rozitis et al. 2020). OVIRS and OTES data taken in combination permit the interpretation that Bennu's spectroscopically active surface is dominated by CM- or CI-chondrite-like material rich in phyllosilicate-mineral products of past aqueous alteration (including hydration–hydroxylation) of a parent or grandparent body, most likely in the grandparent body in the early solar system (Hamilton et al. 2019).

Summary

Spectroscopically estimated hydroxylation states of Ryugu's and Bennu's surfaces vary; Ryugu's surface spectra are consistent with aqueous alteration *and* subsequent thermal dehydroxylation (Sugita et al. 2019) whereas Bennu's are consistent with aqueous alteration *without* subsequent thermal dehydroxylation (Hamilton et al. 2019). NEAs in orbits efficiently accessible by spacecraft from Earth have specific orbital attributes in common, so it is no surprise that both Ryugu and Bennu have similarly low probabilities of specific past insolation heating scenarios (Michel and Delbo 2010; Delbo and Michel 2011). These results suggest low probabilities that Ryugu's or Bennu's surface temperatures reached the realm of thermal dehydroxylation of phyllosilicates.

Variation and Heterogeneity of Fragments and Their Thermal Histories Within and Between Rubble Piles

Michel et al. (2020) modeled impact disruption of 100 km diameter primitive asteroids consisting of hydroxylated (CM and CI) materials by 7–13 km impactors at a variety of conditions below and above the catastrophic disruption threshold. Their numerical simulations yielded the heating above the pre-disruption temperature provided by the energy of the impact for each modeled fragment, and tracked numerous particles (fragments) through disruption to reassembly of dozens

of representative small rubble pile asteroids (mostly ~4 km, near the resolution limit of the numerical simulations) aggregated from the impact-disrupted fragments. Particles originating near the pre-impact surface close to the impact point experienced the most impact-derived heating, while particles originating near the surface but closer to the antipode of the impact experienced the least heating (Michel et al. 2020). Different rubble pile aggregates that accumulated from the debris of the catastrophic impact are composed of different proportions of mixed materials that sampled surfaces at different pre-disruption distances from the impact and different ranges of pre-disruption maximal depth within the parent body (Michel et al. 2020). Michel et al. (2020) find that the populations of ~km-scale rubble pile asteroids resulting from catastrophic disruption of a large hydroxylated asteroid of the assumed composition and size under a given set of assumptions include rubble piles consisting entirely of disrupted fragments that were not heated to the temperature of thermal dehydroxylation, and rubble piles in which some fraction of the fragments was heated beyond the dehydroxylation temperature. The implications for Ryugu and Bennu include an alternative to the hypothesis initially inferred from mission spectroscopy that Ryugu and Bennu had different internal or surface (insolation) heating histories (Hamilton et al. 2019; Kitazato et al. 2019). Instead, Michel et al. (2020) hypothesize that Ryugu and Bennu are each internally homogenous rubble piles but were assembled from ensembles of fragments derived from different regions of the disrupted parent asteroid. The observations and inferences of Morota et al. (2020) are consistent with this hypothesis.

Space-weathered surfaces of returned fragments recovered by sample return missions may reveal evidence for thermal dehydroxylation of asteroid-surface phyllosilicate-rich matrix materials (e.g., Lantz et al. 2018; Thompson et al. 2019) or consequences of space weathering other than phyllosilicate dehydroxylation (Morota et al. 2020). CM material that was aqueously altered and subsequently either dehydroxylated at and near fragment surfaces or space weathered without dehydroxylation at and near fragment surfaces is much more likely to have survived for examination in terrestrial laboratories in mission-returned samples than as meteoroid-surface material.

CONCLUSIONS

A new geothermometer for CM matrix metamorphism is proposed, tested, and applied. A number of CM and closely related chondrites exist for which both matrix EPMA totals and estimated peak

temperatures have been published (all meteorites in Table 1, many in Table 4). T_{peak} values estimated quantitatively using measured EPMA totals and our dehydroxylation thermometer Equation 1 agree closely (when rounded to one significant figure for the reasons discussed above) with previous estimates for most of these meteorites, except for the CY/CM-like Belgica subgroup.

Application of the new dehydroxylation thermometer proposed here to Maribo and Sutter's Mill, CM chondrites with known orbital perihelia, suggests that both (1) passed close enough to the Sun for their surfaces to have been heated by insolation to beyond the T required for the onset of metamorphism as observed in some other CMs, but (2) recovered masses contain CM lithologies that do not exhibit the expected corresponding matrix dehydroxylation or thermal decomposition of tochilinite or TCI. This suggests that insolated-heated meteoroid surfaces would have been lost by ablation during bright flight, and that, if present on asteroid and pre-atmospheric meteoroid surfaces, insolation-heated material is more likely to be encountered among returned asteroid regolith samples than in meteorites.

Consideration of CM matrix T_{peak} in light of recently published results from mission remote sensing and ATCC geochronology focuses new attention on the sources of heat for (1) melting of early accreted ice and associated aqueous alteration of CM anhydrous silicates to phyllosilicates and (2) subsequent dehydroxylation of CM phyllosilicates in ATCCs. Early stellar nucleosynthetic ^{26}Al remains a viable source of heat for aqueous alteration of anhydrous primary silicates to phyllosilicates *prior to* additional heating and dehydroxylation (producing ATCCs). This is supported by the ubiquity of ^{26}Al in the early solar system and the near-ubiquity of abundant phyllosilicates in aqueously altered CM chondrites and as the precursors of dehydroxylated phyllosilicates in ATCCs.

The existence of both aqueously altered CM chondrites and ATCCs implies that some CM were heated only to the point of aqueous alteration and that others experienced additional heating after aqueous alteration. In principle, the two groups could merely sample different less or more (respectively) complete subsets of a range of T_{peak} all driven by a single heat source during a single heating event. Heat for the aqueous alteration stage of any CM could have been produced by ^{26}Al. However, the hypothesis of early solar system heating of CM ATCCs to serpentine dehydroxylation temperatures by decay of ^{26}Al at depth within the pre-disruption parent bodies of rubble-pile asteroids appears to have been refuted by the Rb-Sr ages determined for ATCCs by Amsellem et al. (2020). Other sources of heat have been proposed that could have operated concurrently with still-live early ^{26}Al but also continued to

operate episodically and subjected CM material to T_{peak}s in and beyond the range of serpentine dehydroxylation any time after decay of initial ^{26}Al. These include

- Conversion of kinetic energy to heat in CM chondrite target rock during impact below the catastrophic disruption threshold for the target body, driving widespread subsurface metamorphism heating of target material (Akai 1988; Choe et al. 2010; Davison et al. 2012; Garenne et al. 2014; King et al. 2015a);
- Conversion of kinetic energy to heat in CM chondrite target rock by collisional impact above the catastrophic disruption threshold for the target body, that thermally metamorphosed previously aqueously altered material and immediately disrupted the parent asteroid (Michel et al. 2020);
- Insolation heating during a past orbital epoch of closer perihelion (Michel and Delbo 2010, Delbo and Michel 2011).

In all cases, volumes of aqueously altered but not additionally metamorphosed CM material co-exist with ATCC material in different parts of the target body or its disrupted debris.

The spectroscopic, photometric, and geomorphic observations to date about the hydroxylation–dehydroxylation state of surface materials on Ryugu (Kitazato et al. 2019; Morota et al. 2020) and Bennu (Hamilton et al. 2019) are consistent with any of these three hypotheses. Michel et al. (2020) proposed specifically that Ryugu and Bennu are each internally homogenous (in terms of the degree of phyllosilicate hydroxylation–dehydroxylation) rubble piles that were assembled from fragments derived from different regions of a parent body that had previously been aqueously altered and was then thermally metamorphosed and disrupted by collisional impact. Until returned samples provide direct evidence, the favored hypotheses for the spectroscopically determined hydroxylation states of Ryugu's and Bennu's surfaces remain heating of the pre-disruption planetesimal from which each asteroid was assembled, sufficient for aqueous alteration with (Ryugu) or without (Bennu) subsequent thermal dehydroxylation. Heat for the aqueous alteration stage of any CM could have been produced by ^{26}Al. Heat for dehydroxylation of serpentine-rich CM material was likely produced later, either by impact (e.g., Davison et al. 2012; Michel et al. 2020) any time (including billions of years) after decay of initial ^{26}Al in, and before catastrophic disruption of, the ancestral planetesimal (Hamilton et al. 2019; Sugita et al. 2019) or (low-probability, Michel and Delbo 2010; Delbo and Michel 2011) insolation during a past orbital epoch of closer perihelion, of longer duration and more pervasive effect than that hypothesized for Ryugu by Morota et al. (2020).

Asteroid sample return missions Hayabusa2 and OSIRIS-Rex are designed to acquire granular and fragmental carbonaceous chondrite-like material. As of this writing, samples have already been collected by both spacecraft. The samples are expected to include a variety of particles including long-surface-exposed fragments and material more recently excavated by natural or artificial impact. Subsequent steps involved in ultimately characterizing the returned samples include (1) anticipation of sample attributes expected to occur among returned samples (informed by abundant mission spacecraft data), to refine planning for pre-allocation (basic characterization and preliminary examination) analyses in terrestrial laboratories; and (2) characterization, screening, and selection of specific lithologies among returned samples for diverse highest priority analyses. (3) The last stage in sample characterization is analysis by numerous and diverse techniques, possibly including EPMA, which will allow the new peak-temperature thermometer proposed here to be applied.

How would an abundance of dehydroxylated material in a target asteroid's regolith influence any of these steps? Either an interior or an exterior (surface) setting for the heating would compromise that lithology's ability to host many mission-relevant organic compounds (Delbo and Michel 2011). The dehydroxylation thermometer proposed here may have implications for interpreting sample return mission data and preliminary examination of returned samples.

In the present epoch, thermally driven physical and chemical processes are more intense at the surfaces than in the interiors of NEAs and meteoroids during their orbits around the Sun. Such processes include (1) fragmentation and degradation of rock masses and regolith particles due to thermal fatigue and stress fracturing (e.g., Delbo et al. 2014; Lauretta et al. 2019), (2) breakdown of heat-sensitive organic chemical compounds (Michel and Delbo 2010; Delbo and Michel 2011), and (3) devolatilization of volatile-bearing compounds (e.g., hydrous minerals and hydrous or otherwise volatile-rich amorphous materials; Delbo and Michel 2011; Mazanek et al. 2016; Lauretta et al. 2019). It is beneath the diurnal and annual thermal skin depths that inner solar system small bodies and their granular surface materials are expected to preserve organic compounds and other volatiles least affected by surface (regolithic) processes (Zolensky et al. 2018). Impact cratering, regolith gardening, and thermal stress spallation can excavate and expose long-buried materials to the entire menu of small bodies' surface processes, and can bury previously exposed regolith and surface-exposed fragments. The spectra of recent C-complex sample return mission target asteroid surfaces resemble spectra of aqueously altered (Bennu), and thermally metamorphosed

C chondrites and experimentally heated carbonaceous chondrites (Ryugu). If impact, regolith gardening, and thermal spalling have brought such heated material from the interior of pervasively metamorphosed asteroids and their surface boulders, the regolith represents thermally processed material unlikely to preserve indigenous volatiles (Zolensky et al. 2018). However, if such surface material was heated during a past epoch of more eccentric, small-perihelion orbit, then pristine (aqueously altered but not further heated) volatile-rich material is likely to occur in fresh spall fragments from the interiors of boulders larger than the thermal skin depths (Zolensky et al. 2018). Either way, distinguishing thermally altered carbonaceous chondrite-like returned regolith fragments (e.g., Tonui et al. 2002, 2003, 2014) from the aqueously altered (but not further heated) carbonaceous chondrite lithologies with their higher volatile abundances will be necessary prior to sample return (during the sample return cruise to Earth, using mission data) and during preliminary examination of returned samples in terrestrial laboratories (Zolensky et al. 2018). Spatially resolved spacecraft spectroscopy interpreted with consideration of spectra from relevant carbonaceous chondrite meteorites of diverse degrees of aqueous alteration and subsequent heating (e.g., McAdam et al. 2015) constrains lithologic hydration state and its spatial variation or lack thereof on Ryugu (Kitazato et al. 2019; Morota et al. 2020) and Bennu (Hamilton et al. 2019). Microimaging spectroscopy (Van Gorp et al. 2014; Green et al. 2015; Greenberger et al. 2015; Green et al. 2015; Parra et al. 2020, 2021) of returned samples may serve as a bridge between (1) large-area (>meter-scale spatial resolution) spacecraft spectrophotometry (Hayabusa2 ONC-T, Sugita et al. 2019; OSIRIS-REx MapCam, Rizk et al. 2018) and spectroscopy (Hayabusa2 NIRS3, Kitazato et al. 2019; OSIRIS-REx OVIRS, Reuter et al. 2018; Hamilton et al. 2019) and MASCOT spacecraft MASCam multichannel high (meter to sub-mm) spatial resolution imaging photometry (Jaumann et al. 2017, 2019) and (2) EPMA and other measures of volatile abundance in returned samples.

Further development of quantitative relationships between spectroscopic features and measures of heating and devolatilization in low petrologic-type carbonaceous types are underway since the onset of mission data acquisition at the mission target asteroids Ryugu and Bennu and will continue through return of acquired samples to Earth. After sample return, assaying returned samples of CM lithologies for matrix EPMA totals can establish the maximum temperature to which a given lithology has been exposed, and thereby enable distinguishing fragments with lithologies most likely to preserve unaltered primitive organics from fragments with naturally compromised volatile inventories.

Editorial Handling—Dr. Josep M. Trigo-Rodríguez

Notes

[1] All minerals in humid environments (including laboratories) can have adsorbed/absorbed molecular water in quantities determined by their surface properties and the relative humidity of their environment. All such sorbed water is driven off by mild heating (~100–200 °C). This is the water formerly reported by wet-chemical analysts as $H_2O(-)$. Among silicate minerals, "hydration" and "dehydration" (both terms sensu lato), respectively, are the forward and reverse reactions anhydrous silicate mineral + H_2O ↔ hydrous silicate mineral (e.g., phyllosilicate). Phyllosilicates are layer-structured silicates. Some phyllosilicates (e.g., smectite group minerals) have molecular interlayer water (H_2O), "water of hydration"—usually water of solvation associated with interlayers cations—much of which is driven off by mild heating (~100–200 °C; part of $H_2O[-]$); this is phyllosilicate dehydration sensu stricto. In addition, all phyllosilicates, whether they contain interlayer water or not, contain hydroxyl (OH). Serpentine group minerals, the dominant mineral in CM chondrite matrices (e.g., Howard et al. 2009, 2011, 2015), have only structural OH and minor sorbed (molecular) H_2O, and no interlayer (molecular) water of solvation. Hydroxyl (OH) in phyllosilicates (commonly referred to as "structural water" and reported by wet-chemical analysts as $H_2O[+]$, e.g., Deer et al. 1962; Haramura et al. 1983) can, upon heating, be driven off as molecular water, leaving behind an anhydrous silicate mineral (hydrous silicate mineral → anhydrous silicate mineral + H_2O). Thus, in this sense, phyllosilicates and other silicate minerals with OH are commonly termed "hydrated" silicates—they can be "dehydrated" (evolve molecular water) by (thermally) driving off OH (dehydroxylation). Here, "dehydroxylation" will be used because of the nature of the specific reaction that thermally decomposes serpentine group phyllosilicates, but can be thought of as synonymous with "dehydration" *sensu lato*. A widely used simple reaction for chondrite-relevant minerals is the serpentinization of olivine plus pyroxene— $Mg_2SiO_4 + MgSiO_3 + 2H_2O ↔ Mg_3Si_2O_5(OH)_4$ (see review by Velbel 2014). The forward reaction produces an OH-bearing ("hydrous") mineral from "anhydrous" precursors, producing a "hydrated" mineral; the reverse reaction evolves molecular water from the dehydroxylation ("dehydration") of serpentine.

[2] Rubin et al.'s (2007) petrologic subtypes range from the least-altered known CM chondrite being 2.9 and lower numbers down to 2.0 indicating greater degrees of aqueous alteration. Some workers refer to the most altered CMs as CM1 following Zolensky et al. (1997). See Velbel et al. (2015, their table 1), or Zolensky et al. (2018, their Table 2.2), for how several of these alteration scales relate to one another when applied to the same suite of meteorites.

[3] Ikeda (1992) proposed a new group—CY—for Yamato(Y)-82162, Y-86720, and Belgica(B)-7904. Ikeda (1992) attributed the observed dehydration of matrix phyllosilicates and recrystallization of olivine from hydrous minerals to (1) impact-driven shock heating on parent-body surfaces or (2) thermal metamorphism in the parent body interiors. King et al. (2019a) expanded the CY group to include Y-86029, Y-86789, and Y-980115.

[4] Choe et al. (2010) proposed a Belgica (B)-7904 grouplet that includes the namesake, WIS 91600, Dhofar 225, and Yamato (Y)-86720, and suggested that heating by impact caused the observed dehydroxylation after aqueous alteration. Note that Y-86720 and B-7094 are also part of Ikeda's (1992) CY group.

[5] Serpentine group minerals are the dominant phyllosilicates in most CM chondrites. However, saponite occurs in, and is inferred to be the precursor of dehydroxylation products in, some heated CM chondrites (Kojima et al. 1984; Akai 1988, 1990, 1992; Tomeoka et al. 1989a,1989b; Tomeoka 1990; Ikeda 1992; Kimura and Ikeda 1992; Tonui et al. 2002, 2014; Nakamura 2005), and is interstratified with serpentine in CI chondrites (Brearley and Jones 1998). Saponite has interlayer water that serpentine does not and loses its interlayer $H_2O(-)$ around 100 °C. Saponite loses its structural OH ($H_2O(+)$) at significantly higher temperatures (800–900°C; Kawano and Tomita 1991; Che et al. 2011) than serpentine. Consequently, the equations in this article do not apply to materials dominated by saponite or other clay minerals, and unusual CM chondrites in which the dominant matrix phyllosilicate or residual pre-dehydroxylation phyllosilicate is saponite—for example, Bells (Zolensky et al. 1993; Brearley 1995)—are excluded from this analysis.

[6] Delbo and Michel (2011) erroneously ascribed dehydration and dehydroxylation of C-chondrite phyllosilicates to temperature ranges of 300–670 K (~30–400 °C). Licandro et al. (2007) identified the smectite-group mineral montmorillonite and the serpentine-group mineral antigorite spectroscopically over the 0.35–2.4 μm spectral range on one (B-type) asteroid, selected for study because of its relevance to the asteroid–comet distinction, and not representative of many thousands of other B-type and related (e.g., C-type) asteroids. No 0.7 μm feature was observed. The NIR spectrum (to 2.4 μm) was shown to resemble library spectra of Ivuna (CI) heated to 700 °C and the unusual CI/CM meteorite Yamato-86720 (CM2TIV in the Nakamura [2005] classification). The observed spectral range did not extend to the 2.7–3.1 μm range that includes the widely observed feature that is widely accepted to indicate and characterize octahedral cation-OH bonds of phyllosilicates. Following Licandro et al. (2007), Delbo and Michel (2011) based their inferences about temperature effects on thermal dehydration and dehydroxylation on a compilation of dehydration and dehydroxylation temperatures for the smectite-group minerals montmorillonite, nontronite, and ferruginous smectites (10/14 tabulated items). None of these smectite-group minerals occur in the vast majority of CM chondrites (in which the phyllosilicates are almost exclusively serpentine-group minerals) except Bells in which the smectite-group mineral is saponite (Brearley 1995). Saponite is understood to be the dominant phyllosilicate in CIs. Delbo and Michel's (2011) temperature compilation table 1 does not include data from serpentines or saponite—the phyllosilicates that actually occur in CM and CI chondrites. The text that follows from it (the last paragraph of Delbo and Michel's [2011] section 4) is largely irrelevant to most

actual solar system small bodies carbonaceous CM, CR, and most other related lithologies.

REFERENCES

Akai J. 1988. Incompletely transformed serpentine-type phyllosilicates in the matrix of Antarctic CM chondrites. *Geochimica et Cosmochimica Acta* 52:1593–1599.

Akai J. 1990. Mineralogical evidence of heating events in Antarctic carbonaceous chondrites, Y-86720 and Y-82162. *Proceedings of the NIPR Symposium on Antarctic Meteorites* 3:55–68.

Akai J. 1992. T-T-T diagram of serpentine and saponite, and estimation of metamorphic heating degree of Antarctic carbonaceous chondrites. *Proceedings of the NIPR Symposium on Antarctic Meteorites* 5:120–135.

Alexander C. M. O'D., Bowden R., Fogel M. L., Howard K. T., Herd C. D. K., and Nittler L. R. 2012. The provenances of asteroids, and their contributions to the volatile inventories of the terrestrial planets. *Science* 337:721–723.

Alexander C. M. O'D., Howard K. T., Bowden R., and Fogel M. L. 2013. The classification of CM and CR chondrites using bulk H, C and N abundances and isotopic compositions. *Geochimica et Cosmochimica Acta* 123:244–260.

Alexander C. M. O'D., Bowden R., Fogel M. L., and Howard K. T. 2015. Carbonate abundances and isotopic compositions in chondrites. *Meteoritics & Planetary Science* 50:810–833.

Alizadehhesari K., Golding S. D., and Bhatia S. K. 2012. Kinetics of the dehydroxylation of serpentine. *Energy & Fuels* 26:783–790.

Amsellem E., Moynier F., Mahan B., and Beck P. 2020. Timing of thermal metamorphism in CM chondrites: Implications for Ryugu and Bennu future sample return. *Icarus* 339:113593.

Barber D. J. 1985. Phyllosilicates and other layer-structured materials in stony meteorites. *Clay Minerals* 20:415–454.

Bates H. C., King A. J., Donaldson H. K. L., Boelse N. E., and Russell S. S. 2020. Linking mineralogy and spectroscopy of highly aqueously altered CM and CI carbonaceous chondrites in preparation for primitive asteroid sample return. *Meteoritics & Planetary Science* 55:77–101.

Beck P., Quirico E., Garenne A., Yin Q.-Z., Bonal L., Schmitt B., Montes-Hernandez G., Mo'tagnac G., Chiriac R. and Toche F. 2014. The secondary history of Sutter's Mill CM carbonaceous chondrite based on water abundance and the structure of its organic matter from two clasts. *Meteoritics & Planetary Science* 49:2064–2073.

Beck P., Maturilli A., Garenne A., Vernazza P., Helbert J., Quirico E., and Schmitt B. 2018. What is controlling the reflectance spectra (0.35–150 μm) of hydrated (and dehydrated) carbonaceous chondrites? *Icarus* 313:124–138.

Bibring J.-P., Hamm V., Langevin Y., Pilorget C., Arondel A., Bouzit M., Chaigneau M., Crane B., Darié A., Evesque C., Hansotte J., Gardien V., Gonnod L., Leclech J.-C., Meslier L., Redon T., Tamiatto C., Tosti S., and Thoores N. 2017. The micrOmega investigation onboard Hayabusa2. *Space Science Reviews* 208:401–412.

Binzel R. P., Perozzi E., Rivkin A. S., Rossi A., Harris A. W., Bus S. J., Valsecchi G. B., and Slivan S. M. 2004. Dynamical and compositional assessment of near-Earth object mission targets. *Meteoritics & Planetary Science* 39:351–366.

Bish D. L. and Duffy C. J. 1990. Thermogravimetric analysis of minerals. In *Thermal analysis in clay science*, edited by Stucki J. W. and Bish D. L. Boulder, Colorado: The Clay Minerals Society. pp. 96–157.

Bland P. A., Collins G. S., Davison T. M., Abreu N. M., Ciesla F. J., Muxworthy A. R., and Moore J. 2014. Pressure–temperature evolution of primordial solar system solids during impact-induced compaction. *Nature Communications* 5:5451. https://doi.org/10.1038/ncomms6451.

Bogard D. 1995. Impact ages of meteorites: A synthesis. *Meteoritics* 30:244–268.

Bogard D. D. 2011. K-Ar ages of meteorites: Clues to parent-body thermal histories. *Chemie der Erde* 71:207–226.

Brearley A. J. 1995. Aqueous alteration and brecciation in Bells, an unusual, saponite-bearing, CM chondrite. *Geochimica et Cosmochimica Acta* 59:2291–2317.

Brearley A. J. 2003. Nebular versus parent-body processing. In *Meteorites, comets, and planets*, edited by Davis A. M. Treatise in Geochemistry, Vol. 1, edited by Holland H. D. and Turekian K. K. Oxford: Elsevier-Pergamon. pp. 247–268.

Brearley A. J. 2006. The action of water. In *Meteorites and the early solar system II*, edited by Lauretta D. S. and McSween H. Y. Jr. Tucson, Arizona: University of Arizona Press. pp. 587–624.

Brearley A. J. 2014. Nebular versus parent-body processing. In *Meteorites, comets, and planets*, edited by Davis A. M. Treatise in Geochemistry, Vol. 1, 2nd ed., edited by Holland H. D. and Turekian K. K. Oxford: Elsevier-Pergamon. pp. 309–334.

Brearley A. J. and Jones R. H. 1998. Chondritic meteorites. In *Planetary materials*, edited by Papike J. J. Washington, D.C.: Mineralogical Society of America. pp. 3–01–3-398.

Briani G., Quirico E., Gounelle M., Paulhiac-Pison M., Montagnac G., Beck P., Orthous-Daunay F.-R., Bonal L., Jacquet E., Kearsley A., and Russell S. S. 2013. Short duration thermal metamorphism in CR chondrites. *Geochimica et Cosmochimica Acta* 122:267–279.

Browning L. B., McSween H. Y. Jr. and Zolensky M. E. 2000. On the origin of rim textures surrounding anhydrous

silicate grains in CM carbonaceous chondrites. *Meteoritics & Planetary Science* 35:1015–1023.

Buchanan P. C., Zolensky M. E., and Reid A. M. 1993. Carbonaceous chondrites clasts in the howardites Bholghati and EET87513. *Meteoritics* 28:659–682.

Bunch T. E. and Chang S. 1980. Carbonaceous chondrites - II. Carbonaceous chondrite phyllosilicates and light element geochemistry as indicators of parent body processes and surface conditions. *Geochimica et Cosmochimica Acta* 44:1543–1577.

Burton A. S., Glavin D. P., Elsila J. E., Dworkin J. P., Jenniskens P., and Yin Q.-Z. 2014. The amino acid composition of the Sutter's Mill CM2 carbonaceous chondrite. *Meteoritics & Planetary Science* 49:2074–2086.

Bunch T. E., Chang S., Frick U., Neil J., and Moreland G. 1979. Carbonaceous chondrites—I. Characterization and significance of carbonaceous chondrite (CM) xenoliths in the Jodzie howardite. *Geochimica et Cosmochimica Acta* 43:1727–1742.

Buseck P. R. and Hua X. 1993. Matrices of carbonaceous chondrite meteorites. *Annual Reviews of Earth and Planetary Sciences* 21:255–305.

Busemann H., Alexander C. M. O'D., and Nittler L. R. 2007. Characterization of insoluble organic matter in primitive meteorites by microRaman spectroscopy. *Meteoritics & Planetary Science* 42:1387–1416.

Campins H., de Léon J., Licandro J., Hendrix A., Sánchez J. A., and Ali-Lagoa V. 2018. Compositional diversity among primitive asteroids. In *Primitive meteorites and asteroids: Physical, chemical and spectroscopic observations paving the way for exploration*, edited by Abreu N. M. Cambridge, Massachusetts: Elsevier. pp. 345–369.

Chan Q. H. S., Zolensky M. E., Bodnar R. J., Farley C., and Cheung J. C. H. 2017. Investigation of organo-carbonate associations in carbonaceous chondrites by Raman spectroscopy. *Geochimica et Cosmochimica Acta* 201:392–409.

Che C., Glotch T. D., Bish D. L., Michalski J. R., and Xu W. 2011. Spectroscopic study of the dehydration and/or dehydroxylation of phyllosilicate and zeolite minerals. *Journal of Geophysical Research* 116:E05007.

Chizmadia L. J. and Brearley A. J. 2008. Mineralogy, aqueous alteration, and primitive textural characteristics of fine-grained rims in the Y-791198 CMS carbonaceous chondrite: TEM observations and comparison to ALHA81002. *Geochimica et Cosmochimica Acta* 72:602–625.

Choe W. H., Huber H., Rubin A. E., Kallemeyn G. W., and Wasson J. T. 2010. Compositions and taxonomy of 15 unusual carbonaceous chondrites. *Meteoritics & Planetary Science* 45:531–554.

Christensen P. R., Hamilton V. E., Mehall G. L., Pelham D., O'Donnell W., Anwar S., Bowles H., Chase S., Fahlgren J., Farkas Z., Fisher T., James O., Kubik I., Lazbin I., Miner M., Rassas M., Schulze L., Shamordola K., Tourville T., West G., Woodward R., and Lauretta D. 2018. The OSIRIS-REx Thermal Emission Spectrometer (OTES) instrument. *Space Science Reviews* 214:87.

Clark B. E., Binzel R. P., Howell E. S., Cloutis E. A., Ockert-Bell M., Christensen P., Barucci M. A., DeMeo F., Lauretta D. S., Connolly H. Jr., Soderberg A., Hergenrother C., Lim L., Emery J., and Mueller M. 2011. Asteroid (101955) 1999 RQ36: Spectroscopy from 0.4 to 2.4 μm and meteorite analogs. *Icarus* 216:462–475.

Cloutis E. A., Hudon P., Hiroi T., and Gaffey M. J. 2012. Spectral reflectance properties of carbonaceous chondrites 4: Aqueously altered and thermally metamorphosed meteorites. *Icarus* 220:586–617.

Cloutis E. A., Izawa M. R. M., and Beck P. 2018. Reflectance spectroscopy of chondrites. In *Primitive meteorites and asteroids: Physical, chemical and spectroscopic observations paving the way for exploration*, edited by Abreu A. N. M. Cambridge, Massachusetts: Elsevier. pp. 273–343.

Cody G. D., Alexander C. M. O'D., Yabuta H., Kilcoyne A. L. D., Araki T., Ade H., Dera R., Fogel M., Militzer B., and Mysen B. O. 2008. Organic thermometry for chondritic parent bodies. *Earth and Planetary Science Letters* 272:446–455.

Corrigan C. M., Zolensky M. E., Dahl J., Long M., Weir J., Sapp C., and Burkett P. J. 1997. The porosity and permeability of chondritic meteorites and interplanetary dust particles. *Meteoritics & Planetary Science* 32:509–515.

Davison T. M., Ciesla F. J., and Collins G. S. 2012. Post-impact thermal evolution of porous planetesimals. *Geochimica et Cosmochimica Acta* 95:252–269.

Deer W. A., Howie R. A., and Zussman J. 1962. *Rock forming minerals.* London: Longmans, Green and Co Ltd. 270 p.

Delbo M. and Michel P. 2011. Temperature history and dynamical evolution of (101955) 1999 RQ 36: A potential target for sample return from a primitive asteroid. *Astrophysical Journal Letters* 728:L42–L46.

Delbo M., Libourel G., Wilkerson J., Murdoch N., Michael P., Ramesh K. T., Ganino C., Verat C., and Marchi S. 2014. Thermal fatigue as the origin of regolith on small asteroids. *Nature* 508:233–236.

de Leuw S., Rubin A. E., Schmitt A. K., and Wasson J. T. 2009. ^{53}Mn-^{53}Cr systematics of carbonates in CM chondrites: Implications for the timing and duration of aqueous alteration. *Geochimica et Cosmochimica Acta* 73:7433–7442.

de Leuw S., Rubin A. E., and Wasson J. T. 2010. Carbonates in CM chondrites: Complex formation histories and comparison to carbonates in CI chondrites. *Meteoritics & Planetary Science* 45:513–530.

de Léon J., Campins H., Morate D., De Prá M., Ali-Lagoa V., Licandro J., Rizos J. L., Pinilla-Alonso N., DellaGiustina D. N., Lauretta D. S., Popescu M., and Lorenzi V. 2018. Expected spectral characteristics of (101955) Bennu and (162173) Ryugu, targets of the OSIRIS-REx and Hayabusa2 missions. *Icarus* 313:25–37.

DellaGiustina D. N., Emery J. P., Golish D. R., Rozitis B., Bennett C. A., Burke K. N., Ballouz R.-L., Becker K. J., Christensen P. R., Drouet d'Aubigny C. Y., Hamilton V. E., Reuter D. C., Rizk B., Simon A. A., Asphaug E., Bandfield J. L., Barnouin O. S., Barucci M. A., Bierhaus E. B., Binzel R. P., Bottke W. F., Bowles N. E., Campins H., Clark B. C., Clark B. E., Connolly H. C. Jr., Daly M. G., de Delbo' M., Deshapriya J. D. P., Elder C. M., Fornasier S., Hergenrother C. W., Howell E. S., Jawin E. R., Kaplan H. H., Kareta T. R., Le Corre L., Li J.-Y., Licandro J., Lim L. F., Michel P., Molaro J., Nolan M. C., Pajola M., Popescu M., Rizos Garcia J. L., Ryan A., Schwartz S. R., Shultz N., Siegler M. A., Smith P. H., Tatsumi E., Thomas C. A., Walsh K. J., Wolner C. W. V., Zou X.-D., Lauretta D. S. and The OSIRIS-REx Team. 2019. Properties of rubble-pile asteroid (101955) Bennu from OSIRIS-REx imaging and thermal analysis. *Nature Astronomy* 3:341–351.

DellaGiustina D. N., Burke K. N., Walsh K. J., Smith P. H., Golish D. R., Bierhaus E. B., Ballouz R.-L., Becker T. L.,

Campins H., Tatsumi E., Yumoto K., Sugita S., Prasanna D. J. D., Cloutis E. A., Clark B. E., Hendrix A. R., Sen A., Al Asad M. M., Daly M. G., Applin D. M., Avdellidou C., Barucci M. A., Becker K. J., Bennett C. A., Bottke W. F., Brodbeck J. I., Connolly H. C. Jr., Delbo' M., de Leon J., Drouet d'Aubigny C. Y., Edmundson K. L., Fornasier S., Hamilton V. E., Hasselmann P. H., Hergenrother C. W., Howell E. S., Jawin E. R., Kaplan H. H., Le Corre L., Lim L. F., Li J.-Y., Nolau J., Pajola M., Parkinson A., Popescu M., Porter N. A., Rizk B., Rizos Garcia J. L., Ryan A., Rozitis B., Shultz N. K., Simon A. A., Trang D., Van Auken R. B., Wolner C. W. V., and Lauretta D. S. 2020. Variations in color and reflectance on the surface of asteroid (101955) Bennu. *Science* 370:eabc3660. https://doi.org/10.1126/science.abc3660.

DuFresne E. R. and Anders E. 1962. On the chemical evolution of the carbonaceous chondrites. *Geochimica et Cosmochimica Acta* 26:1085–1114.

Dunn J. G. and Chamberlin A. C. 1991. The effect of stoichiometry on the ignition behaviour of synthetic pyrrhotite. *Journal of Thermal Analysis* 37:1329–1346.

Dunn J. G. 1997. The oxidation of sulphide minerals. *Thermochimica Acta* 300:127–139.

Dunn J. G. and Mackey L. C. 1991. The measurement of ignition temperatures and extents of reaction on iron and iron nickel sulfides. *Journal of Thermal Analysis* 37:2143–2164.

Dyl K. A., Bischoff A., Ziegler K., Young E. D., Wimmer K., and Bland P. A. 2012. Early solar system hydrothermal activity in chondritic asteroids in 1–10-year timescales. *Proceedings of the National Academy of Sciences* 109:18,306–18,311.

Ebert S., Bischoff A., Harries D., Lentfort S., Barrat J.-A., Pack A., Gattacceca J., Visser R., Schmid-Beurmann P., and Kimpel S. 2019. Northwest Africa 11024—A heated and dehydrated unique carbonaceous (CM) Chondrite. *Meteoritics & Planetary Science* 54:328–356.

Endreß M. and Bischoff A. 1993. Mineralogy, degree of brecciation, and aqueous alteration of CI chondrites Orgueil, Ivuna, and Alais. *Meteoritics* 28:345–346.

Eugster O., Eberhardt P., Thalmann C. H., and Weigel A. 1998. Neon-E in CM-2 chondrite LEW90500 and collisional history of CM-2 chondrites, Maralinga, and other CK chondrites. *Geochimica et Cosmochimica Acta* 62:2573–2582.

Faust G. T. and Fahey J. J. 1962. The Serpentine-Group Minerals. *U.S. Geological Survey Professional Paper* 384-A:99.

Fuchs L. H., Olsen E., and Jensen K. J. 1973. Mineralogy, mineral-chemistry, and composition of the Murchison (C2) meteorite. *Smithsonian Contributions to Earth Sciences* 10:39.

Fujiwara A., Kawaguchi J., Yeomans D. K., Abe M., Mukai T., Okada T., Saito J., Yano H., Yoshikawa M., Scheeres D. J., Barnouin-Jha O., Cheng A. F., Demura H., Gaskell R. W., Hirata N., Ikeda H., Kominato T., Miyamoto H., Nakamura A. M., Nakamura R., Sasaki S., and Uesugi K. 2006. The rubble-pile asteroid Itokawa as observed by Hayabusa. *Science* 312:1330–1334.

Garenne A., Beck P., Montes-Hernandez G., Chirc R., Toche F., Quirico E., Bonal L., and Schmitt B. 2014. The abundance and stability of "water" in type 1 and 2 carbonaceous chondrites (CI, CM and CR). *Geochimica et Cosmochimica Acta* 137:93–112.

Garenne A., Beck P., Montes-Hernandez G., Brissaud O., Schmitt B., Quirico E., Bonal L., Beck C., and Howard K. T. 2016. Bidirectional reflectance spectroscopy of carbonaceous chondrites: Implications for water quantification and primary composition. *Icarus* 264:172–183.

Glavin D. P. and Dworkin J. P. 2009. Enrichment of the amino acid L-isovaline by aqueous alteration on CI and CM meteorite parent bodies. *Proceedings of the National Academy of Sciences* 106:5487–5492.

Glavin D. P., Alexander C. M. O'D., Aponte J. C., Dworkin J. P., Elsila J. E., and Yabuta H. 2018. The origin and evolution of organic matter in carbonaceous chondrites and links to their parent bodies. In *Primitive meteorites and asteroids: Physical, chemical and spectroscopic observations paving the way for exploration*, edited by Abreu N. M. Cambridge, Massachusetts: Elsevier. pp. 205–271.

Gounelle M. and Zolensky M. 2001. A terrestrial origin for sulfate veins in CI1 chondrites. *Meteoritics & Planetary Science* 36:1321–1329.

Gounelle M., Zolensky M. E., Liou J.-C., Bland P. A., and Alard O. 2003. Mineralogy of carbonaceous chondritic microclasts in howardites: Identification of C2 fossil micrometeorites. *Geochimica et Cosmochimica Acta* 67:507–527.

Grady M. M. 2000. *Catalog of meteorites*, 5th ed. Cambridge, UK: Cambridge University Press. 689 p.

Green R. O., Ehlmann B. L., Fraeman A. A., Blaney D., Liu Y., Chabot N. L., Murchie S., Wadhwa M., Herd C. D. K., Velbel M. A., Mouroulis P., and Van Gorp B. 2015. Microimaging spectroscopy for the exploration of small bodies: First laboratory measurements of carbonaceous chondrite and HED meteorites and a proposed M6 instrument for in situ measurement (abstract #2154). 46th Lunar and Planetary Science Conference. CD-ROM.

Greenberger R., Mustard J. F., Ehlmann B. L., Blaney D. L., Cloutis E. A., Wilson J. H., Green R. O., and Fraeman A. A. 2015. Imaging spectroscopy of geological samples and outcrops: Novel insights from microns to meters. *GSA Today* 25:4–10. https://doi.org/10.1130/GSATG252A.1.

Grossman J. N., Zolensky M. E., and Tonui E. K. 2005. What are the petrologic types of thermally metamorphosed CM chondrites? (abstract #5169). 68th Annual Meteoritical Society Meeting.

Grott M., Knollenberg J., Hamm M., Ogawa K., Jaumann R., Otto K. A., Delbo M., Michel P., Biele J., Neumann W., Knapmeyer M., Kührt E., Senshu H., Okada T., Helbert J., Maturilli A., Müller N., Hagermann A., Sakatani N., Tanaka S., Arai T., Mottola S., Tachibana S., Pelivan I., Drube L., Vincent J.-B., Yano H., Pilorget C., Matz K. D., Schmitz N., Koncz A., Schröder S. E., Trauthan F., Schlotterer M., Krause C., Ho T.-M., and Moussi-Soffys A. 2019. Low thermal conductivity boulder with high porosity identified on C-type asteroid (162173) Ryugu. *Nature Astronomy* 3:971–976.

Guggenheim S. and Koster van Groos A. F. 2001. Baseline studies of The Clay Mineral Society Source Clays: Thermal analysis. *Clays and Clay Minerals* 49:433–443.

Haack H., Grau T., Bischoff A., Horstmann M., Wasson J., Sørensen A., Laubenstein M., Ott U., Palme H., Gellissen M., Greenwood R. C., Pearson V. K., Franchi I. A., Gabelica Z., and Schmity-Kopplin P. 2012. Maribo—A new CM fall from Denmark. *Meteoritics & Planetary Science* 47:30–50.

Hamilton V. E., Simon A. A., Christensen P. R., Reuter D. C., Clark B. E., Barucci M. A., Bowles N. E., Boynton W. V., Brucato J. R., Cloutis E. A., Connolly H. C. Jr., Donaldson Hanna K. L., Emery J. P., Enos H. L., Fornasier S., Haberle C. W., Hanna R. D., Howell E. S., Kaplan H. H., Keller L. P., Lantz C., Li J.-Y., Lim L. F., McCoy T. J., Merlin F., Nolan M. C., Praet A., Rozitis B., Sandford S. A., Schrader D. L., Thomas C. A., Zou X.-D., Lauretta D. S., and the OSIRIS-REx Team. 2019. Evidence for widespread hydrated minerals on asteroid (101955) Bennu. *Nature Astronomy* 3:332–340.

Hanowski N. P. and Brearley A. J. 2001. Aqueous alteration of chondrules in the CM carbonaceous chondrite, Allan Hills 81002: Implications for parent body alteration. *Geochimica et Cosmochimica Acta* 65:495–518.

Haramura H., Kushiro I., and Yanai K. 1983. Chemical compositions of Antarctic meteorites I. *Proceedings of the Eighth symposium on Antarctic meteorites, Memoirs of National Institute of Polar Research* 30:109–121.

Hasegawa S., Müller T. G., Kawakami K., Kasuga T., Wada T., Ita Y., Takato N., Terada H., Fujiyoshi T., and Abe M. 2008. Albedo, size, and surface characteristics of Hayabusa-2 sample-return target 162173 1999 JU$_3$ from AKARI and Subaru observations. *Publications of the Astronomical Society of Japan* 60:S399–S405.

Herd C. D. K., Blinova A., Simkus D. N., Huang Y., Tarozo R., Alexander C. M. O'D., Gyngard F., Nittler L. R., Cody G. D., Fogel M. L., Kebukawa Y., Kilcoyne A. L. D., Hilts R. W., Slater G. F., Glavin D. P., Dworkin J. P., Callahan M. P., Elsila J. E., De Gregorio B. T., and Stroud R. M. 2011. Origin and evolution of prebiotic organic matter as inferred from the Tagish Lake meteorite. *Science* 322:1304–1307.

Hergenrother C. W., Maleszewski C., Li J.-Y., Pajola M., Chesley S. R., French A. S., Davis A. B., Pelgrift J. Y., Leonard J. M., Shelly F., Liounis A. J., Becker K., Balram-Knutson S. S., Garcia R., Kareta T. R., Adam C., Alkiek K., Bos B. J., Brozović M., Burke K. N., Christensen E., Clark B. E., DellaGiustina D. N., Drouet d'. A. C., Farnocchia D., Howell E. S., Jacobson R. A., Kidd J. N., Lessac-Chenen E. J., Melikyan R., Nolan M. C., Park R. S., Selznick S., Rizk B., and Lauretta D. S. 2020. Photometry of particles ejected from active asteroid (101955) Bennu. *Journal of Geophysical Research: Planets* 125:e2020JE006381.

Hewins R. H., Bourot-Denise M., Zanda B., Leroux H., Barrat J.-A., Humayan M., Göpel G., Greenwood R. C., Franchi I. A., Pont S., Lorand J.-P., Cournède C., Gattacceca J., Rochette P., Kuga M., Marrocchi Y., and Marty B. 2014. The Paris meteorite, the least altered CM chondrite so far. *Geochimica et Cosmochimica Acta* 124:190–222.

Hiroi T., Pieters C. M., Zolensky M. E., and Lipschutz M. E. 1993. Evidence of thermal metamorphism on the C, G, B, and F asteroids. *Science* 261:1016–1018.

Hiroi T., Pieters C. M., Zolensky M. E., and Lipschutz M. E. 1994. Possible thermal metamorphism on the C, G, B, and F asteroids detected from their reflectance spectra in comparison with carbonaceous chondrites. *Proceedings of the NIPR Symposium on Antarctic Meteorites* 7:230–243.

Hiroi T., Zolensky M. E., Pieters C. M., and Lipschutz M. E. 1996. Thermal metamorphism of the C, G, B, and F asteroids seen from the 0.7 μm, 3 μm, and UV absorption strengths in comparison with carbonaceous chondrites. *Meteoritics & Planetary Science* 3:321–327.

Ho T.-M., Baturkin Y., Grimm C., Grundmann J. T., Hobbie C., Ksenik E., Lange C., Sasaki K., Schlotterer M., Talapina M., Termtanasombat N., Wejmo E., Witte L., Wrasmann M., Wübbels G., Rößler J., Ziach C., Findlay R., Biele J., Krause C., Ulamec S., Lange M., Mierheim O., Lichtenheldt R., Maier M., Reill J., Sedlmayr H.-J., Bousquet P., Bellion A., Bompis O., Cenac-Morthe C., Muriel D. M., Fredon S., Jurado E., Canalias E., Jaumann R., Bibring J.-P., Glassmeier K. H., Hercik D., Grott M., Celotti L., Cordero F., Hendrikse J., and Okada T. 2017. MASCOT—The Mobile Asteroid Surface Scout onboard the Hayabusa2 Mission. *Space Science Reviews* 208:339–374.

Howard K. T., Benedix G. K., Bland P. A., and Cressey G. 2009. Modal mineralogy of CM2 chondrites by X-ray diffraction (PSD-XRD). Part 1: Total phyllosilicate abundance and the degree of aqueous alteration. *Geochimica et Cosmochimica Acta* 73:4576–4589.

Howard K. T., Benedix G. K., Bland P. A., and Cressey G. 2011. Modal mineralogy of CM2 chondrites by X-ray diffraction (PSD-XRD). Part 2: Degree, nature and settings of aqueous alteration. *Geochimica et Cosmochimica Acta* 75:2735–2751.

Howard K. T., Alexander C. M. O'D., Schrader D. L., and Dyl K. A. 2015. Classification of hydrous meteorites (CR, CM and C2 ungrouped) by phyllosilicate fraction: PSD-XRD modal mineralogy and planetesimal environments. *Geochimica et Cosmochimica Acta* 149:206–222.

Hršak D., Malina J., and Hadžlpašlć A. B. 2005. The decomposition of serpentine by thermal treatment. *Materiali in Tehnologije* 39:225–227.

Hršak D., Sučik G., and Lazić L. 2008. The thermophysical properties of serpentinite. *Metallurgia* 47:29–31.

Hutchison R. 2004. *Meteorites: A petrologic, chemical and isotopic synthesis*. Cambridge, UK: Cambridge University Press. 506 p.

Ikeda Y. 1992. An overview of the research consortium, "Antarctic carbonaceous chondrites with CI affinities, Yamato-86720, Yamato-82162, and Belgica-7904." *National Institute of Polar Research* 5:49–73.

Ikeda Y., Noguchi T., and Kimura M. 1992. Petrology and mineralogy of the Yamato-86720 carbonaceous chondrite. *National Institute of Polar Research* 5:136–154.

Iwata T., Kitazato K., Abe M., Ohtake M., Arai T., Arai T., Hirata N., Hiroi T., Honda C., Imae N., Komatsu M., Matsunaga T., Matsuoka M., Matsuura S., Nakamura T., Nakato A., Nakauchi Y., Osawa T., Senshu H., Takagi Y., Tsumura K., Takato N., Watanabe S.-I., Barucci M. A., Palomba E., and Ozaki M. 2017. NIRS3: The Near Infrared Spectrometer on Hayabusa2. *Space Science Reviews* 208:317–337.

Jarosewich E. 1990. Chemical analyses of meteorites: A compilation of stony and iron meteorite analyses. *Meteoritics* 25:323–337.

Jaumann R., Schmitz N., Koncz A., Michaelis H., Schröder S. E., Mottola S., Trauthan F., Hoffmann H., Roatsch T., Job D., Kachlicki J., Pforte B., Terzer R., Tschentscher M., Weisse S., Mueller U., Perez-Prieto L., Broll B., Kruselburger A., Ho T.-M., Biele J., Ulamec S., Krause C., Grott M., Bibring J.-P., Watanabe S., Sugita S., Okada T., Yoshikawa M., and Yabuta H. 2017. The camera of the MASCOT asteroid lander on board Hayabusa 2. *Space Science Reviews* 208:375–400.

Jaumann R., Schmitz N., Ho T.-M., Schröder S. E., Otto K. A., Stephan K., Elgner S., Krohn K., Preusker F.,

Scholten F., Biele J., Ulamec S., Krause C., Sugita S., Matz K.-D., Roatsch T., Parekh R., Mottola S., Grott M., Michel P., Trauthan F., Koncz A., Michaelis H., Lange C., Grundmann T. C., Maibaum M., Sasaki K., Wolff F., Reill J., Moussi-Soffys A., Lorda L., Neumann W., Vincent J.-B., Wagner R., Bibring J.-P., Kameda S., Yano H., Watanabe S., Yoshikawa M., Tsuda Y., Okada T., Yoshimitsu T., Mimasu Y., Saiki T., Yabuta H., Rauer H., Honda R., Morota T., Yokota Y., and Kouyama T. 2019. Images from the surface of asteroid Ryugu show rocks similar to carbonaceous chondrite meteorites. *Science* 365:817–820.

Jenniskens P., Fries M. D., Yin Q.-Z., Zolensky M., Krot A. N., Sandford S. A., Sears D., Beauford R., Ebel D. S., Friedrich J. M., Nagashima K., Wimpenny J., Yamakawa A., Nishiizumi K., Hamajima Y., Caffee M. W., Welten K. C., Laubenstein M., Davis A. M., Simon S. B., Heck P. R., Young E. D., Kohl I. E., Thiemens M. H., Nunn M. H., Mikouchi T., Hagiya K., Ohsumi K., Cahill T. A., Lawton J. A., Barnes D., Steele A., Rochette P., Verosub K. L., Gattacceca J., Cooper G., Glavin D. P., Burton A. S., Dworkin J. P., Elsila J. E., Pizzarello S., Ogliore R., Schmitt-Kopplin P., Harir M., Hertkorn N., Verchovsky A., Grady M., Nagao K., Okazaki R., Takechi H., Hiroi T., Smith K., Silber E. A., Brown P. G., Albers J., Klotz D., Hankey M., Matson R., Fries J. A., Walker R. J., Puchtel I., Lee C.-T., Erdman M. E., Eppich G. R., Roeske S., Gabelica Z., Lerche M., Nuevo M., Girten B., and Worden S. P. (the Sutter's Mill Meteorite Consortium). 2012. Radar-enabled recovery of the Sutter's Mill meteorite, a carbonaceous chondrite regolith breccia. *Science* 338:1583–1587.

Kameda S., Suzuki H., Takamatsu T., Cho Y., Yasuda T., Yamada M., Sawada H., Honda R., Morota T., Honda C., Sato M., Okumura Y., Shibasaki K., Ikezawa S., and Sugita S. 2017. Preflight calibration test results for optical navigation camera telescope (ONC-T) onboard the Hayabusa2 spacecraft. *Space Science Reviews* 208:17–31.

Kaplan H. H. and Milliken R. E. 2016. Reflectance spectroscopy for organic detection and quantification in clay-bearing samples: Effects of albedo, clay type, and water content. *Clays and Clay Minerals* 64:167–184.

Kaplan H. H., Hamilton V. E., Howell E. S., Anderson F. S., Barruci M. A., Brucato J., Burbine T. H., Clark B. E., Cloutis E. A., Connolly H. C., Dotto E., Emery J. P., Fornasier S., Lantz C., Lim L. F., Merlin F., Praet A., Reuter D. C., Sandford S. A., and Simon A. A. 2020. Visible–near infrared spectral indices for mapping mineralogy and chemistry with OSIRIS-REx. *Meteoritics & Planetary Science* 55:744–765.

Kawano M. and Tomita K. 1991. Dehydration and rehydration of saponite and vermiculite. *Clays and Clay Minerals* 39:174–183.

Keane J. T. 2019. The geologic history of Bennu. *Nature Geoscience* 12:226.

Kebukawa Y., Nakashima S., Otsuka T., Nakamura-Messenger K., and Zolensky M. E. 2009. Rapid contamination during storage of carbonaceous chondrites prepared for micro FTIR measurements. *Meteoritics & Planetary Science* 44:545–557.

Kimura M. and Ikeda Y. 1992. Mineralogy and petrology of an unusual Belgica-7904 carbonaceous chondrite: Genetic relationships among the components. *Proceedings of the NIPR Symposium on Antarctic Meteorites* 5:74–119.

King A. J., Solomon J. R., Schofield P. F., and Russell S. S. 2015a. Characterising the CI and CI-like carbonaceous chondrites using thermogravimetric analysis and infrared spectroscopy. *Earth, Planets and Space* 67:198.

King A. J., Schofield P. F., Howard K. T., and Russell S. S. 2015b. Modal mineralogy of CI and CI-like chondrites by X-ray diffraction. *Geochimica et Cosmochimica Acta* 165:148–160.

King A. J., Schofield P. F., and Russell S. S. 2017. Type 1 aqueous alteration in CM carbonaceous chondrites: Implications for the evolution of water-rich asteroids. *Meteoritics & Planetary Science* 52:1197–1215.

King A. J., Bates H. C., Krietsch K., Busemann H., Clay P. L., Schofield P. F., and Russell S. S. 2019a. The Yamato-type (CY) carbonaceous chondrite group: Analogues for the surface of asteroid Ryugu? *Geochemistry* 79:125531.

King A. J., Russell S. S., Schofield P. F., Humphreys-Williams E. R., Stekopytov S., Abernathy F. A. J., Verchovsky A. B., and Grady M. M. 2019b. The alteration history of the Jbilet Winselwan CM carbonaceous chondrite: An analog for C-type asteroid sample return. *Meteoritics & Planetary Science* 54:521–543.

Kiryu K., Kebukawa Y., Igisu M., Shibuya T., Zolensky M. E., and Kobayashi K. 2020. Kinetics in thermal evolution of Raman spectra of chondritic organic matter to evaluate thermal history of their parent bodies. *Meteoritics & Planetary Science* 55:1848–1864.

Kitazato K., Milliken R. E., Iwata T., Abe M., Ohtake M., Matsuura S., Arai T., Nakauchi Y., Nakamura T., Matsuoka M., Senshu H., Hirata N., Hiroi T., Pilorget C., Brunetto R., Poulet F., Riu L., Bibring J.-P., Takir D., Domingue D. L., Vilas F., Barucci M. A., Perna D., Palomba E., Galiano A., Tsumura K., Osawa T., Komatsu M., Nakato A., Arai T., Takato N., Matsunaga T., Takagi Y., Matsumoto K., Kouyama T., Yokota Y., Tatsumi E., Sakatani N., Yamamoto Y., Okada T., Sugita S., Honda R., Morota T., Kameda S., Sawada H., Honda C., Yamada M., Suzuki H., Yoshioka K., Hayakawa M., Ogawa K., Cho Y., Shirai K., Shimaki Y., Hirata N., Yamaguchi A., Ogawa N., Terui F., Yamaguchi T., Takei Y., Saiki T., Nakazawa S., Tanaka S., Yoshikawa M., Watanabe S., and Tsuda Y. 2019. The surface composition of asteroid 162173 Ryugu from Hayabusa2 near-infrared spectroscopy. *Science* 364:272–275.

Kojima H., Ikeda Y., and Yanai K. 1984. The alteration of chondrules and matrices in new Antarctic carbonaceous chondrites. *Proceedings of the 9th symposium on Antarctic meteorites, Memoirs of National Institute of Polar Research* 35:184–199.

Krot A. N., Keil K., Goodrich C. A., Scott E. R. D. and Weisberg M. K. 2005. Classification of meteorites. In *Meteorites, comets, and planets*, edited by Davis A. M. Treatise in Geochemistry, Vol. 1, edited by Holland H. D. and Turekian K. K. Oxford: Elsevier-Pergamon. pp. 83–128.

Lantz C., Binzel R. P., and DeMeo F. E. 2018. Space weathering trends on carbonaceous asteroids: A possible explanation for Bennu's blue slope? *Icarus* 302:10–17.

Lauretta D. S., Bartels A. E., Barucci M. A., Bierhaus E. B., Binzel R. P., Bottke W. F., Campins H., Chesley S. R., Clark B. C., Clark B. E., Cloutis E. A., Connolly H. C., Crombie M. K., Delbo M., Dworkin J. P., Emery J. P., Glavin D. P., Hamilton V. E., Hergenrother C. W., Johnson C. L., Keller L. P., Michel P., Nolan M. C.,

Sandford S. A., Scheeres D. J., Simon A. A., Sutter B. M., Vokrouhlicky D., and Walsh K. J. 2015. The OSIRIS-REx target asteroid (101955) Bennu: Constraints on its physical, geological, and dynamical nature from astronomical observations. *Meteoritics & Planetary Science* 50:834–849.

Lauretta D. S., Balram-Knutson S. S., Beshore E., Boynton W. V., Drouet d'. A. C., DellaGiustina D. N., Enos H. L., Gholish D. R., Hergenrother C. W., Howell E. S., Bennett C. A., Morton E. T., Nolan M. C., Rizk B., Roper H. L., Bartels A. E., Bos B. J., Dworkin J. P., Highsmith D. E., Lorenz D. A., Lim L. F., Mink R., Moreau M. C., Nuth J. A., Reuter D. C., Simon A. A., Bierhaus E. B., Bryan B. H., Ballouz R., Barnouin O. S., Binzel R. P., Bottke W. F., Hamilton V. E., Walsh K. J., Chesley S. R., Christensen P. R., Clark B. E., Connolly H. C., Crombie M. K., Daly M. G., Emery J. P., McCoy T. J., McMahon J. W., Scheeres D. J., Messenger S., Nakamura-Messenger K., Righter K., and Sandford S. A. 2017. OSIRIS-REx: Sample return from asteroid (101955) Bennu. *Space Science Reviews* 212:925–984.

Lauretta D. S., Hergenrother C. W., Chesley S. R., Leonard J. M., Pelgrift J. Y., Adam C. D., Al Asad M., Antreasian P. G., Ballouz R.-L., Becker K. J., Bennett C. A., Bos B. J., Bottke W. F., Brozović M., Campins H., Connolly H. C. Jr., Daly M. G., Davis A. B., de León J., DellaGiustina D. N., Drouet d'Aubigny C. Y., Dworkin J. P., Emery J. P., Farnocchia D., Glavin D. P., Golish D. R., Hartzell C. M., Jacobson R. A., Jawin E. R., Jenniskens P., Kidd J. N. Jr., Lessac-Chenen E. J., Li J.-Y., Libourel G., Licandro J., Liounis A. J., Maleszewski C. K., Manzoni C., May B., McCarthy L. K., McMahon J. W., Michel P., Molaro J. L., Moreau M. C., Nelson D. S., Owen W. M. Jr., Rizk B., Roper H. L., Rozitis B., Sahr E. M., Scheeres D. J., Seabrook J. A., Selznick S. H., Takahashi Y., Thuillet F., Tricarico P., Vokrouhlický D., and Wolner C. W. V. 2019. Episodes of particle ejection from the surface of the active asteroid (101955) Bennu. *Science* 366:eaay3544.

Lauretta D. S., Hua X., and Buseck P. R. 2000. Mineralogy of fine-grained rims in the ALH 81002 CM chondrite. *Geochimica et Cosmochimica Acta* 64:3263–3273.

Lee M. R., Lindgren P., Sofe M. R., Alexander C. M. O'D., and Wang J. 2012. Extended chronologies of aqueous alteration in the CM2 carbonaceous chondrites: Evidence from carbonates in Queen Alexandra Range 93005. *Geochimica et Cosmochimica Acta* 92:148–169.

Lee M. R., Lindgren P., and Sofe M. R. 2014. Aragonite, bruennerite, calcite and dolomite in the CM carbonaceous chondrites: High fidelity recorders of progressive parent body aqueous alteration. *Geochimica et Cosmochimica Acta* 144:126–156.

Lee M. R., Lindgren P., King A. J., Greenwood R. C., Franchi I. A., and Sparkes R. 2016. Elephant Moraine 96029, a very mildly aqueously altered and heated CM carbonaceous chondrite: Implications for the drivers of parent body processing. *Geochimica et Cosmochimica Acta* 187:237–259.

Lee M. R., Cohen B. E., King A. J., and Greenwood R. C. 2019. The diversity of CM carbonaceous chondrite parent bodies explored using Lewis Cliff 85311. *Geochimica et Cosmochimica Acta* 264:224–244.

Lee M. R. and Lindgren P. 2016. Aqueous alteration of chondrules from the Murchison CM carbonaceous chondrite: Replacement, pore filling, and the genesis of polyhedral serpentine. *Meteoritics & Planetary Science* 51:1003–1021.

Lentfort S., Bischoff A., Ebert S., and Patzek M. 2021. Classification of CM chondrite breccias—Implications for the evaluation of samples from the OSIRIS-REx and Hayabusa 2 missions. *Meteoritics & Planetary Science* 56:127–147.

Leroux H., Cuvillier P., Zanda B., and Hewins R. H. 2015. GEMS-like material in the matrix of the Paris meteorite and the early stages of alteration of CM chondrites. *Geochimica et Cosmochimica Acta* 170:247–265.

Licandro J., Campins H., Mothé-Diniz T., Pinilla-Alonso N., and de León J. 2007. The nature of comet-asteroid transition object (3200) Phaethon. *Astronomy & Astrophysics* 461:751–757.

Lindgren P., Hanna R. D., Dobson K. J., Tomkinson T., and Lee M. R. 2015. The paradox between low shock-stage and evidence for compaction in CM carbonaceous chondrites explained by multiple low-intensity impacts. *Geochimica et Cosmochimica Acta* 148:159–178.

Lipschutz M. E., Zolensky M. E., and Bell M. S. 1999. New petrographic and trace element data on thermally metamorphosed carbonaceous chondrites. *Antarctic Meteorite Research* 12:57–80.

Losiak A. I. and Velbel M. A. 2011. Evaporite formation during the weathering of Antarctic meteorites—A weathering census analysis based on the ANSMET database. *Meteoritics & Planetary Science* 46:443–458. https://doi.org/10.1111/j.1945-5100.2010.01166.x.

Marchi S., Delbo M., Morbidelli A., Paolicchi P., and Lazzarin M. 2009. Heating of near-Earth objects and meteoroids due to close approaches to the Sun. *Monthly Notices of the Royal Astronomical Society* 400:147–153.

Marrocchi M., Gounelle M., Blanchard I., Caste F., and Kearsley A. T. 2014. The Paris CM chondrite: Secondary minerals and asteroidal processing. *Meteoritics & Planetary Science* 49:1232–1249.

Martinez E. 1961. The effect of particle size on the thermal properties of serpentine minerals. *American Mineralogist* 46:901–912.

Matsumoto M., Tsuchiyama A., Nakato A., Matsuno J., Miyake A., Kataoka A., Ito M., Tomioka N., Kodama Y., Uesugi K., Takeuchi A., Nakano T., and Vaccaro E. 2019. Discovery of fossil asteroidal ice in primitive meteorite Acfer 094. *Science Advances* 5:eaax5078.

Matsuoka K., Nakamura T., Nakamuta Y., and Takaoka N. 1996. Yamato-86789: A heated CM-like carbonaceous chondrite. *Proceedings of the NIPR Symposium on Antarctic Meteorites* 9:20–36.

Mazanek D. D., Reeves D. M., Abell P. A., Asphaug E., Abreu N. M., Bell J. F., Bottke W. F., Britt D. T., Campins H., Chodas P. W., Ernst C. M., Fries M. D., Gertsch L. S., Glavin D. P., Hartzell C. M., Hendrix A. R., Nuth J. A., Scheeres D. J., Sercel J. C., Takir D., and Zacny K. 2016. Asteroid Redirect Mission (ARM) Formulation Assessment and Support Team (FAST). Final Report. NASA Technical Memorandum TM-2016-210911, 130 p.

Mazor E., Heymann D., and Anders E. 1970. Noble gases in carbonaceous chondrites. *Geochimica et Cosmochimica Acta* 34:781–824.

McAdam M., Sunshine J. M., Howard K. T., and McCoy T. M. 2015. Aqueous alteration on asteroids: Linking the mineralogy and spectroscopy of CM and CI chondrites. *Icarus* 245:320–332.

McSween H. Y. Jr. 1979. Alteration in CM carbonaceous chondrites inferred from modal and chemical variations in matrix. *Geochimica et Cosmochimica Acta* 43:1761–1770.

McSween H. Y. Jr. and Richardson S. M. 1977. The composition of carbonaceous chondrite matrix. *Geochimica et Cosmochimica Acta* 41:1145–1161.

Meier M. M. M. 2017. Meteoriteorbits.info—Tracking all known meteorites with photographic orbits (abstract #1178). 48th Lunar and Planetary Science Conference. CD-ROM.

Metzler K. 1995. Aqueous alteration of primary rock on the CM parent body (abstract #1481). 26th Lunar and Planetary Science Conference. CD-ROM.

Metzler K., Bischoff A., and Stoffler D. 1992. Accretionary dust mantles in CM chondrites: Evidence for solar nebula processes. *Geochimica et Cosmochimica Acta* 56:2873–2897.

Michel P., Ballouz R.-L., Barnouin O. S., Jutzi M., Walsh K. J., May B. H., Manzoni C., Richardson D. C., Schwartz S. R., Sugita S., Watanabe S., Miyamoto H., Hirabayashi M., Bottke W. F., Connolly H. C., Yoshikawa M., and Lauretta D. S. 2020. Collisional formation of top-shaped asteroids and implications for the origins of Ryugu and Bennu. *Nature Communications* 11:2655. https://doi.org/10.1038/s41467-020-16433-z.

Michel P. and Delbo M. 2010. Orbital and thermal evolutions of four potential targets for a sample return space mission to a primitive near-Earth asteroid. *Icarus* 209:520–534.

Molaro J. L., Walsh K. J., Jawin E. R., Ballouz R.-L., Bennett C. A., DellaGiustina D. N., Golish D. R., Drouet d'. A. C., Rizk B., Schwartz S. R., Hanna R. D., Martel S. J., Pajola M., Campins H., Ryan A. J., Bottke W. F., and Lauretta D. S. 2020. In situ evidence of thermally induced rock breakdown widespread on Bennu's surface. *Nature Communications* 11:2913. https://doi.org/10.1038/s41467-020-16528-7.

Morlok A., Bischoff A., Stephan T., Floss C., Zinner E. K., and Jessberger E. K. 2006. Brecciation and chemical heterogeneities of CI chondrites. *Geochimica et Cosmochimica Acta* 70:5371–5394.

Morota T., Sugita S., Cho Y., Kanamaru M., Tatsumi E., Sakatani N., Honda R., Hirata N., Kikuchi H., Yamada M., Yokota Y., Kameda S., Matsuoka M., Sawada H., Honda C., Kouyama T., Ogawa K., Suzuki H., Yoshioka K., Hayakawa M., Hirata N., Hirabayashi M., Miyamoto H., Michikami T., Hiroi T., Hemmi R., Barnouin O. S., Ernst C. M., Kitazato K., Nakamura T., Riu L., Senshu H., Kobayashi H., Sasaki S., Komatsu G., Tanabe N., Fujii Y., Irie T., Suemitsu M., Takaki N., Sugimoto C., Yumoto K., Ishida M., Kato H., Moroi K., Domingue D., Michel P., Pilorget C., Iwata T., Abe M., Ohtake M., Nakauchi Y., Tsumura K., Yabuta H., Ishihara Y., Noguchi R., Matsumoto K., Miura A., Namiki N., Tachibana S., Arakawa M., Ikeda H., Wada K., Mizuno T., Hirose C., Hosoda S., Mori O., Shimada T., Soldini S., Tsukizaki R., Yano H., Ozaki M., Takeuchi H., Yamamoto Y., Okada T., Shimaki Y., Shirai K., Iijima Y., Noda H., Kikuchi S., Yamaguchi T., Ogawa N., Ono G., Mimasu Y., Yoshikawa K., Takahashi T., Takei Y., Fujii A., Nakazawa S., Terui F., Tanaka S., Yoshikawa M., Saiki T., Watanabe S., and Tsuda Y. 2020. Sample collection from asteroid (162173) Ryugu by Hayabusa 2: Implications for surface evolution. *Science* 368:654–659.

Moskovitz N. A., Abe S., Pan K.-S., Osip D. J., Pefkou D., Melita M. D., Elias M., Kitazito K., Bus S. J., DeMeo F.

E., Binzel R. P., and Abell P. A. 2013. Rotational characterization of Hayabusa II target Asteroid (162173) 1999 JU$_3$. *Icarus* 224:24–31.

Nakamura T. 2005. Post-hydration thermal metamorphism of carbonaceous chondrites. *Journal of Mineralogical and Petrological Sciences* 100:260–272.

Nakato A., Nakamura T., Kitajima F., and Noguchi T. 2008. Evaluation of dehydration mechanism during heating of hydrous asteroids based on mineralogical and chemical analysis of naturally and experimentally heated CM chondrites. *Earth, Planets and Space* 60:855–864.

Okada T., Fukuhara T., Tanaka S., Taguchi M., Imamura T., Arai T., Senshu H., Ogawa Y., Demura H., Kitazato K., Nakamura R., Kouyama T., Sekiguchi T., Hasegawa S., Matsunaga T., Wada T., Takita J., Sakatani N., Horikawa Y., Endo K., Helbert J., Müller T. G., and Hagermann A. 2017. Thermal infrared imaging experiments of C-type asteroid 162173 Ryugu on Hayabusa2. *Space Science Reviews* 208:255–286.

Okada T., Fukuhara T., Tanaka S., Taguchi M., Arai T., Senshu H., Sakatani N., Shimaki Y., Demura H., Ogawa Y., Suko K., Sekiguchi T., Kouyama T., Takita J., Matsunaga T., Imamura T., Wada T., Hasegawa S., Helbert J., Müller T. G., Hagermann A., Biele J., Grott M., Hamm M., Delbo M., Hirata N., Hirata N., Yamamoto Y., Sugita S., Namiki N., Kitazato K., Arakawa M., Tachibana S., Ikeda H., Ishiguro M., Wada K., Honda C., Honda R., Ishihara Y., Matsumoto K., Matsuoka M., Michikami T., Miura A., Morota T., Noda H., Noguchi R., Ogawa R., Shirai K., Tatsumi E., Yabuta H., Yokota Y., Yamada M., Abe M., Hayakawa M., Iwata T., Ozaki M., Yano H., Hosoda S., Mori O., Sawada H., Shimada T., Takeuchi H., Tsukizaki R., Fujii A., Hirose C., Kikuchi S., Mimasu Y., Ogawa N., Ono G., Takahashi T., Takei Y., Yamaguchi T., Yoshikawa K., Terui F., Saiki T., Nakazawa S., Yoshikawa M., Watanabe S., and Tsuda Y. 2020. Highly porous nature of a primitive asteroid revealed by thermal imaging. *Nature* 579:518–522.

Parra S. A., Ehlmann B. L., Greenberger R. N., Small Z., Mouroulis P., and Velbel M. 2020. Characterizing spectral diversity in carbonaceous chondrites and linking to asteroids with microimaging spectroscopy (abstract #2617). 51st Lunar and Planetary Science Conference. CD-ROM.

Parra S. A., Ehlmann B. L., and Velbel M. 2021. Characterizing spectral diversity in carbonaceous chondrites and linking meteorites to asteroids with microimaging spectroscopy (abstract #2282). 52nd Lunar and Planetary Science Conference. CD-ROM.

Patzek M., Bischoff A., Visser R., and John T. 2018. Mineralogy of volatile-rich clasts in brecciated meteorites. *Meteoritics & Planetary Science* 53:2519–2540.

Perna D., Barucci M. A., Ishiguro M., Alvarez-Candal A., Kuroda D., Yoshikawa M., Kim M.-J., Fornasier S., Hasegawa S., Roh D.-G., Müller T. G., and Kim Y. 2017. Spectral and rotational properties of near-Earth asteroid (162173) Ryugu, target of the Hayabusa2 sample return mission. *Astronomy & Astrophysics* 599:L1.

Pignatelli I., Marrocchi Y., Vacher L. G., Delon R., and Gounelle M. 2016. Multiple precursors of secondary mineralogical assemblages in CM chondrites. *Meteoritics & Planetary Science* 51:785–805.

Pignatelli I., Marrocchi Y., Muglaioli E., Bourdelle F., and Gounelle M. 2017. Mineralogical, crystallographic and

redox features of the earliest stages of fluid alteration in CM chondrites. *Geochimica et Cosmochimica Acta* 209:106–122.

Quirico E., Orthous-Daunay F.-R., Beck P., Bonal L., Brunetto R., Dartois E., Pino T., Montagnac G., Rouzaud J.-N., Engrand C., and Duprat J. 2014. Origin of insoluble organic matter in type 1 and 2 chondrites: New clues, new questions. *Geochimica et Cosmochimica Acta* 136:80–99.

Quirico E., Bonal L., Beck P., Alexander C. M. O'D., Yabuta H., Nakamura T., Nakato A., Flandinet L., Montagnac G., Schmitt-Kopplin P., and Herd C. D. K. 2018. Prevalence and nature of heating processes in CM and C2-ungrouped chondrites as revealed by insoluble organic matter. *Geochimica et Cosmochimica Acta* 241:17–37.

Reddy V., Le Corre L., O'Brien D. P., Nathues A., Cloutis E. A., Durda D. D., Bottke W. F., Bhatt M. U., Nesvorny D., and Buczkowski D. 2012. Delivery of dark material to Vesta via carbonaceous chondritic impacts. *Icarus* 221:544–559.

Reed S. J. B. 1996. *Electron microprobe analysis and scanning electron microscopy in geology.* Cambridge, UK: Cambridge University Press. 201 p.

Reuter D. C., Simon A. A., Hair J., Lunsford A., Manthripragada S., Bly V., Bos B., Brambora C., Caldwell E., Casto G., Dolch Z., Finneran P., Jennings D., Jhbvala M., Matson E., McLelland M., Roher W., Sullivan T., Weigle E., Wen Y., Wilson D., and Lauretta D. S. 2018. The OSIRIS-REx Visible and InfraRed Spectrometer (OVIRS): Spectral maps of the asteroid Bennu. *Space Science Reviews* 214:54.

Rizk B., Drouet d'. A. C., Golish D., Fellows C., Merrill C., Smith P., Walker M. S., Hendershot J. E., Hancock J., Bailey S. H., DellaGiustina D. N., Lauretta D. S., Tanner R., Williams M., Harshman K., Fitzgibbon M., Verts W., Chen J., Connors T., Hamara D., Dowd A., Lowman A., Dubin M., Burt R., Whiteley M., Watson M., McMahon T., Ward M., Booher D., Read M., Williams B., Hunten M., Little E., Saltzman T., Alfred D., O'Dougherty S., Walthall M., Kenagy K., Peterson S., Crowther B., Perry M. L., See C., Selznick S., Sauve C., Beiser M., Black W., Pfisterer R. N., Lancaster A., Oliver S., Oquest C., Crowley D., Morgan C., Castle C., Dominguez R., and Sullivan M. 2018. OCAMS: The OSIRIS-REx camera suite. *Space Science Reviews* 214:26.

Rozitis B., Ryan A. J., Emery J. P., Christensen P. R., Hamilton V. E., Simon A. A., Reuter D. C., Al A. M., Ballouz R.-L., Bandfield J. L., Barnouin O. S., Bennett C. A., Bernacki M., Burke K. N., Cambioni S., Clark B. E., Daly M. G., Delbo M., DellaGiustina D. N., Elder C. M., Hanna R. D., Haberle C. W., Howell E. S., Golish D. R., Jawin E. R., Kaplan H. H., Lim L. F., Molaro J. L., Pino M. D., Nolan M. C., Rizk B., Siegler M. A., Susorney H. C. M., Walsh K. J., and Lauretta D. S. 2020. Asteroid (101955) Bennu's weak boulders and thermally anomalous equator. *Science Advances* 6:eabc3699.

Rubin A. E. 2004. Postshock annealing and postannealing shock in equilibrated ordinary chondrites: Implications for the thermal and shock histories of chondritic asteroids. *Geochimica et Cosmochimica Acta* 38:673–689.

Rubin A. E. 2012. Collisional facilitation of aqueous alteration of CM and CV carbonaceous chondrites. *Geochimica et Cosmochimica Acta* 90:181–194.

Rubin A. E. 2015. An American on Paris: Extent of aqueous alteration of a CM chondrite and the petrography of its

refractory and amoeboid olivine inclusions. *Meteoritics & Planetary Science* 50:1595–1612.

Rubin A. E. and Bottke W. F. 2009. On the origin of shocked and unshocked CM clasts in H-chondrite regolith breccias. *Meteoritics & Planetary Science* 44:701–724.

Rubin A. E., Trigo-Rodríguez J. M., Huber H., and Wasson J. T. 2007. Progressive alteration of CM carbonaceous chondrites. *Geochimica et Cosmochimica Acta* 71:2361–2382.

Schmidt J. S. and Hinrichs R. 2020. Evaluation of terrestrial carbonaceous matter aromatization by Raman spectroscopy and its application to C chondrites. *Meteoritics & Planetary Science* 55:800–817.

Scott E. R. D., Barber D. J., Alexander C. M. O., Hutchison R., and Peck J. A. 1988. Primitive material surviving in chondrites: Matrix. In *Meteorites and the early solar system*, edited by Kerridge J. F., and Matthews M. S. Tucson, Arizona: The University of Arizona Press. pp. 718–745.

Sugita S., Kuroda D., Kameda S., Hasegawa S., Kamata S., Hiroi T., Abe M., Ishiguro M., Takato N., and Yoshikawa M. 2013. Visible spectroscopic observations of asteroid 162173 (1999 JU$_3$) with the Gemini-S telescope (abstract #2591). 44th Lunar and Planetary Science Conference. CD-ROM.

Sugita S., Honda R., Morota T., Kameda S., Sawada H., Tatsumi E., Yamada M., Honda C., Yokota Y., Kouyama T., Sakatani N., Ogawa K., Suzuki H., Okada T., Namiki N., Tanaka S., Iijima Y., Yoshioka K., Hayakawa M., Cho Y., Matsuoka M., Hirata N., Hirata N., Miyamoto H., Domingue D., Hirabayashi M., Nakamura T., Hiroi T., Michikami T., Michel P., Ballouz R.-L., Barnouin O. S., Ernst C. M., Schröder S. E., Kikuchi H., Hemmi R., Komatsu G., Fukuhara T., Taguchi M., Arai T., Senshu H., Demura H., Ogawa Y., Shimaki Y., Sekiguchi T., Müller T. G., Hagermann A., Mizuno T., Noda H., Matsumoto K., Yamada R., Ishihara Y., Ikeda H., Araki H., Yamamoto K., Abe S., Yoshida F., Higuchi A., Sasaki S., Oshigami S., Tsuruta S., Asari K., Tazawa S., Shizugami M., Kimura J., Otsubo T., Yabuta H., Hasegawa S., Ishiguro M., Tachibana S., Palmer E., Gaskell R., Le Corre L., Jaumann R., Otto K., Schmitz N., Abell P. A., Barucci M. A., Zolensky M. E., Vilas F., Thuillet F., Sugimoto C., Takaki N., Suzuki Y., Kamiyoshihara H., Okada M., Nagata K., Fujimoto M., Yoshikawa M., Yamamoto Y., Shirai K., Noguchi R., Ogawa N., Terui F., Kikuchi S., Yamaguchi T., Oki Y., Takao Y., Takeuchi H., Ono G., Mimasu Y., Yoshikawa K., Takahashi T., Takei Y., Fujii A., Hirose C., Nakazawa S., Hosoda S., Mori O., Shimada T., Soldini S., Iwata T., Abe M., Yano H., Tsukizaki R., Ozaki M., Nishiyama K., Saiki T., Watanabe S., and Tsuda Y. 2019. The geomorphology, color, and thermal properties of Ryugu: Implications for parent-body processes. *Science* 364:eaaw0422.

Takir D., Emery J. P., McSween H. Y. Jr., Hibbits C. A., Clark R. N., Pearson N., and Wang A. 2013. Nature and degree of aqueous alteration in CM and CI chondrites. *Meteoritics & Planetary Science* 48:1618–1637.

Takir D., Howard K., Yabuta H., McAdam M., Hibbitts C., and Emery J. 2018. Linking water-rich asteroids and meteorites: implications for asteroid space missions. In *Primitive meteorites and asteroids: Physical, chemical and spectroscopic observations paving the way for exploration.*

edited by Abreu A. N. M. Cambridge, Massachusetts: Elsevier. pp. 371–408.

Telus M., Alexander C. M. O'D., Hauri E. H. and Wang J. 2019. Calcite and dolomite formation in the CM parent body: Insight from in situ C and O isotope analyses. *Geochimica et Cosmochimica Acta* 260:275–291.

Thompson M. S., Loeffler M. J., Morris R. V., Keller L. P., and Christoffersen R. 2019. Spectral and chemical effects of simulated space weathering of the Murchison CM2 carbonaceous chondrite. *Icarus* 319:499–511.

Tomeoka K. 1990. Mineralogy and petrology of Belgica-7904: A new kind of carbonaceous chondrite from Antarctica. *Proceedings of the NIPR Symposium on Antarctic Meteorites* 3:40–54.

Tomeoka K., Kojima H., and Yanai K. 1989a. Yamato-82162: A new kind of CI carbonaceous chondrite found in Antarctica. *Proceedings of the NIPR Symposium on Antarctic Meteorites* 2:36–54.

Tomeoka K., Kojima H., and Yanai K. 1989b. Yamato-86720: A CM carbonaceous chondrite having experienced extensive aqueous alteration and thermal metamorphism. *Proceedings of the NIPR Symposium on Antarctic Meteorites* 2:55–74.

Tonui E. K., Zolensky M. E., and Lipschutz M. E. 2002. Petrography, mineralogy and trace element chemistry of Y-86029, LEW-85332 and Y-793321: Aqueous alteration and heating events. *Antarctic Meteorite Research* 15:38–58.

Tonui E. K., Zolensky M. E., Lipschutz M. E., Wang M.-S., and Nakamura T. 2003. Yamato-86029: Aqueously altered and thermally metamorphosed CI chondrite with unusual textures. *Meteoritics & Planetary Science* 38:269–292.

Tonui E. K., Zolensky M., Hiroi T., Nakamura T., Lipschutz M. E., Wang M.-S., and Okidura K. 2014. Petrographic, chemical and spectroscopic evidence for thermal metamorphism in carbonaceous chondrites I. CI and CM chondrites. *Geochimica et Cosmochimica Acta* 126:284–306.

Trigo-Rodríguez J. M. 2015. Aqueous alteration in chondritic asteroids and comets from the study of carbonaceous chondrites. In *Planetary materials*, edited by Lee M. R. and Leroux H. London: European Mineralogical Union/ Mineralogical Society of Great Britain and Ireland. pp. 67–87.

Trigo-Rodríguez J. M., Rubin A. E., and Wasson J. T. 2006. Non-nebular origin of dark mantles around chondrules and inclusions in CM chondrites. *Geochimica et Cosmochimica Acta* 70:1271–1290.

Trigo-Rodríguez J. M., Rimola A., Tanbakouei S., Cabedo S. V., and Lee M. 2019. Accretion of water in carbonaceous chondrites: Current evidence and implications for the delivery of water to early Earth. *Space Science Reviews* 215:18.

Vacher L. G., Marrocchi Y., Villeneuve J., Verdier-Paoletti M. J., and Gounelle M. 2018. Collisional and alteration history of the CM parent body. *Geochimica et Cosmochimica Acta* 239:213–234.

Vacher L. G., Piralla M., Gounelle M., Bizzarro M., and Marrocchi Y. 2019. Thermal evolution of hydrated asteroids inferred from oxygen isotopes. *Astrophysical Journal Letters* 882:L20.

Van Gorp B., Mouroulis P., Blaney D., Green R. O., Ehlmann B. L., and Rodriguez J. I. 2014. Ultra-compact imaging spectrometer for remote, in situ, and microscopic planetary mineralogy. *Journal of Applied Remote Sensing* 8:084988.

Vaniman D. T. and Chipera S. J. 2006. Transformations of Mg- and Ca-sulfate hydrates in Mars regolith. *American Mineralogist* 91:1628–1642.

Velbel M. A. 1988. The distribution and significance of evaporitic weathering products on Antarctic meteorites. *Meteoritics* 23:151–159.

Vaniman D. T., Bish D. L., Chipera S. J., Fialips C. I., Carey J. W., and Feldman W. C. 2004. Magnesium sulphate salts and the history of water on Mars. *Nature* 431:663–665.

Van Schmus W. R. and Wood J. A. 1967. A chemical petrologic classification for the chondritic meteorites. *Geochimica et Cosmochimica Acta* 31:747–765.

Velbel M. A. 2014. Stoichiometric reactions describing serpentinization of anhydrous primary silicates: A critical appraisal, with application to aqueous alteration of chondrule silicates in CM carbonaceous chondrites. *Clays and Clay Minerals* 62:126–136.

Velbel M. A. and Palmer E. E. 2011. Fine-grained serpentine in CM2 carbonaceous chondrites and its implications for the extent of aqueous alteration on the parent body: A review. *Clays and Clay Minerals* 59:416–432.

Velbel M. A., Tonui E. K., and Zolensky M. E. 2012. Replacement of olivine by serpentine in the carbonaceous chondrite Nogoya (CM2). *Geochimica et Cosmochimica Acta* 87:117–135.

Velbel M. A., Long D. T., and Gooding J. L. 1991. Terrestrial weathering of Antarctic stone meteorites: Formation of Mg-carbonates on ordinary chondrites. *Geochimica et Cosmochimica Acta* 55:67–76.

Velbel M. A., Tonui E. K., and Zolensky M. E. 2015. Replacement of olivine by serpentine in the Queen Alexandra Range 93005 carbonaceous chondrite (CM2): Reactant-product compositional relations, and isovolumetric constraints on reaction stoichiometry and elemental mobility during aqueous alteration. *Geochimica et Cosmochimica Acta* 148:402–425.

Verdier-Paoletti M. J., Marrocchi Y., Avice G., Roskosz M., Gurenko A., and Gounelle M. 2017. Oxygen isotope constraints on the alteration temperatures of CM chondrites. *Earth and Planetary Science Letters* 458:273–281.

Vilas F. 2008. Spectral characteristics of Hayabusa 2 near-Earth asteroid targets 162173 JU3 and 2001 QC34. *The Astronomical Journal* 135:1101–1105.

Viti C. 2010. Serpentine minerals discrimination by thermal analysis. *American Mineralogist* 95:631–638.

Wada K., Grott M., Michel P., Walsh K. J., Barucci A. M., Biele J., Blum J., Ernst C. M., Grundmann J. T., Gundlach B., Hagermann A., Hamm M., Jutzi M., Kim M.-J., Kührt E., Le Corre L., Libourel G., Lichtenheldt R., Maturilli A., Messenger S. R., Michikami T., Miyamoto H., Mottola S., Nakamura A. M., Müller T., Nittler L. R., Ogawa K., Okada T., Palomba E., Sakatani N., Schröder S., Senshu H., Takir D., Zolensky M. E., and International Regolith Science Group (IRSG) in Hayabusa2 project. 2018. Asteroid Ryugu before the Hayabusa2 encounter. *Progress in Earth and Planetary Science* 5:82. https://doi.org/10.1186/s40645-018-0237-y.

Watanabe S., Hirabayashi M., Hirata N., Hirata N., Noguchi R., Shimaki Y., Ikeda H., Tatsumi E., Yoshikawa M., Kikuchi S., Yabuta H., Nakamura T., Tachibana S., Ishihara Y., Morota T., Kitazato K., Sakatani N., Matsumoto K., Wada K., Senshu H., Honda C., Michikami T., Takeuchi H., Kouyama T., Honda R., Kameda S., Fuse

T., Miyamoto H., Komatsu G., Sugita S., Okada T., Namiki N., Arakawa M., Ishiguro M., Abe M., Gaskell R., Palmer E., Barnouin O. S., Michel P., French A. S., McMahon J. W., Scheeres D. J., Abell P. A., Yamamoto Y., Tanaka S., Shirai K., Matsuoka M., Yamada M., Yokota Y., Suzuki H., Yoshioka K., Cho Y., Tanaka S., Nishikawa N., Sugiyama T., Kikuchi H., Hemmi R., Yamaguchi T., Ogawa N., Ono G., Mimasu Y., Yoshikawa K., Takahashi T., Takei Y., Fujii A., Hirose C., Iwata T., Hayakawa M., Hosoda S., Mori O., Sawada H., Shimada T., Soldini S., Yano H., Tsukizaki R., Ozaki M., Iijima Y., Ogawa K., Fujimoto M., Ho T.-M., Moussi A., Jaumann R., Bibring J.-P., Krause C., Terui F., Saiki T., Nakazawa S., and Tsuda Y. 2019. Hayabusa2 arrives at the carbonaceous asteroid 162173 Ryugu—A spinning top–shaped rubble pile. *Science* 364:268–272.

Weisberg M. K., McCoy T. J., and Krot A. N. 2006. Systematics and evaluation of meteorite classification. In *Meteorites and the early solar system II*, edited by Lauretta D. S. and McSween H. Y. Jr. Tucson, Arizona: The University of Arizona Press. pp. 19–52.

Weiss I. M., Muth C., Drumm R., and Kirchner H. L. K. 2018. Thermal decomposition of the amino acids glycine, cysteine, aspartic acid, asparagine, glutamic acid, glutamine, arginine and histidine. *BMC Biophysics* 11:2. https://doi.org/10.1186/s13628-018-0042-4.

Wiik H. B. 1956. The chemical composition of some stony meteorites. *Geochimica et Cosmochimica Acta* 9:279–289.

Yabuta H., Alexander C. M. O'D., Fogel M. L., Kilcoyne A. L. D., and Cody G. D. 2010. A molecular and isotopic study of the macromolecular organic matter of the ungrouped C2 WIS 91600 and its relationship to Tagish Lake and PCA 91008. *Meteoritics & Planetary Science* 45:1446–1460.

Zolensky M. and Ivanov A. 2003. The Kaidun microbreccia meteorite: A harvest from the inner and outer asteroid belt. *Chemie der Erde* 63:185–246.

Zolensky M. and McSween H. Y. Jr. 1988. Aqueous alteration. In *Meteorites and the early solar system*, edited by Kerridge J. F. and Shapley Matthews M. Tucson, Arizona: The University of Arizona Press. pp. 114–143.

Zolensky M. E., Hewins R. H., Mittlefehldt D. W., Lindstrom M. M., Xiao X., and Lipschutz M. E. 1992. Mineralogy, petrology and geochemistry of carbonaceous clasts in the LEW 85300 polymict eucrite. *Meteoritics* 27:596–604.

Zolensky M. E., Barrett R., and Browning L. 1993. Mineralogy and composition of matrix and chondrule rims in carbonaceous chondrites. *Geochimica et Cosmochimica Acta* 57:3123–3148.

Zolensky M. E., Weisberg M. K., Buchanan P. C., and Mittlefehldt D. W. 1996a. Mineralogy of carbonaceous clasts in HED achondrites and the Moon. *Meteoritics & Planetary Science* 31:518–537.

Zolensky M. E., Ivanov A. V., Yang S. V., Mittlefehldt D. W., and Ohsumi K. 1996b. The Kaidun meteorite: Mineralogy of an unusual CM1 lithology. *Meteoritics & Planetary Science* 31:484–493.

Zolensky M. E., Mikouchi T., Fries M., Bodnar R., Jenniskens P., Yin Q., Hagiya K., Ohsumi K., Komatsu M., Colbert M., Hanna R., Maisano J., Ketcham R., Kebukawa Y., Nakamura T., Matsuoka M., Sasaki S., Tsuchiyama A., Gounelle M., Le L., Martinez J., Ross K., and Rahman Z. 2014. Mineralogy and petrography of C asteroid regolith: The Sutter's Mill CM meteorite. *Meteoritics & Planetary Science* 49:1997–2016.

Zolensky M. E., Abreu N. M., Velbel M. A., Rubin A., Chaumard N., Noguchi T., and Michikami T. 2018. Physical, chemical, and petrological characteristics of chondritic materials and their relationships to small solar system bodies. In *Primitive meteorites and asteroids: Physical, chemical and spectroscopic observations paving the way for exploration*, edited by Abreu N. M. Cambridge, Massachusetts: Elsevier. pp. 59–204.

Zolensky M. E., Mittlefehldt D. W., Lipschutz M. E., Wang M.-S., Clayton R. N., Mayeda T. K., Grady M. M., Pillinger C., and Barber D. 1997. CM chondrites exhibit the complete petrologic range from type 2 to 1. *Geochimica et Cosmochimica Acta* 61:5099–5115.